

University of Nevada, Reno

**Enhanced $\alpha7\beta1$ integrin prevents muscle disease in a mouse model
of congenital muscular dystrophy**

A dissertation submitted in partial fulfillment of the
requirements for the degree of Doctor of Philosophy in
Cellular and Molecular Pharmacology and Physiology

By Jinger A. Doe

Dr. Dean J. Burkin/Dissertation Advisor

August, 2011



University of Nevada, Reno
Statewide · Worldwide

THE GRADUATE SCHOOL

We recommend that the dissertation
prepared under our supervision by

JINGER ANN DOE

entitled

**Enhanced Alpha7 Beta1 Integrin Prevents Muscle Disease In A Mouse Model
Of Congenital Muscular Dystrophy**

be accepted in partial fulfillment of the
requirements for the degree of

DOCTOR OF PHILOSOPHY

Dean J. Burkin, Ph.D., Advisor

Normand Leblanc, Ph.D., Committee Member

Cherie Singer, Ph.D., Committee Member

Maria Valencik, Ph.D., Committee Member

Thomas Kidd, Ph.D., Graduate School Representative

Marsha H. Read, Ph. D., Dean, Graduate School

August, 2011

Abstract

Merosin Deficient Congenital Muscular Dystrophy Type 1A (MDC1A) is the most common form of Congenital Muscular Dystrophy (CMD). MDC1A accounts for approximately 40% of all CMD cases. CMD is estimated to have an incidence rate in the United States of 1/100,000 live births. MDC1A is a lethal disease which results from mutations in the *LAMA2* gene leading to either a complete or partial absence of the protein laminin $\alpha 2$. The loss of laminin $\alpha 2$ protein in turn leads to a failure to produce laminin 211 and laminin 221. Laminin 211 is the major laminin component of the basal lamina of mature skeletal muscle while laminin 221 is primarily located at neuromuscular and myotendinous junctions. Patients with MDC1A display a spectrum of clinical signs which correlate with the type of mutation they carry in the *LAMA2* gene. Patients who produce some laminin $\alpha 2$ or who produce a truncated form of the protein tend to have less severe clinical signs and longer life expectancies than patients who produce no laminin $\alpha 2$. Patients with classic MDC1A have mutations which result in either complete absence of or negligible production of laminin $\alpha 2$. Patients who produce no laminin $\alpha 2$ have the most severe clinical signs and shortest life expectancies. MDC1A patients display delayed motor milestones and unsupported sitting is often the maximal motor activity; they are often confined to a wheelchair at a young age. Feeding problems requiring feeding tube placement, and respiratory difficulties requiring positive pressure ventilation are common. It is not unusual for these patients to die within the first decade of life due to respiratory complications.

Secondary to the loss of laminin $\alpha 2$, MDC1A patients display reduced levels of $\alpha 7$ integrin. The $\alpha 7\beta 1$ integrin is one of the main laminin 211/221 receptors in skeletal muscle. The loss of $\alpha 7$ integrin is considered to be due to communication between the extracellular matrix and the cell surface receptors. Primary loss of the $\alpha 7$ integrin is rare and leads to a myopathy in affected individuals. The effect of the secondary loss of the $\alpha 7$ integrin in MDC1A patients has not been evaluated prior to this work.

In order to determine the effect of $\alpha 7$ integrin loss, we enhanced $\alpha 7$ integrin expression in the skeletal muscle of the $dy^W/-$ mouse model of MDC1A. The $dy^W/-$ mouse is one of the most commonly used models of MDC1A and displays altered expression and localization of the $\alpha 7$ integrin with little integrin appropriately localized to the sarcolemma. We accomplished forced expression of $\alpha 7$ integrin by breeding the BX2-10i mouse and $dy^W/-$ mouse over several generations to develop a mouse which lacked laminin $\alpha 2$ and overexpressed $\alpha 7$ integrin in the skeletal muscle. The BX2-10i mouse is a skeletal muscle specific overexpressor of $\alpha 7BX2$ integrin – one of the primary $\alpha 7$ integrin isoforms which binds with laminin in skeletal muscle. These animals contain a transgene which uses the muscle creatine kinase (MCK) promoter to drive $\alpha 7BX2$ integrin production specifically in skeletal muscle. The resultant mouse, designated as $dy^W/-;itga7+$, allowed us to determine the effect of reintroducing $\alpha 7$ integrin back into an MDC1A model, and thus, gave us insight into the role that reduced $\alpha 7$ integrin plays in the pathology of MDC1A.

Dedication

To my family and friends for all their love and support.

To my parents for emphasizing that learning and questioning are two of the greatest things we can do

Acknowledgements

First and foremost I would like to acknowledge my dissertation advisor, Dean J. Burkin. Dr. Burkin has been very encouraging along this journey. He has an infectious enthusiasm for science and genuinely enjoys his laboratory work and the people who work in the laboratory. Dr. Burkin has always had an open door policy which has made this journey not only easier but also more enjoyable. I would also like to thank my dissertation committee: Dr. Maria Valencick, Dr. Cherie Singer, Dr. Normand Leblanc, and Dr. Thomas Kidd. Their support and guidance were very valuable along this journey.

I would like to thank all of the members of the Burkin lab. I would like to especially thank Dr.'s Jennifer V. Welser and Jachinta E. Rooney for teaching me the basics when I first came into the lab and helping with trouble-shooting along the way. They were both always available for questions or to lend an ear. Dr. Ryan Wuebbles was instrumental in all qRT-PCR experiments for which I am thankful. I also need to thank Ms. Rebecca Evans for her assistance with animal husbandry. Ms. Erika Allred also provided valuable assistance in a wide range of projects. I would have been lost without the help of these people. I would also like to thank Dr. Heather Burkin for critically reading my manuscript.

I also need to take the time to thank other investigators for their assistance. Thank you to Dr. Eva Engvall via Dr. Paul Martin (The Ohio State University, Columbus, Ohio) for the dy^W mice, also, Dr. Steven Kaufman (the University of Illinois, Urbana, Champaign, IL) for the BX2#10i mice. I would also like to thank Dr. Kaufman, Dr. Peter Yurchenco (Robert Wood Johnson Medical School, Piscataway, NJ), and Dr. Woo Sun

Keun Song (Gwanju Institute for Science and Technology, Seoul, Korea) for the anti-alpha 7A and alpha 7B, anti-laminin alpha2G, and anti-beta1D integrin antibodies.

I would also like to acknowledge the following funding sources which made this work possible: NIH/NIAMS grant number R01AR053697-01A2, NIH/NINDS grant number R21NS58429-01A1, NIH/NINDS grant number R21NS58429S, and NIH/NIAMS grant number R21AR060769-01.

My parents, Rita Heuser and Thomas Doe and step-parents, Thomas Andrews and Cess Doe have been there for me every step of the way. From when I was young my parents have pushed me academically and taught me that learning is a noble pursuit. They have been supportive of me through this phase of my education and listened to endless presentations without complaint.

Table of Contents

Abstract.....	i
Dedication.....	iii
Acknowledgements.....	iv
Table of Contents.....	vi
List of Tables.....	viii
List of Figures.....	ix
Chapter 1.....	1
Chapter 2.....	14
Chapter 3.....	26
Abstract.....	27
Introduction.....	27
Materials and Methods.....	30
Results.....	36
Discussion.....	46
Acknowledgements.....	50
Table.....	51
Figures.....	52
Addendum.....	57
Chapter 4.....	74
Abstract.....	75
Introduction.....	75
Materials and Methods.....	78
Results.....	80

Discussion.....	82
Figures.....	86
Chapter 5.....	97
Abstract.....	98
Introduction.....	99
Materials and Methods.....	101
Results.....	102
Discussion.....	103
Figures.....	106
Chapter 6.....	111
Appendix.....	119
Appendix A.1.....	120
Abstract.....	121
Introduction.....	121
Materials and methods.....	124
Results.....	129
Discussion.....	136
Acknowledgements.....	142
Figures.....	143
Bibliography.....	160

List of Tables

Table 2.1. Results of RT ² Profiler qPCR array experiments.....	19
Table 3.1. Results of qRT-PCR experiments.....	51
Table S.3.1 Primer sequences for qRT-PCR experiments.....	70

List of Figures

Figure 1.1 Major laminin receptors present in mature skeletal muscle.....	6
Figure 2.1 Breeding scheme used to generate experimental animals.....	24
Figure 2.2 Representative image of dy^W ^{-/-} and dy^W ^{-/-} ; <i>itga7</i> ⁺ animals.....	25
Figure 3.1. Enhanced $\alpha7B$ integrin the muscle of dy^W ^{-/-} ; <i>itga7</i> ⁺ mice.....	52
Figure 3.2 β iD integrin transcript levels comparing wild-type, dy^W ^{-/-} , and dy^W ^{-/-} ; <i>itga7</i> ⁺ animals.....	54
Figure 3.3 Transgenic expression of $\alpha7$ integrin restores sarcolemmal location in dy^W ^{-/-} skeletal muscle.....	55
Figure 3.4. Transgenic expression of $\alpha7$ integrin in the skeletal muscle of dy^W ^{-/-} mice increase longevity but not weight gain.....	57
Figure 3.5. The dy^W ^{-/-} ; <i>itga7</i> ⁺ transgenic mice maintain muscle strength and exhibit increased motor activity.....	58
Figure 3.6. Reduced muscle disease in laminin- $\alpha2$ deficient mice that transgenically express $\alpha7$ integrin.....	60
Figure 3.7. Transgenic expression of $\alpha7$ integrin in the absence of laminin- $\alpha2$ increased expression of galectins-1 and -3 in the muscle of dy^W ^{-/-} mice.....	62
Figure 3.8. Enhanced expression of $\alpha7$ integrin augments the extracellular matrix and slows matrix turnover in the dy^W ^{-/-} mouse.....	64
Figure 3.9. Enhanced expression of $\alpha7$ integrin reduces inflammation in dy^W ^{-/-} muscle.....	66

Figure 3.10. Enhanced $\alpha 7$ integrin expression improves diaphragm pathology in 4-week-old dy^W $-/-$ mice.....	68
Figure S3.1. Muscle specific transgenic expression of the $\alpha 7$ integrin improves myofiber cross-sectional area.....	71
Figure 4.1. α -bungarotoxin staining showing neuromuscular junctions in wild-type, dy^W $-/-$, and dy^W $-/-;itga7+$ animals and graphical representations of neuromuscular size and number.....	86
Figure 4.2. Penh measurements in wild-type, dy^W $-/-$ and dy^W $-/-;itga7+$ animals.....	88
Figure 4.3. Frequency of breathing during methacholine stimulation.....	90
Figure 4.4. Evaluation of total volume breathed in wild-type, dy^W $-/-$, and dy^W $-/-;itga7+$ animals.....	91
Figure 4.5. Comparison of inspiratory times during a methacholine stimulation test at 4-, 6-, and 8-weeks of age.....	93
Figure 4.6. Comparison of expiratory time in wild-type, dy^W $-/-$, and dy^W $-/-;itga7+$ animals during a methacholine stimulation test.....	95
Figure 5.1. Transcription of <i>lgals1</i> and <i>lgals3</i> are altered in the dy^W $-/-$ mouse.....	106
Figure 5.2. Western blotting for galectin-1 in dy^W $-/-$ and wild-type mice at 4- and 8-weeks of age.....	108
Figure 5.3. Immunoblotting experiments for galectin-3 protein in dy^W $-/-$ and wild-type animals.....	110
Figure 6.1. Proposed mechanism of action.....	118
Figure A.1.1. Immunofluorescent staining of C2C12 cells reveals that ECM composition has a profound influence on myoblast phenotype.....	143

Figure A.1.2. Alteration in the time course of changes in membrane currents elicited by switching from isotonic to hypotonic solutions in C2C12 cells plated on fibronectin.....	145
Figure A.1.3. Typical families of membrane current recorded in isotonic and hypotonic conditions from C2C12 myoblasts grown in the absence or presence of matrix proteins.....	147
Figure A.1.4. Voltage-dependence of membrane current recorded in isotonic and hypotonic conditions in C2C12 cells grown in the absence of presence of matrix proteins.....	149
Figure A.1.5. Anion selectivity of hypotonic-induced membrane current recorded from C2C12 cells grown in the absence or presence of matrix proteins.....	151
Figure A.1.6. Selectivity and permeability profiles of hypotonic-induced VSOAC currents in C2C12 myoblasts grown in the absence or presence of matrix proteins.....	153
Figure A.1.7. Tamoxifen sensitivity of the hypotonic-induced VSOAC current recorded in cells grown in the absence or presence of matrix proteins.....	155
Figure A.1.8. Specific genetic β_1 integrin knockdown inhibits the basal and hypotonic-induced VSOAC current in cells plated on fibronectin.....	157

CHAPTER 1

Introduction

Merosin deficient congenital muscular dystrophy 1A (MDC1A)

The congenital muscular dystrophies (CMDs) are some of the most common genetic neuromuscular disorders. The CMDs are comprised of a diverse group of diseases which affect children within the first 6 months of life. Symptoms of CMD include hypotonia, weakness, contractures, and variable disease progression¹⁻³. Further classification of CMD is based upon the specific protein defect. Protein defects have been isolated to extracellular matrix proteins, membrane receptor proteins, and endoplasmic reticulum proteins^{4;5}. Significant regional variability in incidence rates exist with published rates being between 4.7/100,000 in northern Italy and 6.3/100,000 live births in western Sweden; a founder effect is also present^{2;4}.

Merosin Deficient Congenital Muscular Dystrophy Type 1A (MDC1A) is due to a mutation in the *LAMA2* gene. This affects the extracellular matrix proteins laminin 211 and laminin 221. The *LAMA2* gene maps to chromosome 6q22-23 and spans approximately 260 kb with 64 exons^{6;7}. The *LAMA2* gene codes for the protein laminin $\alpha 2$. MDC1A is considered the most common CMD, accounting for 30-40% of all diagnosed cases of CMD⁴. MDC1A is much less common in Asian populations where it has a frequency of 6-7% of CMD cases⁸. Incidence rates for MDC1A in the U.S. are not available.

The severity of MDC1A is variable and correlates well with laminin $\alpha 2$ production. Patients with a mutation that results in no laminin $\alpha 2$ production have more severe clinical signs than those who are able to produce some laminin $\alpha 2$ or a truncated form of laminin $\alpha 2$ ^{9;10}. Patients who suffer from a complete loss of laminin $\alpha 2$ suffer from severe weakness, hypotonia, muscle atrophy, dysmyelinating neuropathy and have

an elevated serum creatine kinase (CK) on blood chemistry panels^{1;5;11}. Feeding difficulties requiring feeding tube placement are not uncommon and respiratory difficulties requiring positive pressure ventilation are common. Maximal motor activity is often unsupported sitting with few patients achieving independent ambulation⁴. A unique characteristic of MDC1A is an increase in brain white matter intensity on T2 weighted MRI which may be associated with seizure-like activity^{4;12}. There is no cure for MDC1A with only palliative therapy available; patients may die as early as the first decade of life, there have been deaths reported as early as 4-months of age^{5;11}.

Laminins

The laminin family of proteins was first described with the isolation and identification of laminin 111 from the Engelbreth-Holm-Swarm (EHS) mouse sarcoma¹³. This was the first time that laminin was described as a distinct basement membrane protein in that it differs from both collagens and fibronectin (which are also produced by the EHS tumor). Laminins are heterotrimeric proteins comprised of an α chain, a β chain, and a γ chain. Laminins have been highly conserved throughout evolution with the earliest laminin believed to be found in *Hydra vulgaris*¹⁴. The α chain is the most variable of the three and confers the binding specificity of the heterotrimer. To date 5 α , 3 β , and 3 γ chains have been identified in mammals which form 16 distinct laminin heterotrimers¹⁵. Laminins are major components of the basal lamina in numerous tissues where they lend structural integrity as well as playing a role in tissue survival, cell movement, and cell differentiation¹⁶. Other components of skeletal muscle basement membrane include collagen IV, nidogens, perlecan, and agrin¹⁶.

Laminin 111 ($\alpha 1$, $\beta 1$, $\gamma 1$) is the predominant laminin isoform during development, including in the basement membrane of developing skeletal muscle; it is replaced by laminins 211 and 221 (laminin 221 is primarily at neuromuscular and myotendinous junctions) in mature skeletal muscle¹⁶⁻¹⁹. At seven weeks of gestation laminin $\alpha 2$ begins to be made and the switch from laminin 111 to laminins 211 and 221 begins with maximum expression at 21-weeks of gestation²⁰⁻²². In mice the switch to laminins 211 and 221 from laminin 111 occurs at embryonic day 11¹⁹. Due to the presence of laminin 111, early muscle development takes place normally in MDC1A patients and mouse models of MDC1A. In developing skeletal muscle laminin 111 anchors the myofibers to the BM. In mature skeletal muscle this role is taken over by laminin 211. Laminin $\alpha 2$ is secreted by muscle cells after undergoing post-translational modifications (they are highly glycosylated) and also undergo post-secretion modifications¹⁶. Laminins $\alpha 4$ and $\alpha 5$ are also present in skeletal muscle and are upregulated in MDC1A patients; however, although this upregulation cannot compensate for the absence of laminin $\alpha 2$ in MDC1A^{16;23}.

Laminin $\alpha 2$ deficient myotubes are unable to properly anchor the cells to the extracellular matrix making them unstable leading to apoptosis^{24;25}. In support of this cultured cells (mouse C2C12 myoblasts and human rhabdomyosarcoma (RD) lines) show differential expression of laminin $\alpha 1$ and $\alpha 2$ chains during differentiation. Laminin $\alpha 2$ expression increases as differentiation proceeds and laminin $\alpha 1$ expression decreases over the same time course. Laminin $\alpha 2$ deficient clones of these cells lines are unable to form stable myotubes and restoration of laminin $\alpha 2$ expression returns myotube stability

²⁴. Laminin $\alpha 2$ deficient myotubes are also associated with decreased regenerative capacity after injury ²⁶.

Schwann cells in the Peripheral Nervous System (PNS) also produce laminin $\alpha 2$. In the absence of laminin $\alpha 2$ the Schwann cells are unable to properly myelinate the nerves, particularly near the Nodes of Ranvier. This is associated with impaired conduction velocity and a resulting peripheral neuropathy ²⁷. Additionally, laminin 221 is essential for the appropriate formation of the neuromuscular junction. The $\beta 2$ chain and the proteoglycan agrin are essential components of the neuromuscular junction ¹⁶. Additional laminin α -chains are expressed in developing peripheral nerves and skeletal muscle including the $\alpha 4$ and $\alpha 5$ chains ¹⁶. These two laminin α -chains are up-regulated in laminin $\alpha 2$ deficient mice and MDC1A patients; however this increase is not compensatory ^{23;28;29}.

In skeletal muscle the two major receptors for laminins 111, 211, and 221 are α -dystroglycan and the $\alpha 7 \beta 1$ integrin (Figure 1.1). α -dystroglycan is a member of the dystrophin glycoprotein complex (DGC) and interacts with laminin $\alpha 2$ via the G-domain (the COOH-terminus) ^{16;30}. The NH₂-terminus of laminin is responsible for polymerization of the individual laminin proteins ³⁰. Alterations to the DGC are associated with multiple types of muscular dystrophy. Absence of the large intracellular protein dystrophin is the cause of Duchenne Muscular Dystrophy (DMD) which is the most common form of muscular dystrophy. DMD patients lose members of the DGC secondary to the loss of dystrophin. The $\alpha 7 \beta 1$ integrin is the second laminin receptor, it also binds with the G-domain of laminin $\alpha 2$ ¹⁶. The $\alpha 7 \beta 1$ integrin can interact with other

ligands such as galectin-1 and fibronectin³¹. MDC1A patients as well as MDC1A mouse models show reduced levels of, or altered localization of $\alpha 7$ integrin protein^{2;32;33}.

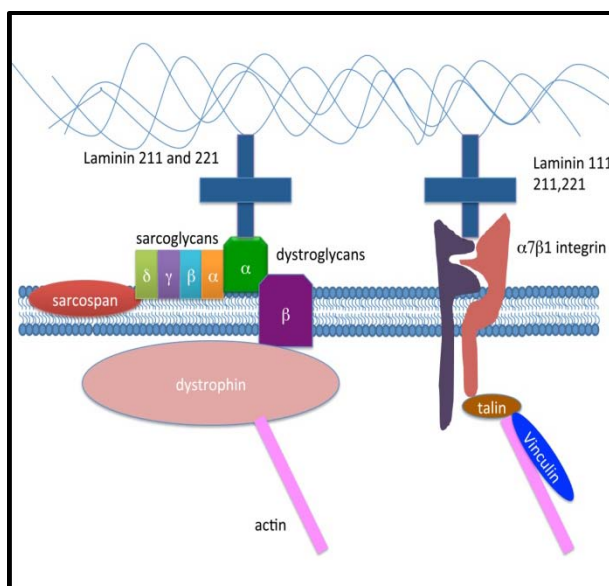


Figure 1.1. Major laminin receptors present in mature skeletal muscle.

The left portion of the panel depicts the dystrophin glycoprotein complex (DGC). The right portion depicts the interaction between the $\alpha 7 \beta 1$ integrin heterodimer and laminin. Defects in the DGC, laminin, and $\alpha 7 \beta 1$ integrin are associated with muscle pathology.

The $\alpha 7 \beta 1$ integrin

The $\alpha 7 \beta 1$ integrin is a member of the integrin family of proteins. It is a heterodimeric protein composed of an α chain and a β chain, which are noncovalently linked³⁴. Integrins are evolutionarily conserved from *Drosophila* to vertebrates^{34;35}. Integrin heterodimers act as leukocyte receptors, RGD receptors (which recognize an arginine, glycine, aspartic acid amino acid sequence), collagen receptors, and laminin receptors³⁴. Patients with a primary mutation in the *ITGA7* gene, which results in a loss of $\alpha 7$ integrin protein, suffer from a congenital myopathy³⁶. $\alpha 7$ integrin was first described in 1992 as a member of the integrin family, which was regulated with muscle development³⁷. Experimentally, animals which are designed to lack both dystrophin and the $\alpha 7$ integrin display a much more severe phenotype than either the *mdx* (a mouse strain which lacks dystrophin) or $\alpha 7$ integrin null animals^{38;39}.

The $\alpha7\beta1$ integrin is one of two major laminin receptors in skeletal muscle (Figure 1.1) ⁴⁰. The $\alpha7$ integrin has three intracellular and two extracellular splice variants which allow it to participate in a variety of signaling cascades. The $\alpha7$ integrin has three alternative intracellular domains ($\alpha7A$, $\alpha7B$, and $\alpha7C$) and two alternative extracellular domains (X1 and X2). The $\alpha7A$ and $\alpha7C$ isoforms are only located in the skeletal muscle, however, the $\alpha7B$ splice variant is located both in the skeletal muscle and outside of it (such as in the vasculature, digestive tract, and nervous system) ⁴¹. The major variants of the $\beta1$ integrin are $\beta1A$ and $\beta1D$ with $\beta1D$ being the primary isoform present in mature skeletal muscle ⁴². Laminin 211 is the major ligand for the $\alpha7\beta1$ integrin although it can interact with alternative laminin isoforms including $\alpha1$, $\alpha4$, and $\alpha5$ *in vivo* as well as galectin-1 and purified fibronectin *in vitro* ^{31;43}.

Patients with Duchenne Muscular Dystrophy (DMD) and the *mdx* mouse (a DMD model) lack the large intracellular protein dystrophin and both show increases in $\alpha7$ integrin expression at the protein and transcript levels ³³. This observation led to further investigation into the role of the $\alpha7\beta1$ integrin in the pathology of dystrophic muscle. To test this role, transgenic mice expressing a rat $\alpha7BX2$ integrin transgene driven by the muscle creatine kinase (MCK) promoter were developed ^{42;44}. Expression of the rat $\alpha7$ integrin transgene also led to an increase in $\beta1$ integrin protein expression. The *mdx/utr^{-/-}* mouse lacks both dystrophin and utrophin proteins and has a severe dystrophic phenotype and dramatically decreased life span. This severe pathology is rescued and the life span increased 3-fold by further enhancing the levels of $\alpha7\beta1$ integrin protein expression in these animals by cross-mating them with the $\alpha7$ integrin transgenic overexpressors ⁴⁵.

MDC1A patients have decreased levels of $\alpha7\beta1$ integrin protein expression^{2;32}. Mouse models for MDC1A also have altered $\alpha7\beta1$ integrin expression when compared to the wild-type at both transcript and protein levels, however there is significant strain variation noted in the literature. The *dy/dy* and *dy^{2J}/dy^{2J}* strain show reduced $\alpha7$ integrin protein and transcript levels^{32;33}. Specifically, the *dy/dy* and *dy^{2J}dy^{2J}* display no sarcolemmal staining for $\alpha7A$ integrin and irregular and patchy staining for $\alpha7B$ integrin³². Conversely, the laboratory generated *dy3k^{-/-}* strain has an increase in $\alpha7$ integrin total protein and transcript. However, these animals showed markedly less $\alpha7$ integrin protein staining at the sarcolemma⁴⁶. The endogenous $\alpha7$ integrin protein and transcript levels have not previously been evaluated in the *dy^W-/-* mouse.

Altered gene expression in dystrophic muscle

Gene expression profiling in various dystrophic muscle has yielded interesting results. Transcript evaluation has also been done in primary myoblasts cultured from DMD patients. Among other results, matrix metalloproteinase 2 (MMP2) and tissue inhibitor of matrix metalloproteinases 1 (TIMP1) had significantly higher transcript than in control cells⁴⁷. The diaphragm muscle of the *dy/dy* mouse has also been evaluated at the gene expression level. The study found 69 genes that were expressed at least two-fold more or less than wild-type animals. Among those genes was *lgals3*, the gene which encodes the lectin-binding protein galectin-3⁴⁸.

Galectins as Biomarkers

Biomarkers are traceable substances which allow physicians to either diagnose diseases, monitor disease progression, or track response to treatment. Two prominently used biomarkers are galectin-1 and galectin-3. The galectins are members of a β -

galactoside binding family of small proteins with a diverse range of functions.

Galectin-1 has a wide array of functions *in vivo*. It is present both intracellularly and extracellularly. One of its roles is in skeletal muscle differentiation where it competes with laminin for binding sites on the $\alpha7\beta1$ integrin^{31;49-51}. It interacts directly with the β -integrin⁴⁹. Camby *et al*⁴⁹ also proposed its use as a potential therapeutic target for muscular dystrophies. They base this proposition on the ability of galectin-1 to increase terminal differentiation and the role it plays in muscle development and regeneration. Even though galectin-1 will inhibit myocyte binding of laminin, it does not prevent the binding of $\alpha7\beta1$ to fibronectin.

Galectin-1 is also produced by a number of tumors and its expression increases as tumor grade increases (i.e. with metastasis)⁵¹. Galectin-1 is also used as a diagnostic and/or prognostic biomarker for several types of cancer including colon carcinomas, pancreatic ductal adenocarcinomas, renal cell carcinomas, prostate cancer, and nonsmall-cell lung cancers⁴⁹. Galectin-1 also plays a role in inflammation as it associates with CD11b, a macrophage and monocyte cell surface protein⁵¹.

Galectin-3 has been used as a biomarker for diseases associated with fibrosis and inflammation such as chronic heart failure, liver cirrhosis and bladder cancer⁵². This is because galectin-3 promotes macrophage activation, fibroblast proliferation and collagen synthesis. In cases of inflammation, galectin-3 is responsible for recruitment of macrophages to the site of trauma causing them to slow down and become more firmly associated with that area^{53;54}. This is accomplished in two ways, first, galectin-3 is chemotactic for monocytes and macrophages, and second, galectin-3 enhances white blood cells attachment to laminin^{53;55;56}. As a biomarker for heart disease, plasma levels

of galectin-3 are used to monitor disease progression and are used as a prognostic marker as well. This is true despite the fact that plasma galectin-3 increases with renal dysfunction and age⁵⁷. In transitional cell carcinomas (TCCs) galectin-3 can be used for diagnosis, staging, and prognosis of disease, in all cases increased levels of galectin-3 correlate with a more negative result. It is also strongly associated with ki67 (a proliferation marker which increases in cases of TCC)⁵⁸. The protein can be detected in the serum, urine, and tumor biopsy samples. The removal of galectin-3 from the circulating blood is accomplished by the liver, which is another reason that galectin-3 levels are elevated in hepatic disease⁵⁹.

Neuromuscular junctions

The laminin β 2 chain is necessary for formation of the neuromuscular junction (NMJ), specifically laminin 221 (α 2 β 2 γ 1) is required as it associates with agrin and the α 7 β 1 integrin, which are also located at the NMJ. Agrin induces ACHR clustering in cultured muscle cells^{16;60-62}. This clustering is mediated by agrin phosphorylation of muscle specific kinase (MuSK)^{16;63-65}. Agrin inserts into the basement membrane by binding with laminin^{61;66-68}. Agrin is also expressed outside of the NMJ and is variable depending on the muscle group⁶¹.

Signaling

The absence of laminins 211 and 221 can have a profound impact on cell signaling cascades, including those related to apoptosis, which is one of the hallmark characteristics of MDC1A. One such cascade is the PI3K/Akt pathway. In normal skeletal muscle laminin binding with the α 7 β 1 integrin causes the phosphorylation of focal adhesion kinase (FAK) by the β 1 integrin chain. FAK then phosphorylates PI3K,

which, in turn, phosphorylates the anti-apoptotic molecule Akt (protein kinase B). Akt then phosphorylates Bad which renders it inactive. In its active state Bad activates cytochrome c in the mitochondria which leads to the release of caspase 9, which activates caspase 3 and begins an apoptotic cycle⁶⁹⁻⁷².

Another way in which the laminin/ α 7 integrin complex affects Akt is via activation of integrin-linked kinase (ILK). ILK binds to both β 1 and β 3 integrins⁷³. ILK then phosphorylates PI3K which can activate Akt. The effects of this are two-fold: activation of mTOR stimulates protein production and inhibition of Bad by phosphorylation, which is anti-apoptotic⁷⁴.

α 7B has four potential phosphorylation sites and an ATP binding site⁷⁵. This makes it an excellent prospect for signaling pathways including the mitogen activated protein kinase (MAPK) pathway. This pathway often ends with the phosphorylation of extracellular signal regulated kinase (ERK)⁷⁶. Evidence for this has been gathered by using both an α 7 integrin knockout mouse and α 7 integrin overexpressing mice. The α 7 integrin knockout mouse displays increased activation of the (MAPK) pathway⁷⁷. As a result of this, the animals display elevated levels of ERK1/2 in their vascular smooth muscle and this can be restored to normal by either forced α 7 integrin expression or use of inhibitors of the MAPK/ERK pathway⁷⁷. When ERK1/2 signaling is returned to normal the vascular smooth muscle cells return to a wild-type phenotype⁷⁷, with the elevated ERK1/2 they displayed an undifferentiated phenotype.

Summary

The main hypothesis of this dissertation is that overexpression of the $\alpha 7$ integrin can alleviate the myopathic phenotype in the dy^W $-/-$ mouse model of MDC1A. MDC1A patients display reduced levels of $\alpha 7$ integrin when biopsy samples are evaluated with immunofluorescence². The $\alpha 7$ integrin can bind multiple ligands and alter signaling pathways^{31;44}. Overexpression of $\alpha 7$ integrin can rescue the phenotype of severely dystrophic mice which lack the large intracellular protein dystrophin and utrophin a similar protein^{42;45}.

Chapter 2 highlights the different models of MDC1A available and the main model used for these studies. It also includes a discussion of early qRT-PCR experiments that were used to narrow the scope of the later experiments included in Chapter 3.

Chapters 3 and 4 detail the characteristics of the dy^W $-/-$; $itga7$ $+$ animals including general pathology, neuromuscular junction pathology, and respiratory function. By forcing expression of $\alpha 7$ integrin in the skeletal muscle we were able to restore the sarcolemmal localization and enhance the expression of the $\alpha 7$ integrin. This work shows, for the first time, that reintroduction of the $\alpha 7$ integrin can alleviate muscle pathology, reduce inflammation, maintain strength, and increase life span in the dy^W $-/-$ mouse. These results indicate that the $\alpha 7$ integrin may be a drugable target for MDC1A therapy either alone or in combination therapies.

Chapter 5 contains conclusions and future directions associated with this work. This work provides evidence that the $\alpha 7$ integrin should be considered as a drugable target for the treatment of MDC1A. It also shows that enhanced $\alpha 7$ integrin expression can maintain respiratory function and improve neuromuscular junction pathology.

This work shows that the $\alpha 7$ integrin should be further explored as a potential therapeutic target for the treatment of MDC1A. The beneficial effects of enhanced $\alpha 7$ integrin expression in the absence of laminins 211 and 221, is due to stabilization and augmentation of the extracellular matrix. This leads to reduced muscle pathology, strength maintenance, reduced diaphragm pathology, and increased longevity in a mouse model of MDC1A. It is also the first time that the role the $\alpha 7$ integrin plays in the pathology of MDC1A has been described. We have also demonstrated, via plethysmography, that the enhanced expression of $\alpha 7$ integrin can lead to maintenance of respiratory function as the dy^W $^{-/-}$ animals age. Additionally, we have identified a potential biomarker (galectin-3) for MDC1A.

CHAPTER 2

**Mouse models of MDC1A and our experimental model,
and early gene expression profiling experiments**

Mouse models for MDC1A

There are several mouse models available for MDC1A. There are three laboratory generated models and two models with spontaneous mutations. There was a third model available but it is no longer in existence. The two models with spontaneous mutations are the dy^{2J}/dy^{2J} and dy/dy mice. The dy^{3K}/dy^{3K} and dy^w/dy^w models were generated to be knockout mice for laminin $\alpha 2$. The dy^{nmf417}/dy^{nmf417} mouse has a single point mutation in the *lama2* gene induced by site-directed mutagenesis. The final mouse model, the dy^{Pas}/dy^{Pas} , was a naturally occurring model that is now extinct.

The dy/dy mouse was first believed to be a model for Duchenne Muscular Dystrophy (DMD). This strain has a spontaneous mutation which has, as of yet, not been identified⁷⁸. The condition is inherited in an autosomal recessive manner. The mice are characterized by a moderate muscular dystrophy that is lethal by 6 months of age, myelination defect, and hearing loss. They produce a greatly reduced amount of normal laminin $\alpha 2$ chain^{20;78-80}. This strain is both phenotypically and genotypically similar to MDC1A which makes it a good model for the disease³. However, the fact that the causal mutation is still unknown which makes genotyping the animals at a young age to start treatments and experiments makes its use as a model less desirable.

The dy^{2J}/dy^{2J} animal is another naturally occurring laminin $\alpha 2$ deficient mouse. It is the result of a single point mutation that results in abnormal splicing of the *lama2* transcript leading to multiple mRNAs being produced. They produce a near normal amount of a truncated laminin $\alpha 2$ protein¹⁶. This mutated laminin is unable to polymerize¹⁶. The mutation is inherited in an autosomal recessive pattern. This mouse is mainly used for evaluation the role of laminin $\alpha 2$ in the development and function of

the neuromuscular junction (NMJ). The NMJ pathology seen includes widening of the synaptic cleft, reduced secondary membrane infoldings and a reduction in current across the synapse^{16;81}. The muscular dystrophy noted in these animals is mild and they have a normal lifespan^{78;79}.

The final spontaneously occurring dy (*lama2*) mutants was the dy^{Pas}/dy^{Pas} mouse, which is now extinct. They were the product of a retrotransposon insertion into the *lama2* gene. This resulted in a complete lack of laminin $\alpha 2$ protein and a severe muscular dystrophy^{20;80}.

A recent member of the dy family of laminin $\alpha 2$ deficient mice is the dy^{nmf417}/dy^{nmf417}. It was generated by Jackson Laboratories site directed mutagenesis program by using N-ethyl-N-nitrosurea to induce a point mutation. These animals display a very mild muscular dystrophy and have a normal life-span. However, similar to the dy^{2J}/dy^{2J} animals they do have a peripheral neuropathy making them a useful model for that aspect of MDC1A^{20;23}.

There are two members of the dy family of mice which were created by targeted disruption of the *lama2* gene, the dy^W/dy^W and dy^{3K}/dy^{dy3K} mice^{78;79;82;83}. Both strain display a severe and progressive muscular dystrophy as well as myelination defects and a peripheral neuropathy md and myelination defects. Both are widely used models for MDC1A.

The dy^W/dy^W animal produces a dramatically reduced amount of truncated laminin $\alpha 2$ protein (they make a small portion of the G-domain of the laminin $\alpha 2$ protein)⁸⁴. They have a severe muscular dystrophy and a dramatically reduced lifespan^{20;82;84}. The mutation is inherited in an autosomal recessive manner. This mouse is

commonly used for research into MDC1A for several reasons. These animals phenocopy MDC1A closely, are easily genotyped at a young age, and are readily available. Their severe phenotype makes them ideal for identification of therapeutic targets and for drug trials.

The final mouse model of MDC1A is the dy^{3K}/dy^{3K} animal, which is a true knock-out of the *lama2* gene. This strain produces no laminin $\alpha 2$ protein and usually dies around four-weeks of age. They also display a severe muscular dystrophy and peripheral neuropathy^{20;83;85;86}. The same traits, which make the dy^W/dy^W animals a frequently used model for MDC1A, hold true for this model as well.

The model of MDC1A, which we used for this work, is the dy^W/dy^W animal. We selected this marker based on its phenotypic correlation with MDC1A and the other characteristics highlighted above. In order to generate animals that were both laminin $\alpha 2$ deficient and overexpressed the $\alpha 7$ integrin in their skeletal muscle we also used the BX2-10i mouse. The BX2-10i mouse has a transgene consisting of rat $\alpha 7$ integrin cDNA driven by the muscle creatine kinase promoter (MCK). The use of the MCK promoter limits expression of the transgene to the skeletal muscle^{42;44;45}. The generation of these animals took several generations due to only being able to breed dy^W heterozygous animals. It is not possible to breed the dy^W/dy^W knockout animals due to their shortened lifespan and defects in spermatogenesis. A flow-chart highlight the breeding scheme used can be found in Figure 2.1 an image of $dy^W/-$ and $dy^W/-;itga7+$ animals is shown in Figure 2.2. All experimental animals came from the final generation noted to keep the genetic background of all experimental animals the same.

Early gene expression profiling experiments

To determine the effect of elevated $\alpha 7$ integrin expression on the regulation of gene expression and to aid in narrowing down future transcript evaluation, qRT-PCR was performed using total RNA isolated from the gastrocnemius muscle of five wild-type, five $dy^{W-/-}$ and five $dy^{W-/-};itga7+$. cDNA was made using the SABioscience RT² First Strand Kit and the RT² SYBR® Green/Rox™ qPCR Master Mix was used to prepare reactions (SA Bioscience). The RT² Profiler PCR Array for mouse extracellular matrix and adhesion molecules was used to evaluate the expression of 84 different extracellular matrix and adhesion molecule genes (SA Bioscience). Up-regulation of Collagen 2A and Timp2 was observed. Down-regulation of Adamts5 and Collagen 6A was noted (amongst other genes). Table 2.1 shows the results of the RT² Profiler Assays. This assay helped to narrow down the genes examined in the experiments of Chapter 3.

We also chose to evaluate galectins -1 and -3. van Lunteren⁴⁸ et al profiled the gene expression changes in dy/dy diaphragm and found that galectin-3 was elevated in the dy/dy animals. In primary DMD myotubes elevated transcripts for MMP-2, TIMP-1, and TIMP-2 have been identified, leading us to examine the expression of these proteins (Chapter 3).

Table 2.1

		Up-Down Regulation (comparing to control group)	
		dy^W-/-	dy^W-/-;itga7+
A01	Adamts1	-100.397	-30.5518
A02	Adamts2	1.8466	5.3275
A03	Adamts5	-1.4911	-24.7244
A04	Adamts8	-1.691	1.0466
A05	Ctnna1	1.3285	3.6785
A06	Ctnna2	2.6281	3.2744
A07	Ctnnb1	-1.2252	-1.2007
A08	Cd44	3.3082	13.3323
A09	Cdh1	-1.1298	-25.6113
A10	Cdh2	-1.7036	-2.4292
A11	Cdh3	-1.1037	2.9774
A12	Cdh4	-3.5776	-7.8622
B01	Cntn1	-1.7565	-4.8964
B02	Colla1	-1.8201	-2.8371
B03	Col2a1	1.1128	24771844.3
B04	Col3a1	2.5475	2.4694
B05	Col4a1	-1.614	-1.349
B06	Col4a2	-1.2051	1.7125

B07	Col4a3	-35.4267	-78.9297
B08	Col5a1	1.5907	1.4712
B09	Col6a1	-1.9693	-89353.7961
B10	Vcan	2.3668	2.7146
B11	Ctgf	2.5147	3.8399
B12	Ecm1	2.7491	6.7024
C01	Emilin1	1.9637	-1.8078
C02	Entpd1	-1.0269	2.8327
C03	Fbln1	2.2507	-1.5562
C04	Fn1	2.3366	1.2511
C05	Hapln1	8.7545	6.4801
C06	Hc	37.6778	25.1294
C07	Icam1	7.3695	5.6507
C08	Itga2	-1.4821	-49.248
C09	Itga3	1.1388	-144.9121
C10	Itga4	1.3901	2.9567
C11	Itga5	1.124	-1.4584
C12	Itgae	248.3663	122.3263
D01	Itgal	-1.192	-15.2482
D02	Itgam	2.1042	3.2663
D03	Itgav	1.8346	3.2811
D04	Itgax	3.589	2.3586

D05	Itgb1	1.5047	2.3909
D06	Itgb2	3.7238	14.6236
D07	Itgb3	2.3369	1.8132
D08	Itgb4	1.1486	-1.5305
D09	Lama1	-2.1293	-7.967
D10	Lama2	-42.645	-36.383
D11	Lama3	1.3547	2.5277
D12	Lamb2	-1.2001	1.5164
E01	Lamb3	-1.2463	-4.6056
E02	Lamc1	-3.9268	-385.4723
E03	Mmp10	-3.5669	-1.0854
E04	Mmp11	2.8806	-1.0677
E05	Mmp12	-2.198	-3.2247
E06	Mmp13	5.15	3.3938
E07	Mmp14	3.2718	2.1454
E08	Mmp15	-2.4377	-8.6237
E09	Mmp1a	-1.1037	2.9774
E10	Mmp2	3.1272	5.4569
E11	Mmp3	29.7973	92.1828
E12	Mmp7	-1.7247	1.9053
F01	Mmp8	-3.0675	-5.5225
F02	Mmp9	-1.4157	1.3427

F03	Ncam1	1.638	1.5007
F04	Ncam2	-1.1037	2.9774
F05	Pecam1	1.1052	-1.6973
F06	Postn	61.0129	5.8287
F07	Sele	17.5613	14.8043
F08	Sell	6.4436	-31.6236
F09	Selp	1.9585	1.9761
F10	Sgce	1.067	1.474
F11	Sparc	2.2102	3.39
F12	Spock1	4.6535	2.9774
G01	Spp1	5.0258	-42.2142
G02	Syt1	2.188	2.3017
G03	Tgfbi	-1.1128	2.0002
G04	Thbs1	4.1959	2.1846
G05	Thbs2	3.6083	5.1254
G06	Thbs3	2.7234	3.485
G07	Timp1	7.1066	6.6706
G08	Timp2	1.0753	74619.6351
G09	Timp3	-21.3661	-55.5505
G10	Tnc	3.766	2.6188
G11	Vcam1	-2.233	1.7172
G12	Vtn	1.4271	2.9332

H01	Gusb	1.1685	-2.2548
H02	Hprt1	1.2142	3.3243
H03	Hsp90ab1	-1.2157	2.8332
H04	Gapdh	-2.5464	-5.9234
H05	Actb	2.1821	1.4181
H06	MGDC	-1.1037	2.9774
H07	RTC	-2.3565	-1.3264
H08	RTC	-2.3206	333.7061
H09	RTC	1.5879	3.1125
H10	PPC	-2.9396	-2.6175
H11	PPC	-4.2694	-2.7881
H12	PPC	-8.056	1.6282

Legend: Red cells = down-regulation, green cells = up-regulation, yellow cells = likely pipetting error. Only changes, which are ≥ 3 -fold, are highlighted.

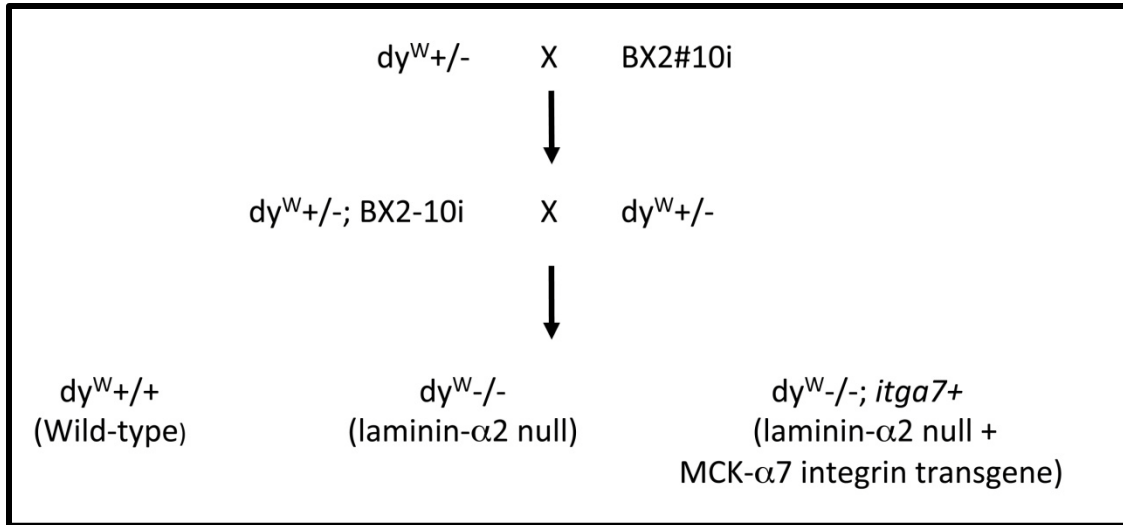


Figure 2.1. Breeding scheme used to generate experimental animals. This flow-chart highlight the production of the wild-type, $dy^{W-/-}$ laminin $\alpha 2$ -deficient, and $dy^{W-/-}; itga7+$ laminin $\alpha 2$ deficient and $\alpha 7$ integrin overexpressing animals used for the following experiments.



Figure 2.2. Representative image of dy^W $^{-/-}$ and dy^W $^{-/-};itga7$ $^{+}$ animals. 8-week old littermates. The black mouse is a dy^W $^{-/-}$ animal while the agouti mouse is a dy^W $^{-/-};itga7$ $^{+}$ mouse. The agouti mouse displays more interest in his environment, greater mobility, normal grooming behaviors, and better hydration status. The dy^W $^{-/-}$ animal was sacrificed soon after this picture was taken due to declining health.

CHAPTER 3

**Transgenic overexpression of the $\alpha 7$ integrin reduces muscle pathology
and improves viability in the dy^W mouse model of
merosin-deficient congenital muscular dystrophy 1A**

Abstract

Merosin-deficient congenital muscular dystrophy (MDC1A) is a devastating neuromuscular disease that results in children being confined to a wheelchair, requiring ventilator assistance to breathe and premature death. MDC1A is caused by mutations in the *LAMA2* gene which results in the partial or complete loss of laminin-211 and laminin-221, the major laminin isoforms found in the basal lamina of skeletal muscle. MDC1A patients exhibit reduced $\alpha7\beta1$ integrin; however, it is unclear how the secondary loss of $\alpha7\beta1$ integrin contributes to MDC1A disease progression. To investigate whether restoring $\alpha7$ integrin expression can alleviate the myopathic phenotype observed in MDC1A, we produced transgenic mice that overexpressed the $\alpha7$ integrin in the skeletal muscle of the $dy^{W/-}$ mouse model of MDC1A. Enhanced expression of the $\alpha7$ integrin restored sarcolemmal localization of the $\alpha7\beta1$ integrin to laminin- $\alpha2$ deficient myofibers, changed the composition of the muscle extracellular matrix, reduced muscle pathology, maintained muscle strength and function, and improved the life expectancy of $dy^{W/-}$ mice. Taken together, these results indicate that enhanced expression of $\alpha7$ integrin prevents muscle disease progression through augmentation and/or stabilization of the existing extracellular matrix in laminin- $\alpha2$ deficient mice and strategies that increase $\alpha7$ integrin in muscle might provide an innovative approach for the treatment of MDC1A.

Introduction

Merosin-deficient congenital muscular dystrophy 1A (MDC1A) is caused by mutations in the *LAMA2* gene resulting in the production of a truncated form or complete

loss of laminin- α 2 protein^{6,7}. The most severe form of MDC1A is associated with mutations that result in a complete loss of laminin- α 2 protein and therefore the absence of laminin-211 and laminin-221 heterotrimers in the basal lamina. MDC1A patients exhibit severe weakness, dysmyelinating neuropathy, hypotonia, muscle atrophy and limited eye movement^{4,12;87}. Patients also exhibit feeding problems and/or respiratory difficulties and often require feeding tube placement or ventilator assistance⁸⁸. Most MDC1A patients are unable to walk without assistance and are confined to a wheelchair⁴. A unique characteristic of MDC1A are changes in brain white-matter that are observed after 6 months of age. These changes might be associated with an increased likelihood of seizure-like activity^{4,12;87}. There is currently no cure or effective treatment for MDC1A and patients die as early as the first decade of life^{4,5}.

Laminin-211 and laminin-221 are the predominant laminin isoforms in the basal lamina of adult skeletal muscle. Laminin-211 is present at the extrajunctional sarcolemma and laminin-221 is enriched at the myotendinous and the neuromuscular junctions^{19;43;89}. Loss of laminin-211 in MDC1A patients and in mouse models of this disease results in an inability of muscle fibers to adhere to the basement membrane and as a result laminin- α 2 null myotubes are unstable and undergo apoptosis^{26;32}. Failed regeneration is also observed in laminin- α 2 deficient myofibers indicating the importance of the laminin-rich microenvironment for muscle repair^{26;90}. In addition, laminin- α 2 is expressed by Schwann cells in the peripheral nervous system and lack of laminin-211 leads to reduced myelination resulting in impaired conduction velocity and peripheral neuropathy^{27;91}.

The α 7 β 1 integrin is a primary laminin receptor expressed in skeletal, cardiac and

vascular smooth muscle^{43;92;93}. The $\alpha 7$ integrin transcript undergoes developmentally regulated RNA splicing to produce three alternative cytoplasmic domains designated $\alpha 7A$, $\alpha 7B$ and $\alpha 7C$ and two alternative extracellular domains designated $\alpha 7X1$ and $\alpha 7X2$ ^{33;75;94;95}. The cytoplasmic domains differ in size, sequence and potential for signal transduction, whereas extracellular domains bind with differential affinities to laminin isoforms^{75;96}. The $\alpha 7B$ cytoplasmic domain is the largest and has a number of regions that could potentially participate in signal transduction⁷⁵.

The $\alpha 7\beta 1$ integrin can bind to multiple laminin isoforms including laminin-111, laminin-211, laminin-221, laminin-332, laminin-411, laminin-511, galectin-1 and fibronectin^{31;43;97}. Mutations in the $\alpha 7$ -integrin-encoding gene (*ITGA7*) cause $\alpha 7$ integrin congenital myopathy and patients' exhibit delayed developmental milestones and impaired mobility³⁶. Mice that lack the $\alpha 7$ integrin develop muscular dystrophy that affects the myotendinous junctions^{36;98-100}. In the adult mouse, the $\alpha 7\beta 1$ integrin is localized at the extrajunctional sarcolemma but is also enriched at neuromuscular and myotendinous junctions where it mediates the adhesion of the muscle fibers to the extracellular matrix^{92;93;101}.

MDC1A patients, *dy/dy*^{-/-} and *dy*^{2J}^{-/-} mouse models have decreased levels of $\alpha 7$ integrin protein in their muscles and this secondary loss of $\alpha 7$ integrin might contribute to disease progression^{2;32;33}. To determine whether restoring $\alpha 7$ integrin expression could serve as a therapeutic strategy in the treatment of MDC1A, we generated transgenic mice that overexpressed the $\alpha 7$ integrin in the skeletal muscle of the *dy*^W^{-/-} mouse model of MDC1A. Transgenic expression of the $\alpha 7$ integrin increased longevity and reduced the

myopathic phenotype of $dy^{W-/-}$ mice. We show that these beneficial changes were achieved through augmenting and/or stabilizing the existing extracellular matrix in laminin- $\alpha 2$ deficient muscle. Our data demonstrate, for what we believe to be the first time, that the $\alpha 7$ integrin is a major modifier of disease progression in laminin- $\alpha 2$ deficient mice and might be a novel drug target for the treatment of MDC1A.

Materials and Methods

Generation of laminin- $\alpha 2$ deficient mice which overexpress $\alpha 7$ integrin in skeletal muscle

All experiments involving mice were approved by the University of Nevada, Reno Institutional Animal Care and Use Committee. Transgenic $\alpha 7$ integrin $dy^{W-/-}$ mice were generated by breeding mice that overexpressed the $\alpha 7BX2$ integrin in skeletal muscle⁴² with $dy^{W+/-}$ animals⁸². Resultant pups which were heterozygous for the laminin- $\alpha 2$ mutant allele and positive for the $\alpha 7BX2$ transgene were bred to $dy^{W+/-}$ mice. The male pups from these matings included $dy^{W+/+};itga7-$ (wild-type), $dy^{W-/-};itga7-$ ($dy^{W-/-}$) (laminin- $\alpha 2$ deficient) and $dy^{W-/-};itga7+$ (laminin- $\alpha 2$ deficient that overexpress the $\alpha 7BX2$ integrin) mice. Male littermates were used as controls for all experiments. Genomic DNA was isolated from tail biopsies taken at 10 days of age using the Wizard SV Genomic DNA Purification System (Promega, Madison, WI). Polymerase chain reaction (PCR) was used as previously described to detect the laminin- $\alpha 2$ allele and the $\alpha 7BX2$ transgene^{45;82;102}. The $dy^{W+/-}$ mice were a gift from Dr. Eva Engvall via Dr. Paul Martin (The Ohio State University, Columbus, OH).

Isolation of Skeletal Muscle

Four-week-old wild-type, $dy^{W/-}$ and $dy^{W/-};itga7+$ male mice were sacrificed by CO₂ asphyxiation followed by cervical dislocation in accordance with a protocol approved by the University of Nevada Reno Animal Care and Use Committee. Skeletal muscles were dissected and flash frozen in liquid nitrogen cooled isopentane. Tissues were stored at -80°C.

Western blot analysis

Gastrocnemius muscles from 4 week old male mice were pulverized with a mortar and pestle cooled in liquid nitrogen. Protein was extracted in RIPA buffer (50mM HEPES pH 7.4, 150mM NaCl, 1mM Na₃VO₄, 10mM NaF, 0.5% Triton X-100, 0.5% NP50, 10% glycerol, 2mM PMSF and a 1:200 dilution of Protease Inhibitor Cocktail Set III) and quantified using a Bradford assay (Bio-Rad Laboratories Inc, Hercules, CA). Proteins were separated by SDS-PAGE. The $\alpha 7$ integrin was detected with a 1:1000 dilution of anti- $\alpha 7B$ antibody overnight loading 10 μ g of protein. Integrin $\alpha 7A$ was also loaded at 10 μ g and was detected using 1:1000 dilution of CDB 345 antibody overnight (a kind gift from Stephen Kauffman, University of Illinois, Urbana-Champaign, IL). Integrin $\alpha 3$ was quantified using the AB1920 antibody (Chemicon), again 10 μ g of protein was used. The $\beta 1D$ integrin was visualized using $\beta 1D$ -antibody (a kind gift from Woo Keun Song, Gwanju Institute for Science and Technology, South Korea) overnight. All primary antibodies were followed by a 1:5000 goat-anti-rabbit-IgG secondary antibody (Li-Cor Biosciences, Lincoln, NE) for 1 hour. Galectin-1 (50 μ g) was detected with a 1:1000 dilution of H00003956-D01P (Abnova, Walnut, CA). Galectin-3 was detected with a 1:1000 dilution of ab53082 (Abcam, Cambridge, MA). Galectin-3 blots used differential

loading: 100 μ g wild-type, 50 μ g *dy*^W^{-/-}, and 25 μ g for *dy*^W^{-/-};*itga7*⁺; this was done to keep the protein detected in the linear range. Immunoblots were normalized by using a 1:5000 dilution of an anti- α -tubulin (AbCam, Cambridge, MA) antibody followed by a 1:5000 dilution of goat-anti-mouse-IgG secondary antibody. Band intensities were determined with an Odyssey Imaging System.

Immunofluorescence

Cryosections (8 μ m) of 4 week old male Tibialis Anterior (TA) muscle were cut using a LeicaCM 1850 cryostat and mounted onto pre-cleaned Surgipath slides. Sections were fixed using 4% paraformaldehyde (PFA) for 2 or 5 minutes then rehydrated using Phosphate Buffered Saline (PBS). Slides were blocked in 5% Bovine Serum Albumin (BSA) in PBS then incubated with antibodies against laminin- α 2G or β 1D integrin, as previously described⁹⁰. For detection of Galectin-1 H00003959-D01P (Abnova) antibody was used. Galectin-3 was visualized using ab53082 (Abcam). Antibody T3413 (Sigma) was used to detect Tenascin C. MMP2 and TIMP1 were detected using antibodies ab37150 and ab86482 respectively (Abcam). Slides were then incubated using an appropriate secondary, which was a FITC-anti-rabbit-IgG in all cases except for Tenascin C which was a FITC-conjugated anti-rat-IgG secondary antibody was used. For detection of spectrin, slides were fixed for 1 minute in ice cold acetone then treated with the M.O.M™ kit according to package instructions (FMK-2201 Vector Laboratories, inc. Burlingame, CA). A mouse monoclonal anti-spectrin antibody (Novo Castra NCL-spec2) was then used at 1:100 for 30 minutes followed by a FITC-conjugated anti-mouse-IgG secondary antibody at 1:1000 for 1 hour. Slides were mounted using Vectashield

with DAPI and imaged using a Zeiss Axioskop 2 Plus fluorescence microscope. Images were captured using a Zeiss AxioCam HRc digital camera with Axiovision 4.1 software.

Inflammatory Cell Infiltrate

TA muscle cryosections from four-week-old mice were fixed in 4% PFA for 5 minutes followed by rehydration with PBS. Slides were incubated with FITC-conjugated rat anti-mouse-CD11b antibody (BD Biosciences, San Jose, CA) at 1:1000 for 1 hour to detect macrophages in the muscle tissue. Slides were washed with PBS and mounted using Vectashield with DAPI. Muscle sections from five mice of each genotype were analyzed and CD11b positive cells per 20 fields at 400X magnification were counted. A Zeiss Axioskop 2 Plus fluorescent microscope was used to view the slides and images were captured using a Zeiss AxioCam HRc digital camera with Axiovision 4.1 software

Confocal microscopy

The TA muscles from 4-week-old male mice from each genotype were sectioned and subjected to immunofluorescence. For detection of $\alpha 7B$ integrin sections were fixed in ice cold acetone (-20°C) for 1 minute then rehydrated using phosphate-buffered saline (PBS). Cryosections were blocked in a 5% BSA in PBS solution for 20 minutes followed by incubation with CDB347 (which recognizes the cytoplasmic domain of both mouse and rat $\alpha 7B$ integrin) or anti- $\beta 1D$ A2-integrin antibodies for 1 hour. Slides were then washed with 1% BSA in PBS and incubated with FITC-conjugated anti-rabbit-IgG antibody for 1 hour. Slides were again washed with 1% BSA in PBS. To outline the myofibers sections were incubated with rhodamine labeled wheat germ agglutinin for 30 minutes. Slides were mounted using Vectashield with DAPI. Images were captured

using an Olympus FluoviewTM Confocal Scanning System.

Survival and weight gain analysis

Male mice were allowed to age and monitored daily for weight loss and any signs of pain, distress or illness. A weight loss of >10% over a one week period was also considered a terminal sign and the animals were humanely euthanized. Weights from animals of each genotype were compared at 3, 8, and 12 weeks of age.

Grip strength and activity assays

The forelimb grip strength of 4- and 8- week-old male wild-type, $dy^{W/-}$ and $dy^{W/-};itga7+$ mice were measured using a SDI Grip Strength System and a Chatillon DFE Digital Force Gauge (San Diego Instruments, Inc., San Diego, CA) as per a standard protocol. Five consecutive tests were performed for each mouse and the data averaged for each mouse genotype. In order to assess mobility 4- and 8- week old male wild-type, $dy^{W/-}$ and $dy^{W/-};itga7+$ mice were placed in a clean cage by themselves and monitored for five minutes. Periods of moving about the cage, standing up, and digging were considered times of activity. Additionally during this time period the number of times the mouse stood up was recorded. Stand up testing was only performed on animals that were physically able to stand up. Some mice were excluded from these samples owing to the extent of their peripheral neuropathy.

Hematoxylin and Eosin Staining

Cryosections from 4 week-old TA and diaphragm muscle were stained using hematoxylin and eosin, as previously described¹⁰³ and were used to determine the percentage of myofibers that contained CLN using a Zeiss Axioskop 2 plus fluorescence

microscope¹⁰³. A minimum of 1000 fibers per animal (5 animals per group) were counted and the percentage of myofibers with centrally located nuclei calculated. Images were captured using a Zeiss AxioCam HRC digital camera and Axiovision 4.1 software.

Myofiber Area Determination

Cryosections from TA and diaphragm muscles from 4-week-old mice were fixed for 5 minutes in 4% paraformaldehyde (PFA) and rehydrated in PBS. Myofibers were outlined with 2 μ g/ml Oregon Green-488 conjugated WGA (Molecular Bioprobes, Eugene, OR) for 30 minutes. Sections were then washed with PBS for 15 minutes and mounted in Vectashield. A minimum of 1000 fibers per animal with five animals per group were assessed for the TA muscle. For diaphragm muscle a minimum of 500 fibers per animal with five animals per genotyped were used. Myofiber cross-sectional area was determined with a Zeiss Axioskop 2 Plus fluorescent microscope and images were captured with a Zeiss AxioCam HRC digital camera with Axiovision 4.1 software.

Quantitative real-time PCR analysis

Total RNA was purified from five 4 week old male mice wild-type, $dy^{W/-}$, and $dy^{W/-};itga7+$ gastrocnemius muscles using Trizol (Invitrogen, Carlsbad, CA) reagent. After the concentration was determined, mRNA was pooled equally by genotype for cDNA production. The cDNA was prepared from 4 μ g of pooled total RNA with random hexamers and Superscript III (Invitrogen, Carlsbad, CA) using standard procedures. Quantitative real-time PCR was conducted with 50pg total cDNA using SYBR Green Jumpstart (Sigma-Aldrich, St Louis, MO) with primer sequences to mouse extracellular matrix genes are listed in Table S1 and levels were normalized to that of *Gapdh*. The

fold change over wild-type was calculated using the $\Delta\Delta\text{Ct}$ method after normalization and the average fold change in transcript and (\pm s.e.m.) were calculated.

Statistics

Data is reported as the mean \pm standard deviation. One way analysis of variance (ANOVA) was used to compare animals across groups. Kaplan-Meier Log-Rank test was used to determine significance of life span changes. Myofiber cross-sectional area was analyzed using the GLIMMIX statistical analysis package in SAS. A p-value of <0.05 was considered significant.

Results

The $\alpha7\text{B}$ integrin is overexpressed in the muscle of $dy^{W-/-};itga7+$ transgenic mice

To determine whether overexpression of the $\alpha7$ integrin in laminin- $\alpha2$ deficient muscle could alleviate disease progression, transgenic mice were generated in which rat $\alpha7\text{BX2}$ integrin expression was driven by the muscle creatine kinase (*Mck*, also known as *Ckm*) promoter, which we designate as *itga7+* mice. These mice were bred with $dy^{W+/-}$ animals to generate $dy^{W-/-};itga7+$ mice. Pups were genotyped at 10 days of age for the laminin- $\alpha2$ mutant and wild-type alleles and *itga7* transgene as previously described

45;82;102 .

To confirm that the presence of the transgene resulted in increased $\alpha7$ integrin in dy^W muscle quantitative real-time PCR (qRT-PCR) and immunoblotting were performed on mouse tibialis anterior (TA) and gastrocnemius muscle. qRT-PCR experiments showed a 4.1-fold increase in $\alpha7$ integrin transcript in the $dy^{W-/-}$ muscle compared with that in wild-type muscle, whereas $dy^{W-/-};itga7+$ mice exhibited a 17-fold increase in $\alpha7$

integrin transcript in muscle compared with that in wild-type (Table 3.1).

Immunoblotting confirmed a 2.8-fold increase in $\alpha7B$ integrin in the muscle of $dy^{W/-};itga7+$ mice (Figures 3.1A and 3.1C). There was a 67.5% and 83.2% reduction in $\alpha7A$ integrin in the muscles $dy^{W/-}$ and $dy^{W/-};itga7+$ animals respectively compared to wild-type (Figures 3.1A and 3.1B). Analysis of other laminin-binding integrins in skeletal muscle revealed a 86% and 61.5% reduction in $\alpha3$ integrin protein in $dy^{W/-}$ and $dy^{W/-};itga7+$ animals respectively compared with that in wild-type (Figure 3.1D). Finally no significant change in $\beta1D$ integrin protein was observed in any of the genotypes (Figure 3.1E). qRT-PCR was also performed to determine the effect of enhanced $\alpha7$ integrin expression on $\beta1D$ transcript levels. We found that $\beta1D$ transcript was elevated in both the $dy^{W/-}$ and $dy^{W/-};itga7+$ animals. The $dy^{W/-}$ animals had the greatest levels of $\beta1D$ transcript (Figure 3.2).

Together these results indicate the MCK- $\alpha7BX2$ integrin increased both the transcript and protein level expression of $\alpha7BX2$ in the skeletal muscle of $dy^{W/-}$ mice without altering the expression of other laminin-binding integrin isoforms and chains.

Transgenic expression of the $\alpha7$ integrin in $dy^{W/-}$ muscle restores sarcolemmal localization of the $\alpha7\beta1$ integrin

Previous studies have shown that loss of laminin- $\alpha2$ results in reduced sarcolemmal localization of $\alpha7$ integrin^{2;32;33}. Immunofluorescence was used to determine whether forced expression of $\alpha7$ integrin restored sarcolemmal localization of the $\alpha7\beta1$ integrin in skeletal muscle. Immunofluorescence analysis confirmed that

whereas wild-type mice exhibited substantial laminin- $\alpha 2$ in the basal lamina, $dy^{W/-}$ and $dy^{W/-};itga7+$ mice were negative for laminin- $\alpha 2$ and produced only negligible amounts of the laminin- $\alpha 2$ globular domain (Figure 3.3A) which is consistent with previous studies⁸⁴. The localization of $\beta 1D$ integrin was examined in wild-type, $dy^{W/-}$ and $dy^{W/-};itga7+$ TA muscle (Figure 3.3A). Compared with that in wild-type mice, $dy^{W/-}$ muscle exhibited a reduced sarcolemmal localization of $\beta 1D$ integrin. By contrast, transgenic overexpression of the $\alpha 7$ integrin restored sarcolemmal localization of $\beta 1D$ integrin in TA muscle. Spectrin levels were the same in all three genotypes and were used as a positive control for immunofluorescence.

To examine whether transgenic overexpression restored the sarcolemmal localization of the $\alpha 7$ integrin in muscle, TA cryosections were stained for $\alpha 7B$ integrin (green) and with rhodamine labeled wheat germ agglutinin (WGA) (red) which binds N-acetylglucosamine-labeled sugar residues in the basal lamina and high-resolution confocal microscopy was used to assess sarcolemmal localization of $\alpha 7$ integrin (Figure 3.3B). Wild-type and $dy^{W/-};itga7+$ muscle exhibited colocalization of the $\alpha 7$ integrin and WGA (indicated by the yellow staining), as well as sharp sarcolemmal staining for $\alpha 7$ integrin (Figure 3.3B). By contrast, the $dy^{W/-}$ animals showed little colocalization between $\alpha 7$ integrin and the WGA, and did not show sharp $\alpha 7$ integrin sarcolemmal localization (Figure 3.3B). Together these data indicate that transgenic expression of the $\alpha 7$ integrin in $dy^{W/-}$ muscle restored sarcolemmal localization of the $\alpha 7\beta 1$ integrin in laminin- $\alpha 2$ deficient muscle.

Transgenic overexpression of $\alpha 7$ integrin increases the longevity of $dy^{W/-}$ mice

MDC1A patients and the $dy^{W/-}$ mouse model exhibit severe muscle wasting that results in reduced life expectancy^{4;5}. We next investigated whether transgenic overexpression of $\alpha7$ integrin improved the longevity of $dy^{W/-}$ animals. Kaplan-Meier survival analysis revealed that 50% of $dy^{W/-}$ mice died by 70 days of age (Figure 3.4A). By contrast, 50% of $dy^{W/-};itga7+$ mice survived beyond 140 days of age (Figure 3.4A). The oldest $dy^{W/-}$ mouse lived to 132 days, whereas the oldest $dy^{W/-};itga7+$ animal lived to 318 days which represents a 2.4-fold increase in life expectancy (Figure 3.4A). These results indicate that increasing $\alpha7$ integrin expression in skeletal muscle substantially improves the life expectancy of laminin- $\alpha2$ deficient mice.

MDC1A patients exhibit reduced body weight and muscle strength^{4;5}. We next examined whether transgenic expression of the $\alpha7$ integrin improved the body weight and muscle strength and function of $dy^{W/-}$ mice. Compared with that of wild-type mice both $dy^{W/-}$ and $dy^{W/-};itga7+$ mice had reduced body weight at 3, 8 and 12 weeks of age with no difference between these laminin- $\alpha2$ deficient mice (Figure 3.4B). This indicates that the transgene is not effective at restoring body weight to that of wild-type animals.

We next examined muscle strength. Forelimb grip strength was measured to analyze overall forelimb muscle strength. Compared to four week old wild-type mice, both $dy^{W/-}$ and $dy^{W/-};itga7+$ mice exhibited a 36.4% and 30.8% reduction respectively in forelimb grip strength compared with that of wild-type mice, with no difference between these laminin- $\alpha2$ null animals (Figure 3.5A). However, when the animals were re-evaluated at 8 weeks of age, $dy^{W/-}$ animals showed a 55% reduction in grip strength compared to wild-type while $dy^{W/-};itga7+$ mice showed only a 24.8% reduction in grip

strength compared with that of wild-type (Figure 3.5A). This indicates that while the $dy^{W/-}$ animals progressively got weaker, enhanced levels of $\alpha7$ integrin in the $dy^{W/-};itga7+$ animals preserved muscle strength over time.

We next evaluated two different measures of activity in 4- and 8- week old animals. Measurement of overall activity over a 5 minute period when a mouse is introduced into a new cage revealed that at four weeks of age there was no significant difference between wild-type, $dy^{W/-}$ and $dy^{W/-};itga7+$ mice (Figure 3.5B). By contrast, at 8 weeks of age, wild-type and $dy^{W/-};itga7+$ mice animals exhibited a 1.8-fold and 1.5-fold increase in active time respectively compared with that of $dy^{W/-}$ animals. There was no significant difference between the wild-type and $dy^{W/-};itga7+$ animals (Figure 3.5B). Finally, stand-up activity of animals introduced to a new cage over a 5 minute period was assessed on mice capable of standing up. At four weeks of age there was no significant difference between the genotypes (Figure 3.5C). At eight weeks of age wild-type and $dy^{W/-};itga7+$ animals exhibited a 5.2-fold and 4.2-fold increase in standup activity compared with that of $dy^{W/-}$ animals (Figure 3.5C). Together these results indicate transgenic expression of the $\alpha7$ integrin maintained muscle strength and activity in the $dy^{W/-}$ mouse model of MDC1A.

Transgenic overexpression of $\alpha7$ integrin reduces skeletal muscle pathology in $dy^{W/-}$ mice

To determine whether enhanced $\alpha7$ integrin expression prevented skeletal muscle pathology in laminin- $\alpha2$ -deficient mice, TA muscle cryosections from 4-week-old wild-type, $dy^{W/-}$ and $dy^{W/-};itga7+$ mice were stained with hematoxylin and eosin (H&E). Compared with that in wild-type mice, $dy^{W/-}$ TA muscle showed greater variation in

myofiber size, presence of centrally located nuclei (CLN), fibrosis and inflammatory cell infiltrate (Figure 3.6A). The $dy^{W/-};itga7+$ muscle exhibited less muscle pathology, including fewer myofibers with CLN, less inflammatory infiltrate, and less variation in myofiber size (Figure 3.6A).

The requirement for muscle repair was determined by evaluating the percentage of myofibers containing centrally located nuclei (CLN). CLN are an indicator of muscle degeneration and regeneration, which requires satellite cell activation to repair damaged myofibers¹⁰⁴. Compared with 4-week-old wild-type mice, which showed few myofibers with CLN, 4 week old $dy^{W/-}$ TA muscle exhibited 4.8-fold increase in myofibers with centrally located nuclei (Fig. 2.6B). There was a 66.5% reduction in the percentage of CLN in the $dy^{W/-};itga7+$ compared with that in the $dy^{W/-}$ animals, although the level of CLN in these mice was still elevated compared with that in wild-type (Figure 3.6B). These results indicate transgenic expression of the $\alpha7$ integrin in the skeletal muscle results in reduced muscle pathology and fewer myofibers with CLN than in $dy^{W/-}$ mice.

MDC1A patients and $dy^{W/-}$ mice exhibit substantial myofiber size variation and the presence of a large number of hypotrophic muscle fibers. Measurements of myofiber cross-sectional area were used to determine whether transgenic expression of the $\alpha7$ integrin improved this aspect of muscle pathology. Compared with that of wild-type with a mean myofiber cross-sectional area of $16.1\mu\text{m}^2$, $dy^{W/-}$ TA muscle had a mean myofiber cross-sectional area of $9.5\mu\text{m}^2$, with a curve shifted to the left indicating increased numbers of hypotrophic muscle fibers (Figure 3.6C). By contrast, TA myofibers in $dy^{W/-};itga7+$ mice had a mean cross-sectional area of $11.5\mu\text{m}^2$ (Figure 3.6C). These results

indicate that transgenic expression of the $\alpha 7$ integrin in skeletal muscle of laminin- $\alpha 2$ -null mice reduced the variation in myofiber size and improved the myofiber cross-sectional area. At the maximum frequency of occurrence the $dy^{W/-}$ mice have significantly smaller fibers than the wild-type mice. There was no significant difference between the $dy^{W/-}$ and $dy^{W/-};itga7+$ or between the $dy^{W/-};itga7+$ and wild-type mice (supplementary material Figure 3.1). This indicates transgenic mice that overexpress the $\alpha 7$ integrin in muscle have fewer hypotrophic fibers compared with $dy^{W/-}$ animals and are more similar to wild-type.

Transgenic $\alpha 7$ integrin expression alters the composition of the extracellular matrix in laminin- $\alpha 2$ deficient muscle.

The loss of laminin-211 and 221 in the muscle extracellular matrix is the underlying cause of muscle disease in MDC1A. Given that the $\alpha 7$ integrin is the primary laminin receptor in muscle we next determined the mechanism by which increased $\alpha 7\beta 1$ integrin rescued $dy^{W/-}$ mice in the absence of its laminin-211-laminin-221 ligand. qRT-PCR was used to examine the expression profile of genes encoding an array of extracellular matrix proteins in the gastrocnemius muscle of 4-week-old wild-type, $dy^{W/-}$ and $dy^{W/-};itga7+$ mice. qRT-PCR revealed that $dy^{W/-}$ mice exhibited increased levels of several transcripts: a disintegrin and metalloproteinase with thrombospondin motifs 5 (*Adamts5*), agrin (*Agrn*), collagen 6A1 (*Col6A1*), galectin-1 (*Lgals1*), galectin-3 (*Lgals3*), matrix metalloproteinase 2 (*Mmp2*), integrin $\alpha 3$ (*Itga3*), integrin $\alpha 6$ (*Itga6*), integrin $\alpha 7$ (*Itga7*), laminin- $\alpha 4$ (*Lama4*), laminin- $\alpha 5$ (*Lama5*), nidogen 1 (*Nid1*), tenascin C (*Tnc*), tissue inhibitor of metalloproteinase 1 (*Timp1*) and tissue inhibitor of metalloproteinase 2

(*Timp2*) transcripts compared with that in wild-type (Table 3.1). Transgenic expression of the $\alpha7$ integrin in $dy^{W/-};itga7+$ mice resulted in reduced levels of agrin and Mmp2 transcripts compared with $dy^{W/-}$ mice (Table 3.1). Transgenic expression of the $\alpha7$ integrin in $dy^{W/-};itga7+$ mice resulted in increased levels of transcripts for *Col6A1*, *Lgals1*, *Lgals3*, *Itga3*, *Itga6*, *Itga7*, *Tnc* and *Timp1* compared with that in $dy^{W/-}$ mice (Table 3.1).

The $\alpha7\beta1$ integrin has been shown to interact with galectin-1 in cultured muscle cells³¹ and we next determined whether transgenic expression of the $\alpha7$ integrin altered expression of galectin-1 and -3 in the muscle of laminin- $\alpha2$ null mice. Compared with that in wild-type mice, the level of galectin-1 transcript was increased 9.2-fold in $dy^{W/-}$ muscle and 12.1-fold in $dy^{W/-};itga7+$ animals (Table 3.1). This increase in galectin-1 transcript correlated with a 1.8-fold increase in galectin-1 protein in $dy^{W/-};itga7+$ animals compared with that in wild-type (Figure 3.7A). These results indicate an increase in galectin-1 protein in the gastrocnemius muscle of $dy^{W/-};itga7+$ animals.

Galectin-3 transcript was increased 70-fold and 80-fold in 4-week-old $dy^{W/-}$ and $dy^{W/-};itga7+$ muscle respectively compared with that in wild-type mice (Table 3.1). This increase in galectin-3 transcript resulted in a 2-fold increase in galectin-3 protein in $dy^{W/-}$ mice and a 7-fold increase in galectin-3 protein in $dy^{W/-};itga7+$ animals compared with that in wild-type (Figure 3.7B). These results indicate that loss of laminin- $\alpha2$ results in increased galectin-3 in the muscle extracellular matrix of $dy^{W/-}$ mice and that transgenic expression of $\alpha7$ integrin further enhanced the levels of galectin-3 in laminin- $\alpha2$ deficient muscle.

In laminin- α 2-deficient muscle, tenascin C is normally localized at the myotendinous junctions and has been shown to be enriched at extrajunctional sites of laminin- α 2 deficient muscle which correlate with regions of muscle regeneration¹⁰⁵. qRT-PCR was used to examine whether transgenic overexpression of the α 7 integrin altered the expression of tenascin C in the muscle of $dy^{W/-}$ mice. qRT-PCR confirmed a 28-fold increase in tenascin C transcript in the gastrocnemius muscle of $dy^{W/-}$ mice and a 49-fold increase in tenascin C transcript in $dy^{W/-};itga7+$ gastrocnemius muscle compared with that in wild-type (Table 3.1). These results indicate transgenic expression of the α 7 integrin augmented tenascin C transcription in laminin- α 2 null muscle.

Immunofluorescence was used to confirm the qRT-PCR and immunoblotting for several proteins. Immunofluorescence also demonstrated increased extracellular galectin-1, galectin-3, and Tenascin C in the extracellular matrix with galectin-3 and tenascin C being more prevalent in the $dy^{W/-};itga7+$ mice (Figure 3.8). Immunostaining demonstrated reduced MMP2 and increased TIMP1 in the extracellular matrix of the $dy^{W/-};itga7+$ mice compared with that in the $dy^{W/-}$ mice (Figure 3.8). These results support the idea that overexpression of the α 7 integrin results in both augmentation and stabilization of the existing extracellular matrix in $dy^{W/-};itga7+$ animals.

Inflammatory infiltrate is reduced in dy^W muscle with enhanced α 7 integrin

Inflammatory cell infiltration (particularly by the monocyte or macrophage line) is a hallmark of MDC1A¹⁰⁶. To determine whether overexpression of the α 7 integrin reduced inflammation in $dy^{W/-};itga7+$ muscle, CD11b was used as a marker for the presence of macrophages in skeletal muscle (Figure 3.9A). Compared with that in the 4-

week-old wild-type TA muscle, $dy^{W/-}$ TA muscle exhibited an 11.1-fold increase in CD11b positive cells (Figure 3.9B). By contrast, 4-week-old $dy^{W/-};itga7+$ showed a 55.3% decrease in the number of CD11b positive cells compared with that in $dy^{W/-}$ TA muscle (Figure 3.9B). These results indicate transgenic overexpression of the $\alpha7$ integrin reduced the level of macrophage-mediated inflammation in $dy^{W/-}$ muscle.

Transgenic expression of $\alpha7$ integrin prevents muscle disease progression in the diaphragm of dy^W mice

MDC1A patients exhibit severe restrictive respiratory syndrome and require ventilator assistance to breathe as a result of severe diaphragm muscle pathology⁴. Histological analysis and measurements of myofiber area were used to examine whether transgenic expression of the $\alpha7$ integrin prevented the onset of severe diaphragm muscle pathology. Hematoxylin and eosin studies revealed that transgenic expression of the $\alpha7$ integrin in 4-week-old $dy^{W/-}$ diaphragm muscle resulted in reduced mononuclear cell infiltrate, hypotrophic muscle fibers, centrally located nuclei and fibrosis (Figure 3.10A).

Analysis of myofiber cross-sectional areas confirmed the improvement in the muscle pathology observed in the histological studies. Compared with wild-type mice, which have peak myofiber cross-sectional area of between 3.5-4.5 μm^2 , $dy^{W/-}$ muscle exhibited a large number of hypotrophic muscle fibers with a peak myofiber area of only 2 μm^2 (Figure 3.10B). By contrast, $dy^{W/-};itga7+$ diaphragm myofibers exhibited a peak myofiber area of between 3.5-5 μm^2 and a curve more similar to that of wild-type (Figure 3.10B). At the maximum frequency myofiber area, all three groups were significantly different from one another (Supplemental Figure 3.1). These results indicate that

transgenic expression of the $\alpha 7$ integrin prevents muscle disease progression in the diaphragm of laminin- $\alpha 2$ null mice.

Discussion

Merosin deficient congenital muscular dystrophy (MDC1A) is considered one of the most common congenital muscular dystrophies. Classic MDC1A is associated with a complete loss of laminin- $\alpha 2$ and has the most severe clinical signs with severe muscle weakness, hypotonia, and muscle atrophy. Feeding and respiratory difficulties are common and patients often require either feeding tube placement or positive pressure ventilation. Maximal motor activity is often unsupported sitting with few patients achieving independent ambulation⁴. There is currently no cure or effective treatment for MDC1A and patients often die at a young age from respiratory insufficiency⁵.

The observation of reduced $\alpha 7$ integrin in MDC1A muscle has led to the proposal that the secondary loss of $\alpha 7$ integrin may contribute to the myopathic phenotype observed in MDC1A patients and laminin- $\alpha 2$ null mice^{2;32;33}. Because $\alpha 7$ integrin congenital myopathy does not phenocopy MDC1A, disease progression must involve more than loss of the $\alpha 7$ integrin receptor, however, given that the $\alpha 7\beta 1$ integrin binds to multiple ligands, restoring $\alpha 7\beta 1$ integrin receptor in skeletal muscle might improve muscle integrity and reduce the myopathy associated with disease progression.

Previous studies have shown a loss of $\alpha 7$ integrin from the skeletal muscle of *dy/dy* and *dy^{2J}/dy^{2J}* mouse models of MDC1A^{32;33;107}. Our results show the *dy^{W/-}* muscle exhibits reduced $\alpha 7$ integrin expression and loss of sarcolemmal localization of the $\alpha 7\beta 1$ integrin. Studies have suggested transcriptional regulation between laminin and $\alpha 7$

integrin in muscle³³ and the small amount of truncated laminin- α 2 globular domain produced in $dy^{W/-}$ muscle⁸⁴ which might be sufficient to promote some α 7 integrin expression but insufficient for the correct sarcolemmal localization in muscle. In this study, we show that transgenic overexpression of the α 7 integrin in $dy^{W/-}$ mice resulted in sarcolemmal localization of the α 7 β 1 integrin. Restoring sarcolemmal localization of the α 7 β 1 integrin reduced muscle pathology, maintained muscle strength and increased survival of $dy^{W/-}$ mice. Taken together, our data support the hypothesis that secondary loss of α 7 integrin contributes to muscle disease progression and restoring sarcolemmal localization might reduce the myopathy in MDC1A.

Studies have indicated that the α 7 β 1 integrin might act to modulate the organization and deposition of the muscle extracellular matrix^{30;103}. To investigate the mechanism by which enhanced α 7 integrin expression improved the myopathic phenotype in the absence of the laminin-211-221 ligand, we examined changes in levels of other extracellular matrix proteins and enzymes that regulate the extracellular matrix. MDC1A patients and laminin- α 2 deficient mice have increased laminin- α 4 and laminin- α 5 chains; however previous studies have indicated that the increase in these laminin isoforms are unlikely to rescue of the myopathic phenotype^{28;29;108}. Transgenic expression of α 7 integrin did not further increase α 7A integrin isoform or α 3 integrin in skeletal muscle, indicating that these laminin and integrin isoforms do not play a role in the rescue of laminin- α 2 deficient mice that overexpress α 7 integrin in skeletal muscle.

Our analysis of extracellular matrix proteins in the $dy^{W/-}$ muscle basal lamina revealed that transgenic expression of the α 7 integrin resulted in reduced expression of

Mmp2 and increased levels of Timp1. Mmp2 is associated with the breakdown of the basal lamina, whereas Timp1 acts to inhibit the activity of matrix metalloproteinases, such as Mmp2¹⁰⁹. Reduced Mmp2 and increased Timp1 in the muscle of $\alpha7$ integrin transgenic $dy^{W/-}$ mice indicate that increased $\alpha7\beta1$ integrin acts to stabilize the basal lamina by affecting the expression of enzymes that degrade and remodel the muscle extracellular matrix.

The $\alpha7\beta1$ integrin has been shown to directly bind galectin-1³¹. Galectin-1 (L-14) is a lactoside binding protein that has been shown to inhibit myoblast adhesion by blocking the interaction of laminin to integrins. Galectin-3 has also been shown to mediate cell adhesion and regulate the cell signaling pathways involved in apoptosis, cell proliferation, inflammation, and gene transcription¹¹⁰. Galectin-3 binds extracellular matrix proteins including laminin and tenascin C and has been shown to bind directly to integrins. In breast carcinoma cells, galectin-3 has been shown to mediate $\beta1$ integrin endocytosis¹¹¹. In this study we show that both galectin-1 and -3 are increased in $dy^{W/-}$ muscle and further increased in $dy^{W/-};itga7+$ skeletal muscle that transgenically overexpress the $\alpha7$ integrin. These results suggest that, in the absence of laminin-211, expression of galectin-1 and -3 are increased and might serve as biomarkers for disease progression. Because the $\alpha7\beta1$ integrin has been previously shown to bind galectin-1, our results suggest that rescue of laminin- $\alpha2$ deficient muscle by overexpression of the $\alpha7$ integrin is mediated through interactions of the $\alpha7\beta1$ integrin with galectin-1 and/or galectin-3 to stabilize myofibers.

Although tenascin C is normally localized and enriched at myotendinous junctions in wild-type muscle, in $dy^{W/-}$ laminin- $\alpha 2$ deficient mice, tenascin C is found around regenerating myofibers, sites of inflammation and extrajunctional sites¹⁰⁵. Our study shows that transgenic expression the $\alpha 7$ integrin resulted in increased tenascin C transcript in $dy^{W/-}$ muscle. Because transgenic expression of the $\alpha 7$ integrin results in a reduced percentage of myofibers with centrally located nuclei (and therefore reduced muscle regeneration) and decreased inflammation, these results indicate that increased $\alpha 7\beta 1$ integrin stabilizes the existing extracellular matrix, including tenascin C in $dy^{W/-}$ muscle.

Approaches toward the treatment of MDC1A have targeted apoptosis in mouse models through the inhibition of Bax, transgenic expression of the anti-apoptotic protein Bcl-2 and treatment with the anti-apoptotic drugs doxycycline^{112;113} or omigapil¹¹⁴. Another approach has focused on restoring or improving the muscle extracellular matrix through transgenic expression, in mouse models, of laminin- $\alpha 1$ ^{29;107}, laminin- $\alpha 2$, mini-agrin¹¹⁵ and N-acetylgalactosamine transferase¹⁰⁴. Our results indicate that increased expression of the $\alpha 7\beta 1$ integrin receptor in muscle improves adhesion of myofibers to the endogenous basal lamina to reduce muscle disease progression and maintain muscle strength in the $dy^{W/-}$ mouse model of MDC1A. Results from this study indicate that compounds that increase $\alpha 7$ integrin expression in laminin- $\alpha 2$ deficient muscle might provide a novel therapeutic approach for the treatment of MDC1A.

Acknowledgements

The authors thank Drs. Paul Martin and Eva Engvall for the dy^W mice and Dr. Stephen Kaufman (University of Illinois, Urbana-Champaign, IL) for the anti- $\alpha 7$ integrin antibodies. The authors thank Ms. Rebecca Evans and Honglin Tian for technical assistance, Dr. Heather Burkin for critically reading the manuscript and Dr. George Fernandez for statistical analysis. This study was supported by NIH/NCRR 5P20RR015581 and NIH/NIAMS R01AR053697. Deposited in PMC for release after 12 months.

Table 3.1

Gene Name	dy ^{W^{-/-}} (fold increase over Wild-type)	dy ^{W^{-/-}} ;itga7+ (fold increase over Wild-type)	Significant Change (dy ^{W^{-/-}} vs dy ^{W^{-/-}} ;itga7+) (p-value <0.05)
<i>Adamts5</i>	1.97 ± 0.14	2.33 ± 0.08	No
<i>Agrn</i>	9.23 ± 0.53	6.55 ± 0.15	Yes
<i>Col6a1</i>	5.56 ± 0.27	7.45 ± 0.51	Yes
<i>Lgals1</i>	9.19 ± 0.28	12.13 ± 0.31	Yes
<i>Lgala3</i>	70.02 ± 0.83	80.43 ± 1.96	Yes
<i>Mmp2</i>	19.21 ± 0.86	12.40 ± 0.43	Yes
<i>Itga3</i>	4.99 ± 0.41	4.53 ± 0.23	No
<i>Itga6</i>	2.68 ± 0.09	3.71 ± 0.09	Yes
<i>Itga7</i>	4.08 ± 0.11	17.15 ± 0.42	Yes
<i>Lama4</i>	11.96 ± 0.40	12.60 ± 0.90	No
<i>Lama5</i>	5.63 ± 0.34	6.16 ± 0.34	No
<i>Nid1</i>	4.32 ± 1.56	6.07 ± 1.33	No
<i>Tnc</i>	28.05 ± 1.30	49.60 ± 3.64	Yes
<i>Timp1</i>	276.20 ± 22.35	328.56 ± 20.40	Yes
<i>Timp2</i>	6.30 ± 0.18	6.34 ± 0.21	No

Results are the fold increase in expression compared with that in wild-type mice.

Significance is taken as P<0.05.

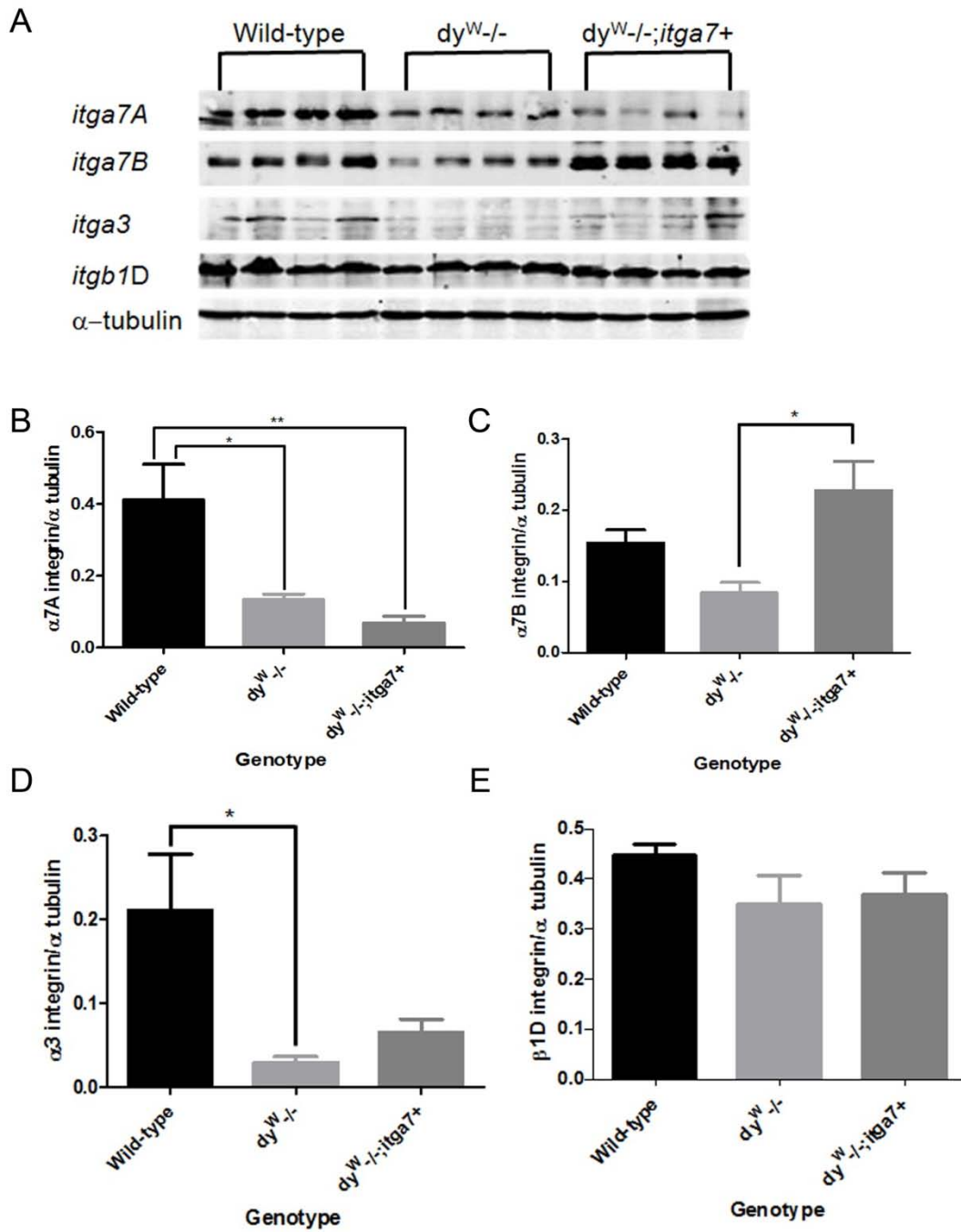


Figure 3.1. Enhanced $\alpha 7B$ integrin in the muscle of $dy^{W-/-};itga7^+$ mice. (A)

Immunoblot showing protein levels of $\alpha 7A$ integrin, $\alpha 7B$ integrin, $\alpha 3$ integrin, and $\beta 1D$

integrin in wild-type, $dy^{W/-}$, and $dy^{W/-};itga7+$ animals. α -tubulin was used to normalize protein loading. (B) Densitometry analysis of $\alpha7A$ integrin indicating that both the $dy^{W/-}$ animals (* $p < 0.05$) and the $dy^{W/-};itga7+$ animals have significantly reduced levels of $\alpha7A$ integrin (** $p < 0.01$). (C) Densitometry showing that $\alpha7B$ integrin is significantly elevated in the $dy^{W/-};itga7+$ animals when compared with the $dy^{W/-}$ animals (* $p < 0.05$). (D) Protein quantitation for $\alpha3$ integrin showing a significant reduction in protein levels in the $dy^{W/-}$ animals compared with wild-type (* $p < 0.05$) with no other significant changes. (E) No differences in $\beta1D$ protein levels were observed amongst the three genotypes analyzed.

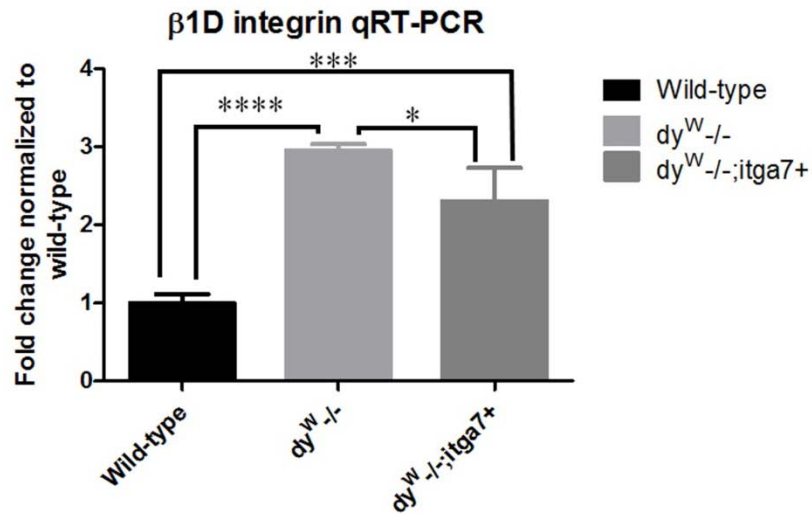


Figure 3.2. β 1D integrin transcript levels comparing wild-type, $dy^{W-/-}$, and $dy^{W-/-};itga7+$ animals. There is significantly elevated β 1D integrin transcript production in both the $dy^{W-/-}$ and $dy^{W-/-};itga7+$ animals. The $dy^{W-/-}$ mice have the largest amount of transcript present * $P < 0.05$, *** $P < 0.001$, **** $P < 0.0001$

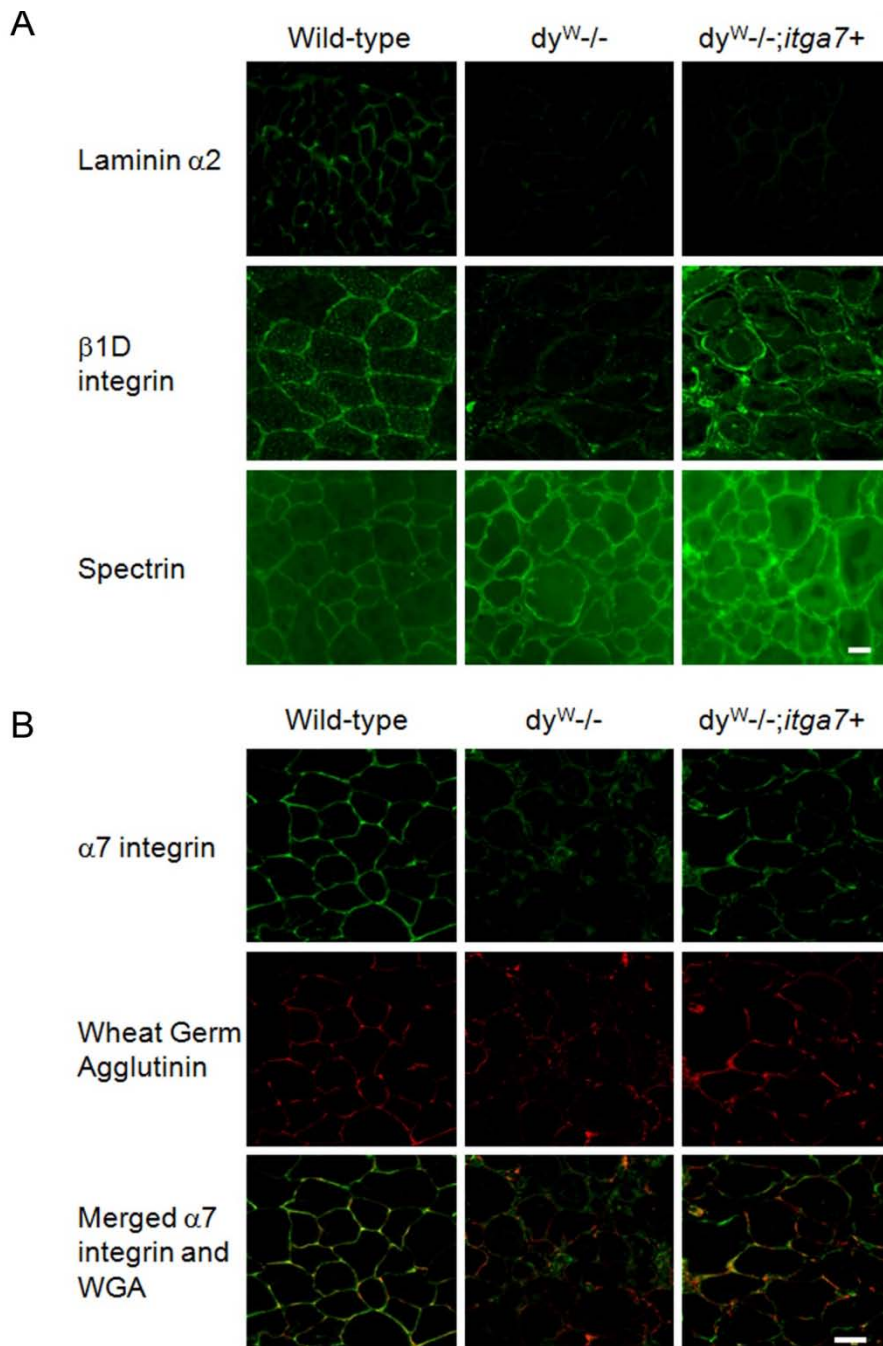
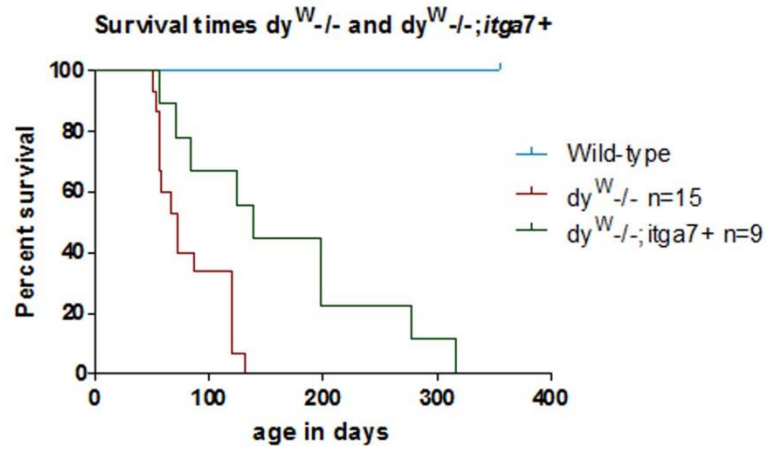


Figure 3.3. Transgenic expression of $\alpha 7$ integrin restores sarcolemmal location in $dy^{W-/-}$ skeletal muscle. (A) Immunofluorescence using TA muscle from 4-week-old male mice was used to confirm the absence of laminin- $\alpha 2$ protein in $dy^{W-/-}$ muscle. Wild-type TA muscle shows sarcolemmal staining for laminin- $\alpha 2$ which is not present in $dy^{W-/-}$

or $dy^{W-/-};itga7+$ animals. Sections were also incubated with anti- β 1D antibody to visualize β 1D integrin. Scale Bar = 20 μ m. (B) High resolution confocal microscopy of TA muscle using rhodamine labeled WGA to highlight the sarcolemma, and CDB347 antibody to visualize α 7B integrin was performed. The increased yellow colocalization signal in the $dy^{W-/-};itga7+$ animals indicates restoration of sarcolemmal localization of the α 7 integrin. Scale bar = 30 μ m.

A



B

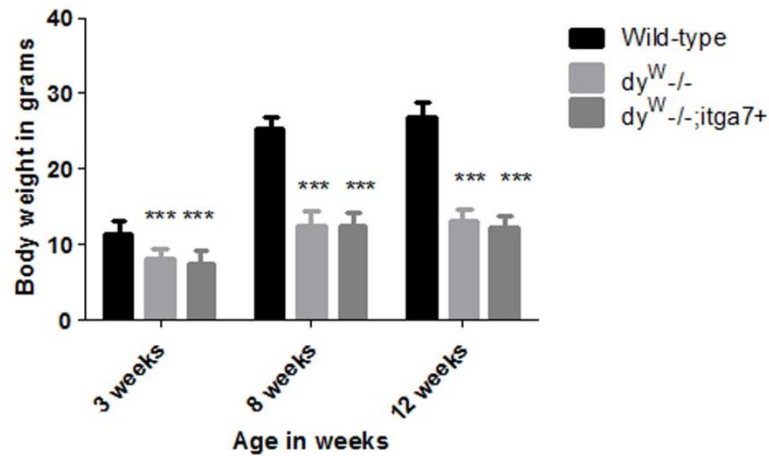


Figure 3.4. Transgenic expression of $\alpha 7$ integrin in the skeletal muscle of $dy^{W-/-}$ mice increases longevity but not weight gain. (A) Kaplan-Meier survival curve shows $dy^{W-/-};itga7+$ (n=9) animals have a median life expectancy that is 2.0-fold longer compared to their $dy^{W-/-}$ (n=15) littermates (* $p < 0.05$). (B) Analysis of body weights shows that wild-type mice are heavier than both $dy^{W-/-};itga7+$ and $dy^{W-/-}$ animals at all ages analyzed (** $p < 0.001$).

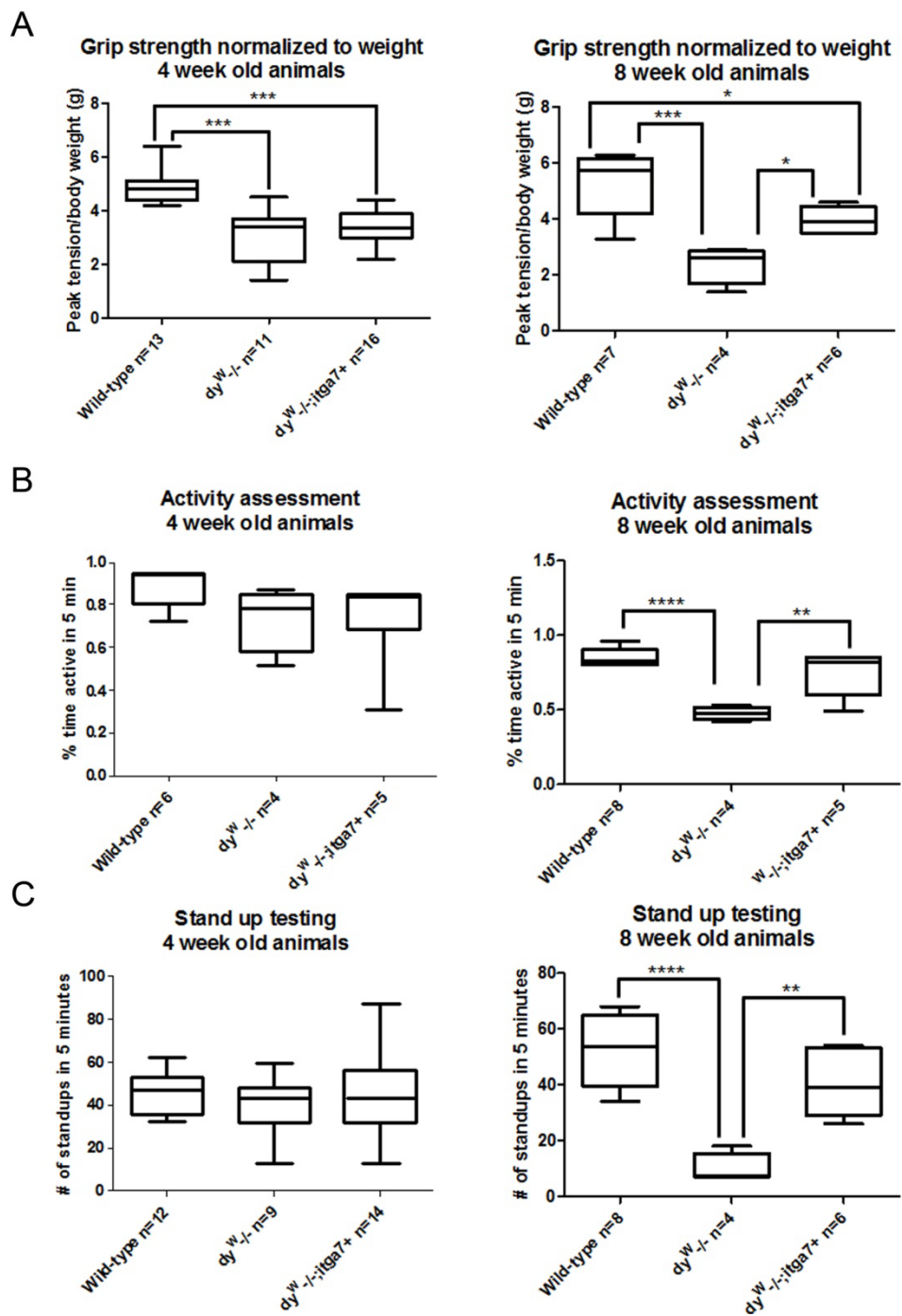


Figure 3.5. The *dy*^{W/-};*itga7*⁺ transgenic mice maintain muscle strength and exhibit increased motor activity. (A) Box and whiskers plot of forelimb grip strength at four

weeks of age showing that $dy^{W/-}$ and $dy^{W/-};itga7+$ mice are weaker than the wild-type animals ($***p<0.001$). At eight weeks of age wild-type ($***p<0.001$) and $dy^{W/-};itga7+$ animals ($*p<0.05$) are significantly stronger than $dy^{W/-}$ mice. (B) Box and whiskers plot of activity, as measured by the amount of active time over a 5 minute period. At four weeks of age there is no significant difference between any of the genotypes analyzed ($p>0.05$). At eight weeks of age wild-type and $dy^{W/-};itga7+$ mice were significantly more active than $dy^{W/-}$ animals. There was no significant difference in the activity levels of 8 week old wild-type and $dy^{W/-};itga7+$ mice. (C) Box and whiskers plot of stand up activity over a five minute period. At four weeks of age there were no significant differences between the genotypes. At eight weeks of age, wild-type and $dy^{W/-};itga7+$ animals exhibited significantly more stand ups compared to $dy^{W/-}$ animals. There was no significant difference in stand up activity between the $dy^{W/-};itga7+$ and wild-type animals. $*P<0.05$; $**P<0.01$; $***P<0.0001$. For each plot the box represents 1st quartile, mean and 3rd quartile and the whiskers represent minimum and maximum values.

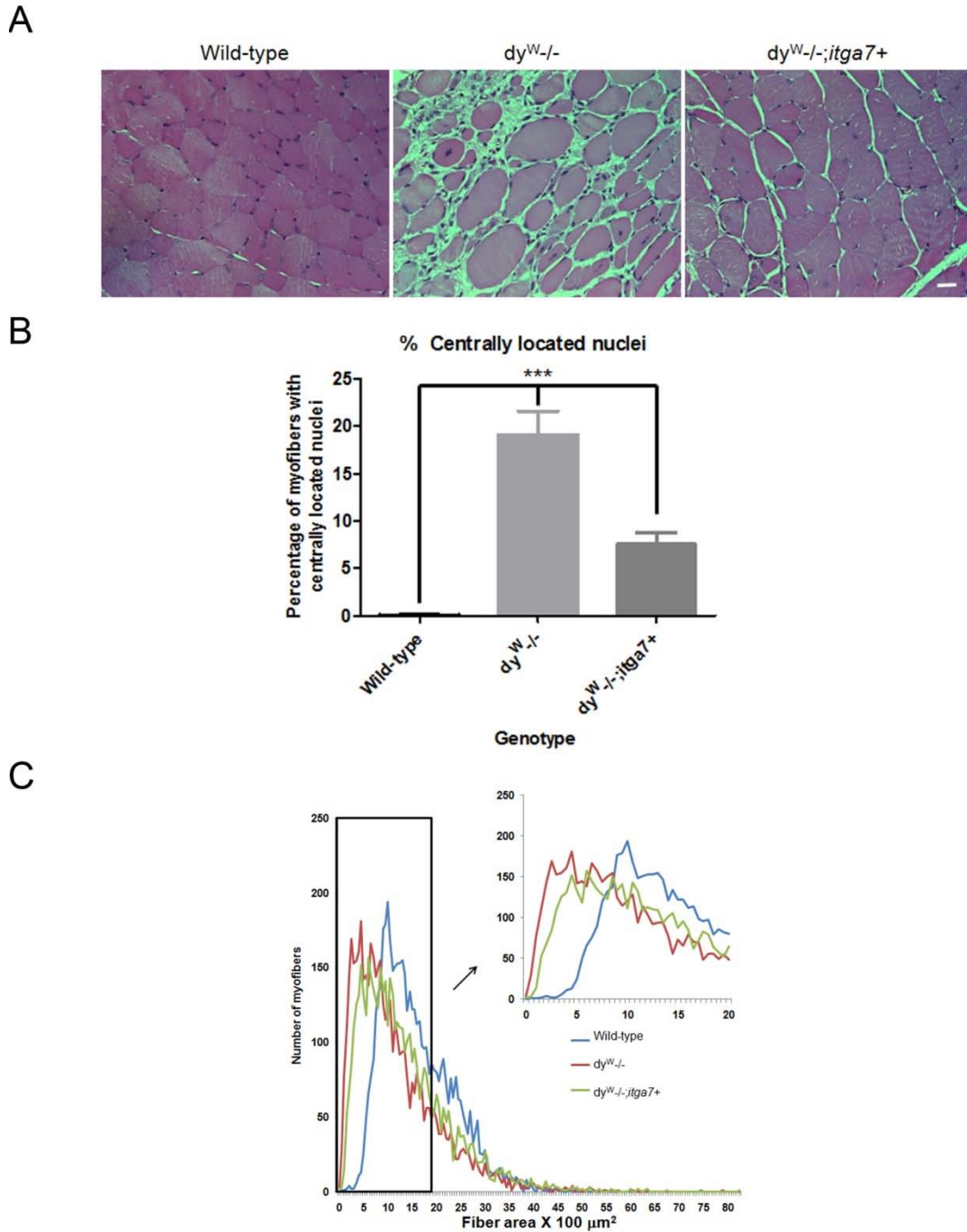


Figure 3.6. Reduced muscle disease in laminin- $\alpha 2$ deficient mice that transgenically express $\alpha 7$ integrin. (A) H&E staining of sections from TA muscles from 4-week-old mice shows more muscle pathology in $dy^{W/-}$ mice compared with that in wild-type. The

TA muscle of $dy^{W/-};itga7+$ mice exhibited reduced muscle pathology. Scale bar = 20 μ m.

(B) The percentage of myofibers containing centrally located nuclei was used to evaluate muscle repair in TA muscles from 4-week-old mice. Compared with that in wild-type, $dy^{W/-}$ showed a 19-fold increase in the percentage of myofibers containing centrally located nuclei. By contrast, $dy^{W/-};itga7+$ TA muscle showed a 66.5% reduction in the percentage of myofibers with centrally located nuclei (** $p < 0.001$). **(C)** Myofiber cross-sectional area revealed $dy^{W/-};itga7+$ animals have a fiber size distribution closer to that of wild-type animals than to $dy^{W/-}$ mice (Supplementary material figure S2.1).

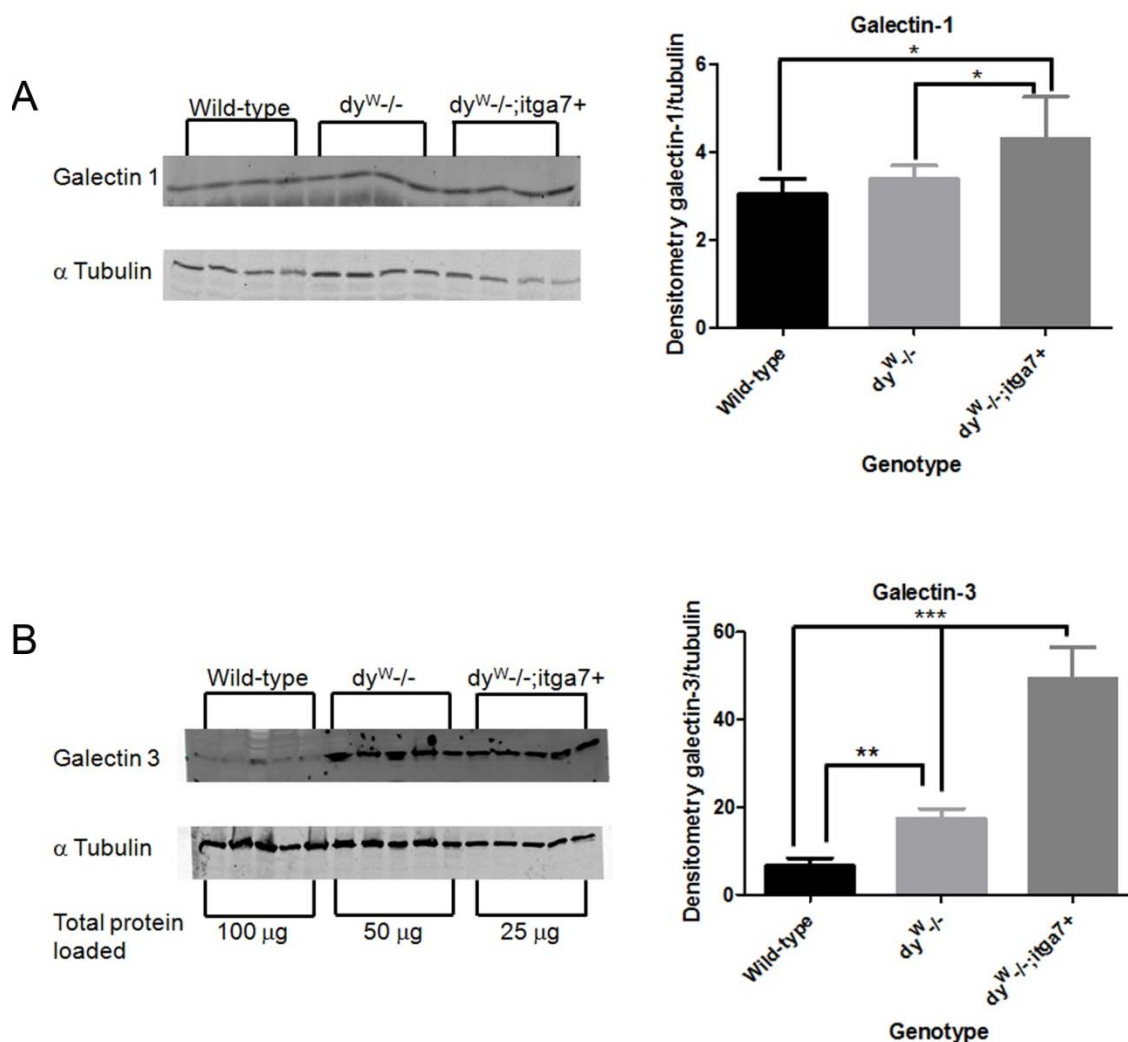


Figure 3.7. Transgenic expression of $\alpha 7$ integrin in the absence of laminin- $\alpha 2$ increased expression of galectin-1 and -3 in the muscle of $dy^{W-/-}$ mice. (A)

Immunoblot of galectin-1 protein (50 μ g protein lysate used) showing that 4-week-old $dy^{W-/-};itga7^+$ animals have a 1.4-fold increase in galectin-1 protein compared to wild-type and $dy^{W-/-}$ (* $p < 0.05$). (B) Immunoblot of galectin-3 protein required differential protein loading across the genotypes as follows: wild-type=100 μ g, $dy^{W-/-}$ =50 μ g, and $dy^{W-/-};itga7^+$ =25 μ g. Quantitative analysis revealed 4-week-old $dy^{W-/-}$ mice have 2-fold more galectin-3 compared with that in wild type animals (** $p < 0.01$). The $dy^{W-/-};itga7^+$

animals have 7-fold and 2.9-fold more galectin-3 protein compared with that in both wild-type and $dy^{W/-}$ animals respectively (** $p < 0.001$).

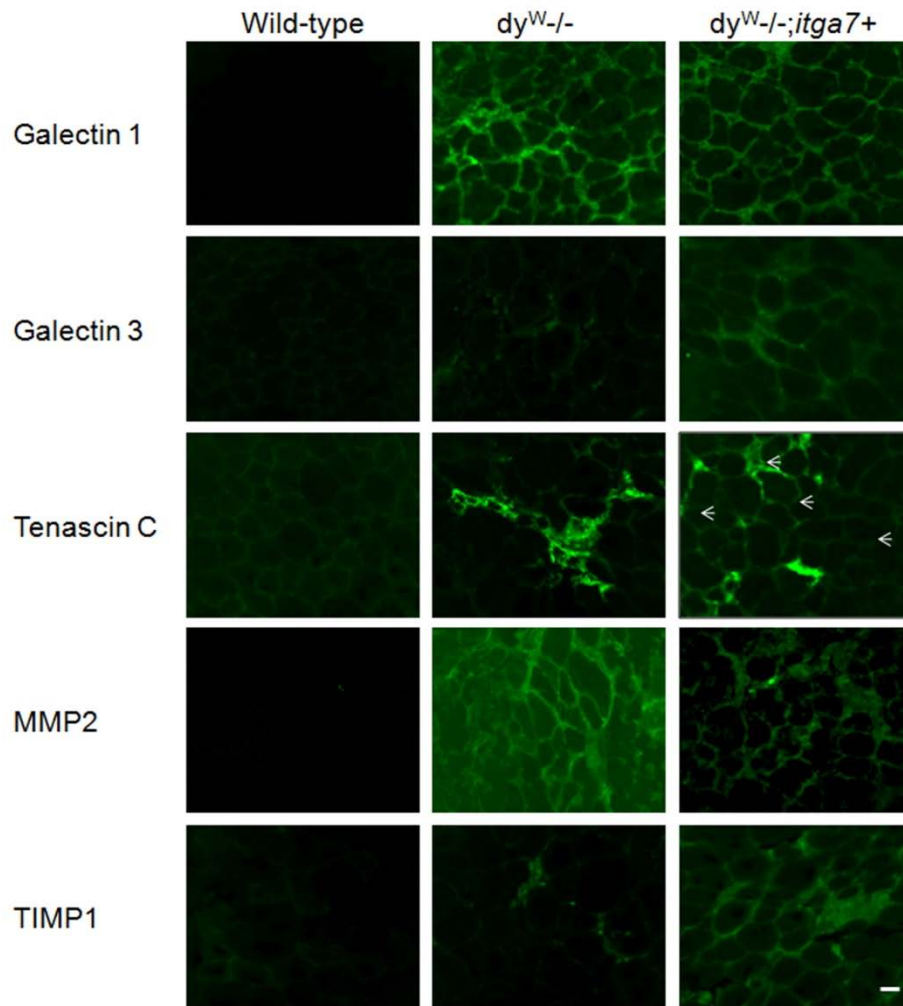


Figure 3.8. Enhanced expression of $\alpha 7$ integrin augments the extracellular matrix and slows matrix turnover in the $dy^{W-/-}$ mouse. Immunofluorescence was used to evaluate extracellular matrix proteins and associated proteins. Galectin-1 was found to be elevated in both the $dy^{W-/-}$ and $dy^{W-/-};itga7+$ animals when compared with that in the wild-type. The $dy^{W-/-};itga7+$ animals had the greatest amount of staining for galectin-3 with some staining present in the $dy^{W-/-}$ animals and none in wild-type controls. Tenascin C was found in areas of inflammation in the $dy^{W-/-}$ animals, whereas it was more dispersedly located in the $dy^{W-/-};itga7+$ animals (arrows). Matrix Metalloproteinase 2

(MMP2) was highest in the $dy^{W-/-}$ animals. Overexpression of $\alpha 7$ integrin led to reduced staining for MMP2 in the $dy^{W-/-};itga7+$ animals. Conversely, Tissue Inhibitor of Metalloproteinases 1 (TIMP1) was found to be elevated by enhanced $\alpha 7$ integrin expression in the $dy^{W-/-};itga7+$ mice compared with both $dy^{W-/-}$ and wild-type animals (Scale bar= 20 μm).

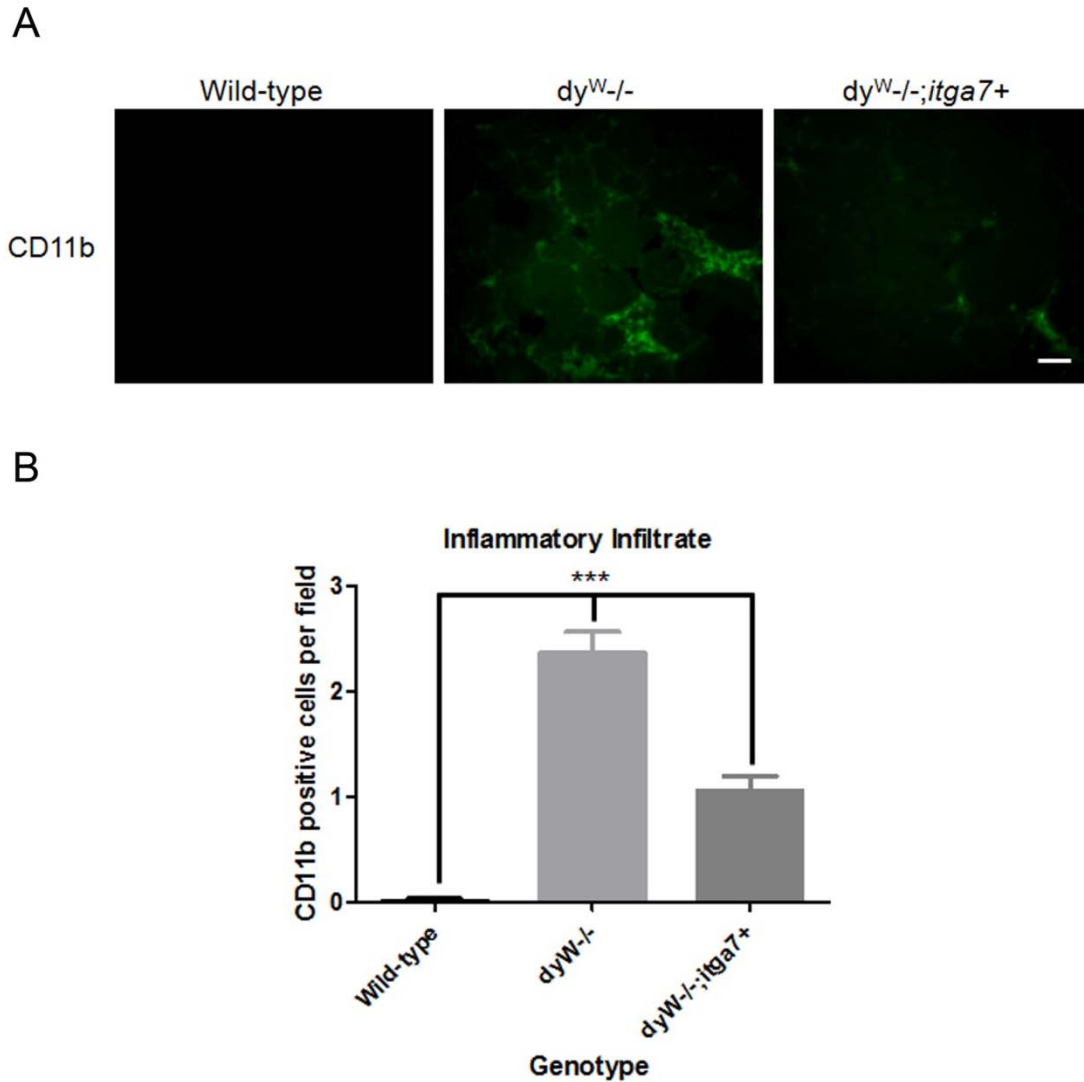


Figure 3.9. Enhanced expression of $\alpha7$ integrin reduces inflammation in $dy^{W-/-}$ muscle. (A) Immunofluorescence of TA muscles from 4-week-old mice with anti-CD11b, a marker for macrophages. Compared with wild-type mice, $dy^{W-/-}$ mice have an increased number of CD11b positive macrophages. The $dy^{W-/-};itga7+$ animals have less inflammatory cell infiltration compared with $dy^{W-/-}$ animals (Scale bar= 20 μ m). (B) Quantification revealed that $dy^{W-/-}$ mice have a 2.4-fold increase in CD11b positive macrophages in TA muscle compared with the number in wild-type mice. By contrast,

$dy^{W-/-};itga7+$ animals exhibited a 55.3% decrease in CD11b positive macrophages in TA muscle compared with the number in $dy^{W-/-}$ (***) $p < 0.001$ for all groups).

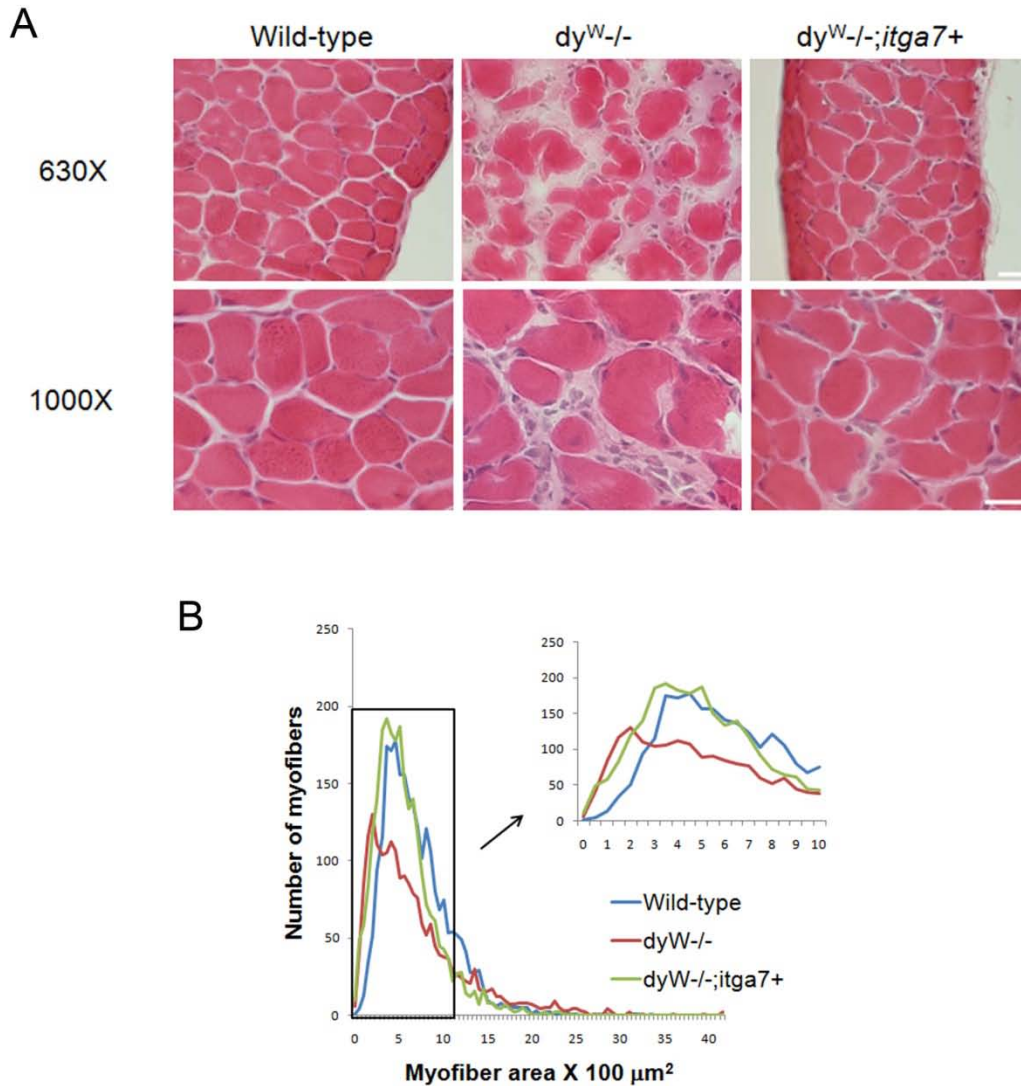


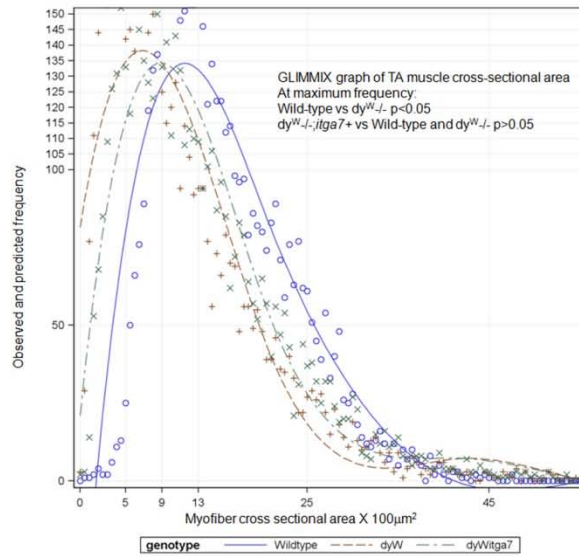
Figure 3.10. Enhanced $\alpha 7$ integrin expression improves diaphragm pathology in 4-week-old $dy^{W-/-}$ mice. (A) Hematoxylin and eosin staining of diaphragm muscle from 4-week-old $dy^{W-/-}$ mice exhibit variation in myofiber size, presence of centrally located nuclei and fibrosis. By contrast, the $dy^{W-/-};itga7+$ diaphragm shows reduced muscle pathology. Scale bar=20 μm . (B) Cross-sectional myofiber area of the diaphragm muscle

of 4-week-old animals shows that the $dy^{W/-};itga7+$ mice have a myofiber cross-sectional area more similar to wild-type animals than that observed in $dy^{W/-}$ mice (see also supplementary material Fig. S2.1).

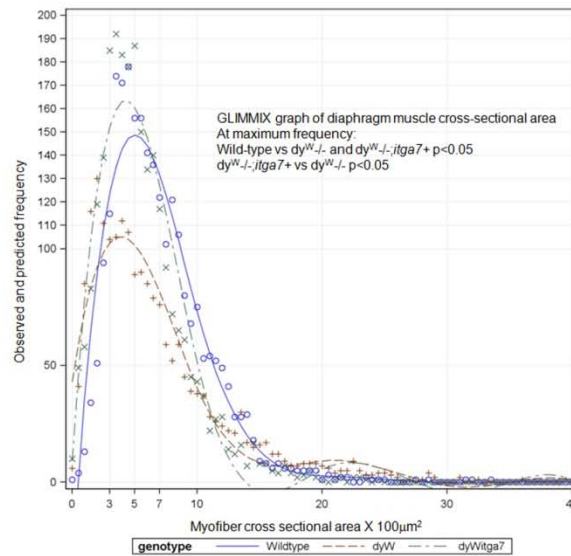
Supplemental material Table S3.1

Gene name	Forward Primer	Reverse Primer
Adamts5	gaagagggccatataccgttct	caggacacctgcatattgggaac
Agri	tgcgctccactgtgaaggtaa	ccatctgtgtccaattgtgtggca
B1D	gaaaatgaatgccaagtgggacac	gagaccagctttacgtccatagtttgattct
Col6a1	attacggatggacgttctgacactca	gataagccttggcaggaatgacattga
Lgals1	gccagcaacctgaatctcaaacct	ctgtctttccaggttcagcaca
Lgals3	gcacagtgaaacccaacgcaa	tgtcctgcttcgtgttacacaca
Mmp2	cctaagctcatgcagactcctg	cttccaaacttcacgctcttgagact
Itga3	ccttcagacacctccaacattacca	gtagggatgctggttctcaggaa
Itga6	gcttccatagatgtcaccgctgct	gcaagaacagccaggaggatgat
Itga7	gatcgtccgagccaacatcaca	ctaacagcccagccagcact
Lama4	ggaatacctgaacgtgcatatgaga	gtgcatctgccatcacagagattct
Lama5	ctacatgcagctgaagggtgctga	ggtgccaccgtccatcacaaa
Nid1	caccaaccggaggattctcgca	agcccttcgagaactttgctct
Tnc	acctgagcaaaatcacagcccaa	gatctaccattgtgatagttcatggagtca
Timp1	actctgagcctgctcagcaa	cgccacaaacagtgagtgtcact
Timp2	gtgagcgagaaggaggtggattc	tcgatgtctttgcaggctccttga
Gapdh	caatgtgtccgtcgtggatctga	gagttgctgttgaagtcgcagga

A



B



Supplemental material Figure S3. 1. Muscle specific transgenic expression of the $\alpha 7$ integrin improves myofiber cross-sectional area. (A) SAS GLIMMIX statistical analysis of the TA muscle myofiber cross-sectional area in wild-type, $dy^{W-/-}$ and $dy^{W-/-}$

;itga7+ mice. At maximal frequency the myofibers area of the $dy^{W/-};itga7+$ mice is not statistically different from the wild-type or $dy^{W/-}$ animals. In contrast, there is a significant difference between the fiber sizes of the wild-type and $dy^{W/-}$ animals (* $p < 0.05$). (B) SAS GLIMMIX statistical analysis of diaphragm myofiber cross-sectional area in wild-type, $dy^{W/-}$ and $dy^{W/-};itga7$ mice. At maximum frequency the myofibers size differs significantly between all three genotypes. However, the overall curve for the $dy^{W/-};itga7+$ mice is more similar to that for wild-type mice.

Reprinted with permission of The Company Of Biologists Limited. Published as:

Transgenic overexpression of the $\alpha 7$ integrin reduces muscle pathology and improves viability in the dyW mouse model of merosin-deficient congenital muscular dystrophy type 1A. Doe JA, Wuebbles RD, Allred ET, Rooney JE, Elorza M, and Burkin DJ. Journal of Cell Science 2011 Jul1;124(Pt13):2287-97.

Chapter 4

Neuromuscular junction pathology and pulmonary testing of wild-type, dy^W $-/-$, and dy^W $-/-$; $itga7$ $+$ animals

Abstract

Merosin deficient congenital muscular dystrophy type 1A (MDC1A) is caused by a mutation in the *LAMA2* gene which leads to a loss of laminins 211 and 221. These two laminins, particularly laminin 221, are crucial members of the extracellular matrix at neuromuscular junctions in skeletal muscle. Without laminins 211 and 221 the neuromuscular junctions are unable to form properly leaving the junctions smaller in size and reduced in number. Secondary to the loss of laminins 211 and 221 there is a reduction in $\alpha7\beta1$ integrin. The $\alpha7\beta1$ integrin is one of the main binding partners for laminins 211 and 221 both at the neuromuscular junction and extrajunctionally. By using a transgenic approach to enhance $\alpha7$ integrin expression, we were able to partially rescue the neuromuscular junction abnormalities in the $dy^W/-$ mouse model for MDC1A. The main cause of death in MDC1A patients is respiratory failure. Using a flow whole body plethysmography system (FWBP) we were able to evaluate the $dy^W/-$ mouse, as well as transgenic, skeletal muscle specific overexpressors of $\alpha7$ integrin, in multiple areas of respiratory function. To our knowledge this is the first time that plethysmography has been used to evaluate the $dy^W/-$ mouse model of MDC1A.

Introduction

Neuromuscular junctions (NMJs) are highly specialized areas of the sarcolemma where acetylcholine receptors (AChRs) congregate. AChRs in the postsynaptic cleft are of the nicotinic type (nAChR) and are ligand gated ion channels¹¹⁶. Stimulation of the nAChR leads to sarcolemmal depolarization caused by the influx of cations – specifically

Na^+ , K^+ , and, to a lesser extent, Ca^{2+} ¹¹⁶. This is the first step in muscle contraction as it leads to activation of voltage gated ion channels and in turn to contraction.

nAChRs aggregate in areas of the sarcolemma, which are characterized by high concentrations of cholesterol and sphingolipids (lipid rafts). This process is driven by agrin activation of muscle specific tyrosine kinase (MuSK) leading to actin polymerization and raft formation. This lipid raft formation leads to nAChR clustering^{61;117;118}. Agrin is a heparin sulfate proteoglycan found in many tissues. In mature skeletal muscle, it is found at the neuromuscular junction as well as extrajunctionally. In addition to inducing AChR clustering, agrin can bind with laminins 111, 211, and 221, and α -dystroglycan^{61;119;120}. Moll *et al*¹¹⁹ found that overexpression of a truncated agrin isoform could partially rescue the dystrophic phenotype of the $\text{dy}^{\text{W}}/-$ mouse. Laminins 111, 211, and 221 can also induce AChR clustering⁹³. Agrin, $\alpha 7\beta 1$ integrin, and the different laminin isoforms act synergistically to form NMJs^{92;93}.

The $\alpha 7\beta 1$ integrin is located at all NMJs where it associates with agrin and laminin 111, 211, and 221 and physically interacts with the nAChR (the α -chain). The $\alpha 7\beta 1$ integrin is not a passive member of the NMJ, it is involved with all steps of NMJ formation⁹². In order to evaluate the effect of enhancing $\alpha 7$ integrin on the neuromuscular junction, we bred the dy^{W} mouse, a model of MDC1A, with the BX2-10i mouse which overexpresses $\alpha 7\text{BX}2$ integrin in the skeletal muscle. The overexpression of $\alpha 7\text{BX}2$ was essential as only $\alpha 7$ integrin which is comprised of the X2 extracellular domain is found in the NMJ. Both the $\alpha 7\text{A}$ and $\alpha 7\text{B}$ cytoplasmic splice variants are located at the NMJ^{92;101}. The resultant mouse was laminin $\alpha 2$ deficient and

overexpressed the $\alpha 7$ integrin in the skeletal muscle and is designated as $dy^{W/-/-}; itga7+$. We found that enhanced $\alpha 7$ integrin expression could partially restore both the numbers of NMJs as well as the size of the junctions (both of which are reduced in the $dy^{W/-/-}$ mouse).

We have recently shown that enhanced $\alpha 7$ integrin expression rescues the $dy^{W/-/-}$ mouse model of MDC1A. To further define the mechanism of this rescue we evaluated NMJ and respiratory pathology. Patients with MDC1A and the $dy^{W/-/-}$ mouse model suffer from a dysmyelinating peripheral neuropathy and reduced expression of the $\alpha 7$ integrin. The reduced expression of $\alpha 7$ integrin may also contribute to the peripheral nerve pathology by affecting NMJ formation. If we lessen the NMJ pathology of the $dy^{W/-/-}$ mouse by enhanced expression of $\alpha 7$ integrin we may have another mechanism for the rescue seen.

The main cause of mortality in MDC1A patients is respiratory failure due to pathology in the diaphragm and intercostal muscles. NMJs are critical for the diaphragm to function properly and the $\alpha 7$ integrin is needed for proper AChR aggregation. We have shown that enhanced $\alpha 7$ integrin expression can increase the life expectancy and improve diaphragm pathology in $dy^{W/-/-}$ mice ¹²¹. This increased longevity may be due to improvement in diaphragm function; therefore, we examined the effect of enhanced $\alpha 7$ integrin expression on respiratory function at the whole animal level.

Plethysmography is a technique used to measure changes in pressures or flow in specific areas of the body. We applied the technique of flow whole body plethysmography (FWBP) to assess various components of airway function in response

to methacholine. Methacholine is an AChR agonist. AChRs are members of the NMJ and are found, among other locations, in the airway where they innervate airway smooth muscle. Stimulation of the NMJs results in bronchiole constriction and therefore, changes in airflow and pressures throughout the respiratory tree¹²². This makes methacholine stimulation testing, during which a patient is subjected to differing concentrations of nebulized methacholine while respiratory parameters are monitored, a powerful clinical tool for the diagnosis of asthma, systemic sclerosis-associated interstitial lung disease (SSc-ILD), allergic airway hyper-reactivity, and other pulmonary conditions¹²²⁻¹²⁴. Methacholine challenge responses have also been shown to be independent of animal age as balb/c mice between the ages of 2 and 8 weeks of age have similar responses¹²⁴.

In this study we show that enhanced expression of $\alpha 7$ integrin maintains respiratory function and decreases NMJ pathology in the $dy^W/-$ mouse. These studies indicate that the $\alpha 7$ integrin plays a role in maintaining diaphragm muscle function.

Materials and Methods

Neuromuscular junction detection

Triceps muscle from five animals of each genotype at eight-weeks of age $dy^{W+/+}$, $dy^{W/-}$, and $dy^{W/-};itga7+$, animals were embedded in OCT (TissueTek). 8 μ m sections at the midbelly level were placed onto precleaned Surgipath Slides. Sections were fixed using 4% paraformaldehyde for 5 minutes and blocked using 5% Bovine Serum Albumin (BSA) in phosphate buffered saline (PBS) for 1 hour. Sections were then incubated with rhodamine labeled α -bungarotoxin. Slides were mounted using Vectashield with DAPI (Vector). Slides were observed using a Zeiss Axioskop 2 Plus fluorescent microscope,

images were captured using a Zeiss AxioCam HRc digital camera and data was evaluated using Axiovision 4.1 software.

Neuromuscular junction counting and area determination

To determine the number of neuromuscular junctions present, the number of neuromuscular junctions in 20 63X fields which contained at least 1 receptor were counted. 5 animals of each genotype were evaluated. To determine the area of the neuromuscular junctions the Axiovision 4.1 software was used to determine the area of 20 neuromuscular junctions per mouse. 5 mice of each genotype were evaluated for a total of 100 neuromuscular junctions per genotype.

Plethysmography

Animals were subjected to plethysmography at 4, 6, and 8 weeks of age. Animals from each genotype ($dy^W_{+/+}$, $dy^W_{-/-}$, and $dy^W_{-/-;itga7+}$) were used. Animals were placed in the plethysmography chamber (unrestrained) and then subjected to increasing doses of aerosolized methacholine, after an initial time period to acclimate to the chamber. First mice were exposed to aerosolized PBS to gather base line data, followed by increasing doses of methacholine (6.25, 12.5, 25, 50, and 100mg/ml). Experimental values were automatically collected by the pneumatograph in the wall of the chamber. FinePointe software (Buxco©) was used to collect data.

Statistics

One and two way ANOVA were used to determine statistical significance using GraphPad Prism.

Results

dy^W;itga7⁺ animals have an intermediate phenotype between wild-type and dy^W-/- animals of neuromuscular junction number and size

α -bungarotoxin was used to visualize the NMJs via fluorescent microscopy and shows the differences in size and number between the three genotypes (Figure 4.1.A). NMJs were quantified over 20, 63X fields that contained at least one receptor (Figure 4.1B). The number of NMJs in the dy^W-/- animals was significantly lower when compared to wild-type animals. The dy^W-/-;itga7⁺ animals displayed an intermediate phenotype with the number of junctions not being significantly different than either the wild-type or dy^W-/- animals. Both dy^W-/- and dy^W-/-;itga7⁺ animals had significantly smaller NMJs than wild-type animals (Figure 4.1C). There was no difference in sizes of the AChR in the two laminin α 2 deficient genotypes. These results indicate a partial rescue of the NMJ in the dy^W-/-;itga7⁺ animals. There was no significant rescue in the size of the NMJs.

Enhanced α 7 integrin in the dy^W-/- mouse helps maintain respiratory function over time.

A whole body flow plethysmograph was used to measure several variables related to respiratory function. Methacholine stimulation was used to simulate airway irritation. Most parameters (excluding frequency of breathing) were normalized to body weight to take into account the size difference between the wild-type animals and the dy^W-/- and dy^W-/-;itga7⁺ animals. Parameters were normalized to body weight to take into account the air displacement by the animals. Most plethysmography studies use mice of approximately the same size (balb/c, age-matched animals) so the effect of weight is less

apparent than with the animals which we used where the $dy^W/-/$ and $dy^W/-/;itga7+$ animals are significantly smaller than the wild-type animals¹²¹.

Penh was measured during a methacholine stimulation test. There was no significant difference in Penh between the three different genotypes studied at either 4-, 6-, or 8-weeks of age (Figure 4.2). However, at 8-weeks of age a trend towards higher Penh is present in the $dy^W/-/$ mice when compared to the wild-type and $dy^W/-/;itga7+$ animals (Figure 3.2C). This occurs in the 25, 50, and 100 mg/ml challenge doses. More animals in the cohort may lead to this trend being statistically significant.

Frequency of breathing was also measured during the methacholine stimulation. No significant differences were present across the genotypes (Figure 4.3). This parameter was independent of animal weight (data not shown). Total volume of air breathed during the methacholine stimulation was significantly greater in both $dy^W/-/$ and $dy^W/-/;itga7+$ animals at 4-weeks of age at all doses of methacholine administered with the exception of 12.5mg/ml (Figure 4.4A). It was not significantly different between any of the genotypes at either 6- or 8-weeks of age (Figure 4.4 B and C).

At all ages tested the $dy^W/-/$ animals had a significantly longer inspiratory time than the wild-type animals at the 100mg/ml dose (Figure 4.5A-C). At 4-weeks-of age the $dy^W/-/$ animals had a 2-fold increase in inspiratory time, this increased to a 2.3 fold increase at 6-weeks-of-age and a 2.4 fold increase at 8-weeks-of-age compared to wild-type animals. The $dy^W/-/;itga7+$ animals were not statistically different than either the wild-type or $dy^W/-/$ mice. This indicates that the presence of the $\alpha7$ integrin transgene is able to restore the inspiratory time back to near wild-type levels. More animals are necessary to confirm this trend.

Expiratory time did not differ significantly between the three genotypes at 4-weeks of age (Figure 4.6A). At 6- and 8-weeks of age there is a significant difference between the wild-type and $dy^W/-$ animals at the 100mg/ml dose of the methacholine stimulation test (Figure 4.6B and 4.6C). The $dy^W/-$ animals have a significantly longer expiration time at those points (3.2 and 2.6 fold respectively). The $dy^W/-;itga7+$ animals are not significantly different from either the wild-type or $dy^W/-$ animals at any age point. Taken together with the reduction in inspiratory time, these data show that enhanced $\alpha7$ integrin expression in skeletal muscle (in this case the diaphragm) is able to improve respiratory function during both the inspiratory and expiratory phases of respiration.

Discussion

Neuromuscular junction pathology is reduced in the $dy^W/-;itga7+$ animals

Patients with MDC1A display a peripheral neuropathy, which is due to the Schwann cells requiring laminin 211 to appropriately form the myelin sheath. The $dy^W/-$ mice also display a peripheral neuropathy and show reduced levels of appropriately localized $\alpha7$ integrin¹²¹. The reduced levels of $\alpha7$ integrin may contribute to the peripheral neuropathy by contributing to NMJ pathology. Therefore, by increasing $\alpha7$ integrin expression we may be able to partially alleviate the NMJ pathology because $\alpha7$ integrin plays a role in AChR clustering^{92;93;121}. The diaphragm muscle is a skeletal muscle which leads us to believe that our $\alpha7BX2$ transgene will be expressed in it and may then lead to increased NMJs which would help lessen diaphragm pathology. This led us to the hypothesis that the $dy^W/-$ animals should have NMJ pathology and that

enhanced $\alpha 7$ integrin expression should improve the phenotype seen. By evaluating midbelly triceps brachii cryosections we determined that the $dy^W/-/$ mice have both a reduced number and size of NMJs. We determined that the overexpression of $\alpha 7$ integrin in the skeletal muscle could increase the number of NMJs present to near wild-type levels. Also, the presence of the $\alpha 7BX2$ transgene increased the size of the neuromuscular junctions, though not significantly.

α -bungarotoxin was used to highlight the reduced size and numbers of NMJs in the absence of laminin- $\alpha 2$. We show that enhanced $\alpha 7$ integrin increases the number of NMJs in the absence of laminin $\alpha 2$. The $dy^W/-/;itga7+$ animals display an intermediate phenotype between the wild-type animals and $dy^W/-/$ animals in that the number of NMJs is not significantly different when compared to either wild-type or $dy^W/-/$ animals. The size of the NMJs in the $dy^W/-/$ animals is reduced compared to wild-type and that the overexpression of $\alpha 7$ integrin increases the size of the NMJs. By increasing the number of NMJs in the skeletal muscle (triceps brachii) we should also have increased the number of NMJs in the diaphragm. Improving diaphragm NMJ pathology may be contributing to the increased life expectancy seen in the $dy^W/-/;itga7+$ animals.

Pulmonary function

The majority of MDC1A patients die due to respiratory failure or complications from requiring positive pressure ventilation¹²⁵. Our previous work showed an improvement in diaphragm pathology in the $dy^W/-/;itga7+$ animals compared to dy^W animals¹²¹. This led us to hypothesize that pulmonary function would be improved by enhanced expression of $\alpha 7$ integrin in the diaphragm. We assessed respiratory function

by performing flow whole body flow plethysmography and a methacholine stimulation test on wild-type, $dy^W-/-$, and $dy^W-/-;itga7+$ animals at 4-, 6-, and 8-weeks of age.

The use of WBP and parameters derived from it are controversial in the field. This is mainly because most of the parameters measured are not specific to any single pulmonary disease but can be applied to many and the results may be confounded by environmental factors making interpretation difficult ^{126;127}. Lunblad et al, ¹²⁷ took it a step further and stated that unrestrained WBP, and Penh in particular, should not be used as indicators of lung function or bronchial sensitivity. They report that unrestrained WBP should only be used with anesthetized animals where the conditions can be more thoroughly controlled ¹²⁷.

One of the more controversial parameters measured by WBP is “enhanced pause” (Penh). Penh can be measured using flow plethysmography ¹²⁶⁻¹²⁸. Proponents of Penh find that it is a measure of overall pulmonary function and that it is beneficial to measure during asthma or allergy testing involving a methacholine stimulation test. It is also argued that since Penh is derived from a flow WBP and represents differences in the inspiratory and expiratory wave forms making it independent of many environmental factors ^{126;128}. Penh has also been shown to correlate with airway hyperresponsiveness in mice ¹²⁹. Opponents of its use state that Penh can be influenced by a number of environmental factors (such as humidity) and that it is too nonspecific to be beneficial. Others have presented data which show that Penh and lung compliance and resistance are not well correlated, particularly in C57/bl6 animals ¹³⁰. Our data show a trend towards compromised pulmonary function at 8 weeks of age during the methacholine stimulation

in the dy^W animals which would correlate well with death due to respiratory failure. A larger n number is needed to determine if this trend will hold.

There was no significant difference between the three genotypes, at any dose, in frequency of breathing. Breathing frequency is controlled by the autonomic nervous system and the cardio-respiratory center in the brain. If the dy^W animals were significantly more hypoxic than either the dy^W ; *itga7*⁺ or wild-type animals we would expect their respiratory rate to increase. The animals in all three genotypes breathed similar volumes of air as well indicating that at the ages evaluated the respiratory tract is able to compensate for any impairment present.

We do have evidence for some level of impairment though when we evaluate the total volume of air breathed along with the inspiratory and expiratory times. The dy^W animals had significantly longer inspiratory and expiratory times at the upper doses of methacholine. These results indicate that it takes these animals a longer amount of time to breathe the same volume of air. The length of the inspiratory and expiratory time can be related to diaphragm function. Therefore, the dy^W animals may be suffering from respiratory pathology at 8-weeks of age.

In total, our data indicate that enhanced expression of $\alpha 7$ integrin can improve neuromuscular junction pathology by increasing the number of AChRs and can improve respiratory function by improving inspiratory and expiratory time in older dy^W mice. Additional animals are needed for plethysmography studies to determine if other beneficial effects are present.

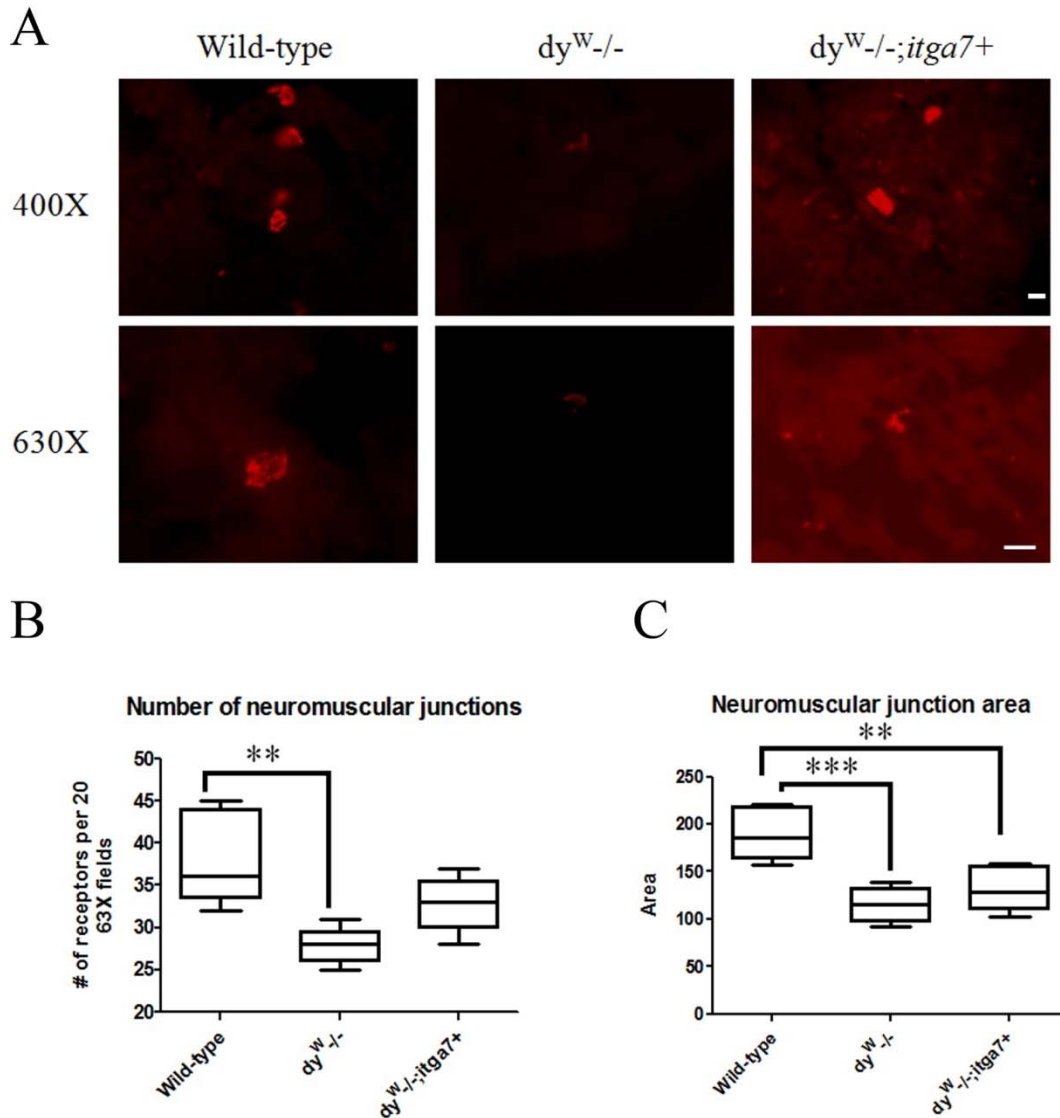


Figure 4.1. α -bungarotoxin staining showing neuromuscular junctions in wild-type, $dy^{W/-}$, and $dy^{W/-};itga7+$ animals and graphical representations of neuromuscular junction number and size. (A) α -bungarotoxin staining showing that the $dy^{W/-}$ mouse displays fewer and smaller acetylcholine receptors than wild-type. The $dy^{W/-};itga7+$ animals displays smaller sized acetylcholine receptors but similar numbers of acetylcholine receptors to wild-type. Scale bar = $20\mu m$ (B) The $dy^{W/-}$ mice have reduced

number of acetylcholine receptors present at the midbelly level of the triceps muscle. The $dy^{W-/-};itga7+$ animals display an intermediate number of acetylcholine receptors ($P>0.05$ compared to both wild-type and $dy^{W-/-}$ animals). (C) Both $dy^{W-/-}$ and $dy^{W-/-};itga7+$ animals have smaller acetylcholine receptors compared with wild type (** $P<0.01$ and *** $P<0.001$).

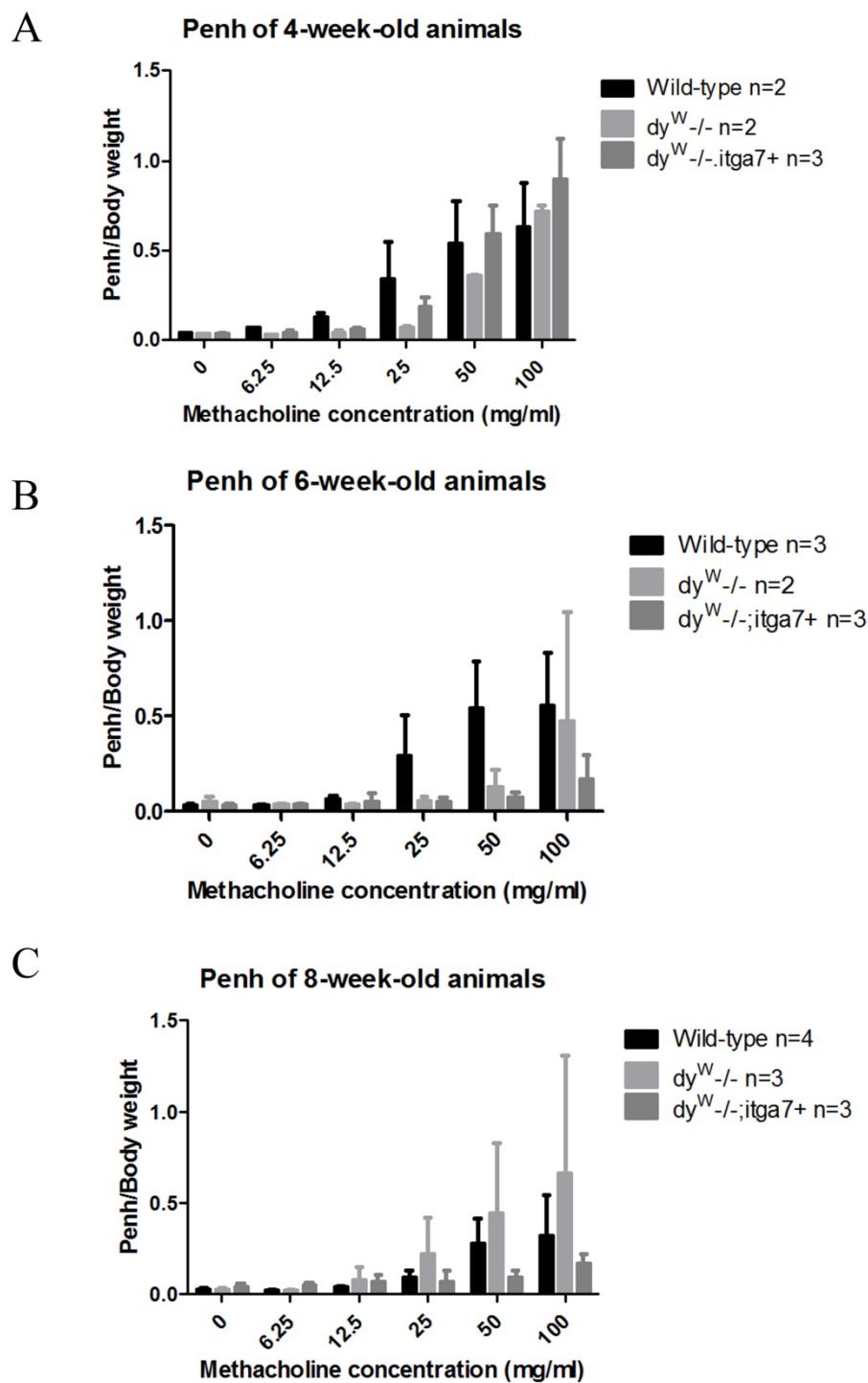


Figure 4.2. Penh measurement in wild-type, $dy^{W-/-}$ and $dy^{W-/-};itga7+$ animals. (A and B) There is no significant difference in Penh between the genotypes at any age or any

methacholine dose. (C) There is a trend towards higher Penh in the dy^W -/- animals at 25, 50, and 100mg/ml methacholine.

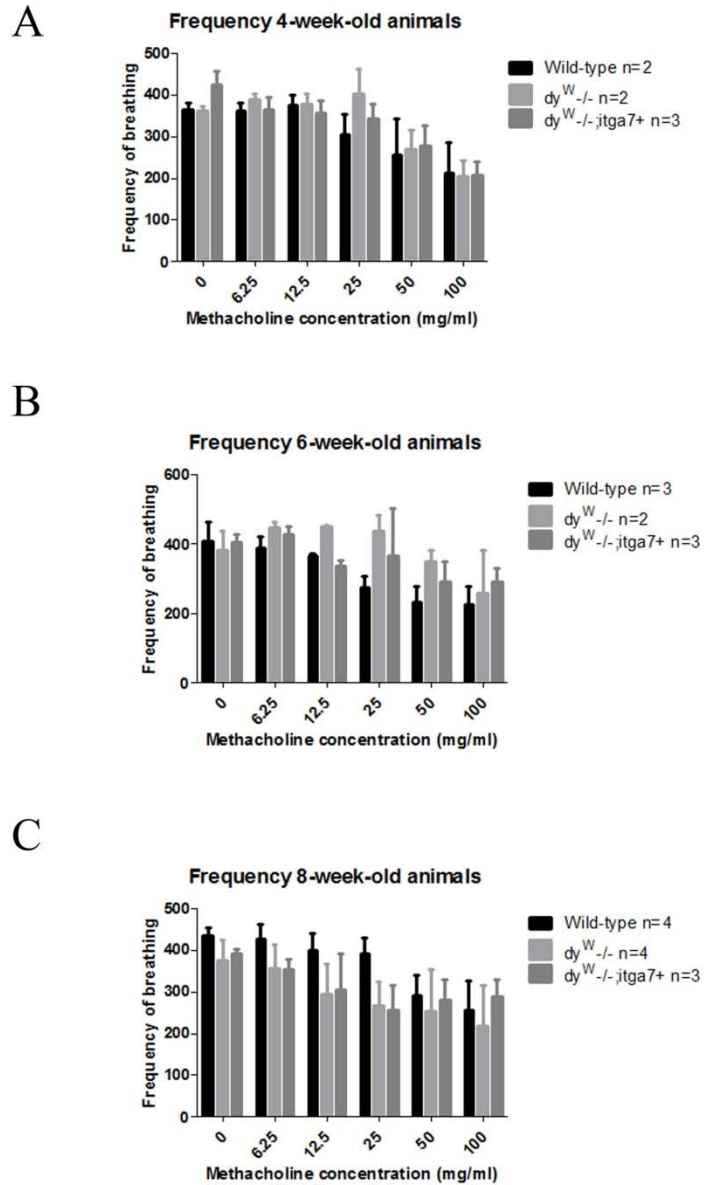


Figure 4.3. Frequency of breathing during methacholine stimulation. There is no significant difference in the frequency of respiration at any age or any methacholine dose.

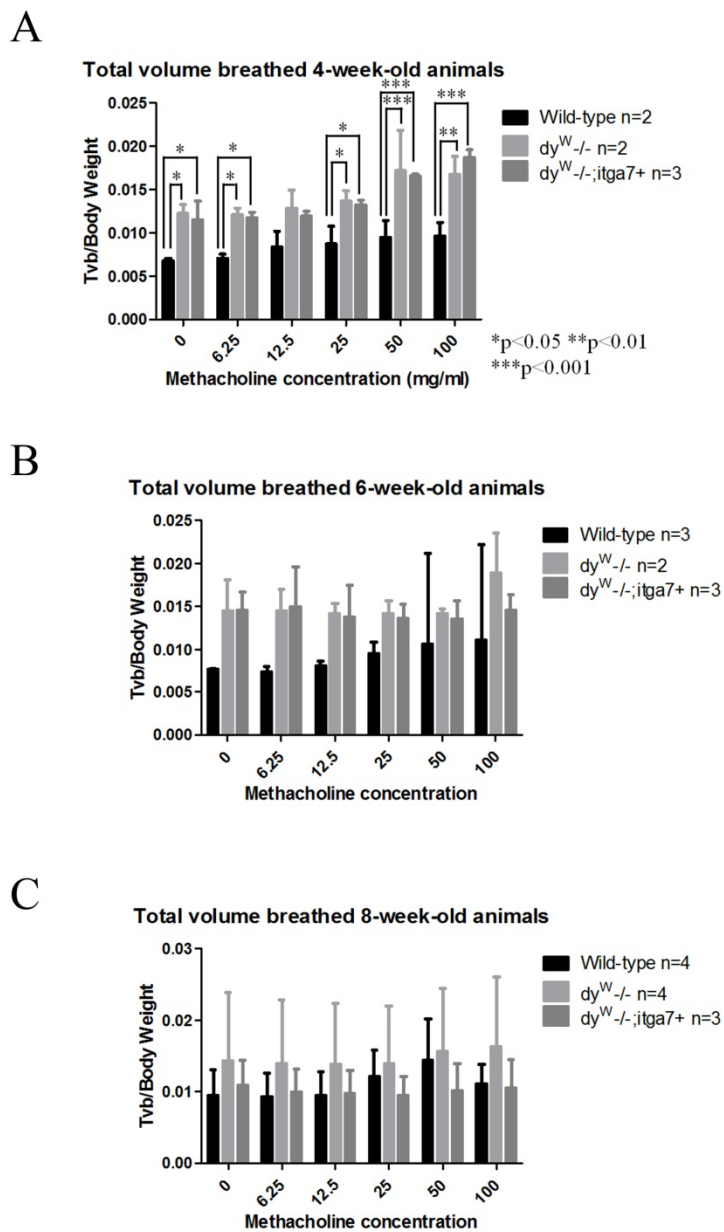
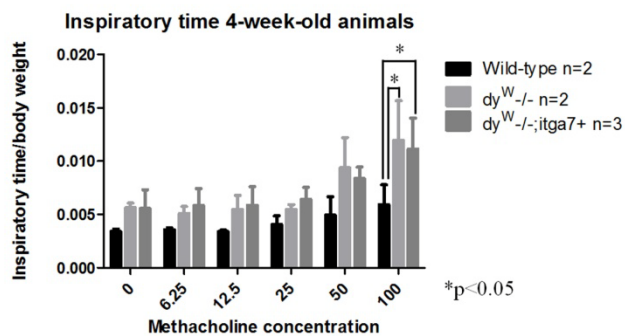


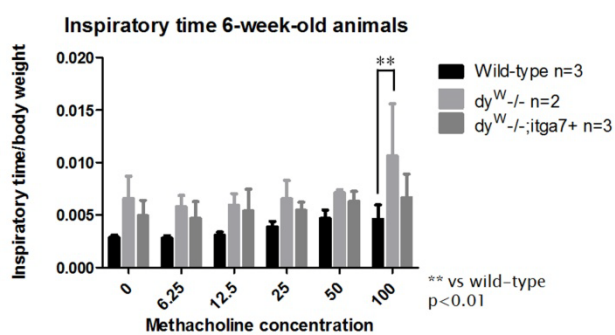
Figure 4.4. Evaluation of total volume breathed in wild-type, $dy^{W-/-}$, and $dy^{W-/-};itga7+$ animals. (A) The total volume of air breathed is significantly higher in both $dy^{W-/-}$ and $dy^{W-/-};itga7+$ animals at all doses of methacholine except for the 12.5 mg/ml

methacholine dose. (B and C) There is no difference in total volume of air breathed between any of the genotypes. (* $P < 0.05$, ** $P < 0.01$, *** $P < 0.001$)

A



B



C

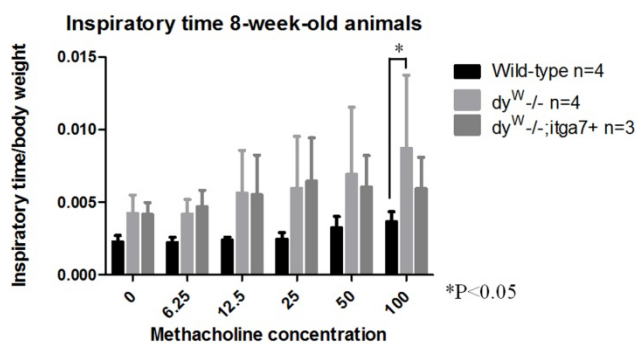


Figure 4.5. Comparison of inspiratory times during a methacholine stimulation test at 4-, 6-, and 8-weeks of age. (A) At 100mg/ml methacholine dose there is a significant difference between the $dy^{W-/-}$ and $dy^{W-/-};itga7+$ animals (B and C) There is a significant

increase in inspiratory time in the dy^W -/- animals compared to wild-type at 100mg/ml methacholine. (* $P < 0.05$, ** $P < 0.01$).

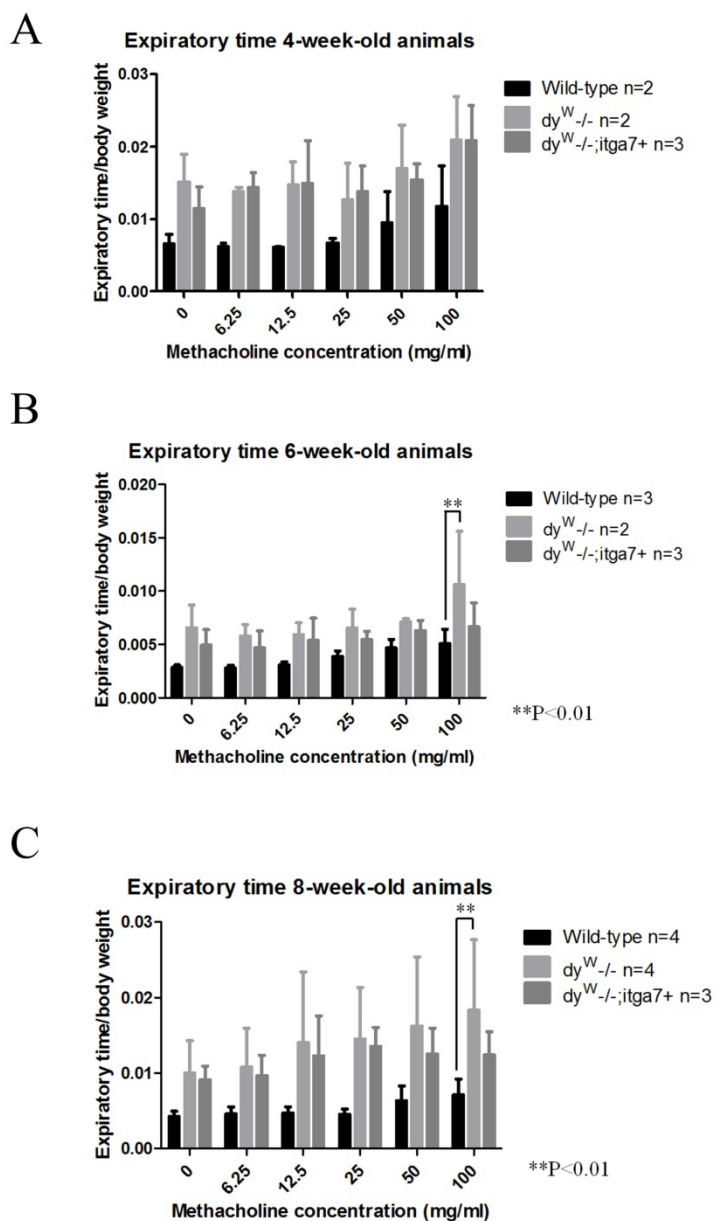


Figure 4.6. Comparison of expiratory time in wild-type, $dy^{W-/-}$, and $dy^{W-/-};itga7+$ animals during a methacholine stimulation test. (A) There is no significant difference across the genotypes at 4-weeks of age. (B) At 6-weeks of age the $dy^{W-/-}$ animals have a significantly longer expiratory time compared to wild-type animals at a methacholine dose of 100mg/ml. (C) At 8-weeks of age and dose of 2 of aerosolized methacholine, the

dy^W -/- animals have a significantly longer expiratory time compared to wild-type.

(**P<0.01)

Chapter 5

Investigation of galectins 1 and 3 as potential biomarkers for MDC1A

Abstract

Merosin deficient congenital muscular dystrophy type 1A (MDC1A) is a devastating, genetic, neuromuscular disorder. MDC1A is caused by mutations in the *LAMA2* gene, which can result in complete loss of, reduction of, or production of a truncated form of laminins-211 and -221. Laminins-211 and -221 are critical components of the extracellular matrix in mature skeletal muscle. This loss of laminin 211/221 results in a severe muscular dystrophy characterized by severe weakness and hypotonia, joint contractures, and limited eye movement. Patients with MDC1A are only rarely capable of independent ambulation. There is currently no cure for MDC1A and only palliative therapy is available for patients. However, recent work has brought potential therapies to the light including targeting anti-apoptotic proteins, enhancing expression of the protein agrin, increased expression of $\alpha7$ integrin, and expression of laminin $\alpha1$. With potential therapeutic agents and targets becoming more prevalent, the need for biomarkers to monitor disease progression has become greater. Biomarkers are small molecules, which can be followed with disease progression usually in either blood or urine. Biomarkers can be used both to follow treatment efficiency and as prognostic indicators. Previously we have identified galectin-1 and galectin-3 as potential biomarkers for MDC1A. In this study we have further evaluated galectin-1 and galectin-3 as possible biomarkers for MDC1A. We have identified galectin-3 as a possible biomarker to follow disease progression in MDC1A. Galectin-3 is used as a prognostic indicator and to monitor treatment response in several types of cancer. The main hypothesis of this work is that galectin-1, galectin-3, or both can be used as biomarkers for MDC1A.

Introduction

Merosin deficient congenital muscular dystrophy type 1A (MDC1A) is a devastating, lethal disease. It is caused by a mutation which leads to either a complete or partial loss of laminins -211 and -221. This is due to a mutation in the *LAMA2* gene, which encodes the protein laminin- α 2. Laminin- α 2 is the α -chain which is present in both the laminin-211 and laminin-221 heterotrimers. The G-domain of the α -chain confers the majority of the binding specificity of the laminin heterotrimer. In skeletal muscle the major laminin receptors are the α 7 β 1 integrin, which displays altered localization or expression in models of MDC1A, and α -dystroglycan (a member of the dystrophin glycoprotein complex).

There is neither a cure nor specific treatment available for MDC1A and patient care is limited to palliative measures. Recently there has been an increase in potential therapeutic agents or targets including omigapil¹¹⁴ and doxycycline¹¹³ both of which reduce apoptosis. With potential therapeutic agents or targets on the rise it is imperative that tools be found which can monitor disease progression and treatment efficacy. These tools should be able to be used with minimally invasive or non-invasive collection procedures; muscle biopsies are too invasive, painful, and impractical to perform on a regular basis as a therapeutic monitoring device. This biomarker needs to be accurate and reproducible; serum creatine kinase is highly variable both in the same patient and across patients¹³¹. Recently we have shown that galectin-1 and -3 are elevated in the dy^W mouse model of MDC1A¹²¹. In this study we show that galectin-3 can be used to follow disease progression in the dy^W mouse.

Lectins bind carbohydrates and are divided into two categories – the C-type lectins and the S-type lectins¹³². The C-type lectins require calcium to function while the S-type lectins do not. The C-type lectins include selectins and pentraxins. The S-type lectins are the galectins. They are found both intracellularly and extracellularly (associated with the extracellular matrix). They are exported via non-traditional pathways as they do not contain extracellular transport sequences^{49;132-135}.

Galectins are small β -galactoside binding proteins in the lectin family¹³⁶. Galectins bind to N-acetyllactosamine. There are currently 15 identified galectin proteins in vertebrates^{49;134}. Galectins have been identified in vertebrates (including fish, birds and amphibians), invertebrates (worms and insects) and “lower animals” (sponges and fungi)¹³⁴. They play a role in the modulation of inflammation, cancer metastasis, cell-extracellular matrix interactions and cell attachment/differentiation¹³⁶.

Galectin-1 and galectin-3 are two of the most studied galectins. Galectin-1 forms a homodimer with a single carbohydrate recognition signal while galectin-3 has a unique N-terminus and is referred to as a “chimeric” galectin^{133;137;138}. Both galectin-1 and galectin-3 play a role in the regulation of inflammation¹³⁶. Galectin-1 can interact with a number of glycosylated proteins including both laminins and the $\alpha 7\beta 1$ integrin⁴⁹. Both are used as biomarkers for several different types of diseases including several forms of cancer and congestive heart failure. The usefulness of galectins-1 and -3 is enhanced by the ability to detect the proteins in serum and urine. They are also good candidates for MDC1A biomarkers because inflammation is a hallmark of MDC1A muscle. Galectin-1 has also been shown to bind to the $\alpha 7$ integrin where it competes with laminin for binding sites^{49;132}.

Materials and methods

Western blotting

Gastrocnemius muscles from 4- and 8-week old male wild-type and $dy^W/-$ animals were pulverized with a mortar and pestle cooled in liquid nitrogen. Protein was extracted in RIPA buffer (50mM Hepes pH7.4, 150mM NaCl, 1mM Na_3VO_4 , 10mM NaF, 0.5% Triton X-100, 0.5% NP40, 10% glycerol, 2mM PMSF, and a 1:200 dilution of Protease Inhibitor Cocktail Set III) and quantified using a Bradford assay (Bio-Rad Laboratories Inc, Hercules, CA). Proteins were separated by SDS-PAGE. Galectin-1 was detected using a 1:1000 dilution of anti-galectin-1 antibody (H00003956-D01P Abnova, Walnut, CA). Galectin-3 was detected using a 1:1000 dilution of anti-galectin-3-antibody (ab53082, Abcam). Blots were incubated with primary antibody overnight at 4°C. Blots were then incubated with a 1:5000 dilution of goat-anti-rabbit-IgG secondary antibody (Li-Cor Biosciences, Lincoln, NE) for 1 hour. Blots were imaged using an Odyssey Imaging System and bands were quantified using the same system. Blots were normalized to α -tubulin using a 1:5000 dilution of an anti- α -tubulin antibody (AbCam, Cambridge, MA) followed by a goat-anti-mouse-IgG secondary antibody (Li-Cor Biosciences, Lincoln, NE).

Quantitative real-time PCR

Total RNA was isolated from five animals of each genotype (wild-type and $dy^W/-$) at 4- and 8-weeks of age using the Trizol method (Invitrogen, Carlsbad, CA). The concentration of RNA was determined and pooled equally by genotype. cDNA was prepared using random hexamers and Superscript III (Invitrogen, Carlsbad, CA) using standard procedures and 3 μ g of pooled RNA. Quantitative real-time PCR was performed

using 50pg of cDNA using SYBR Green Jumpstart (Sigma-Aldrich, St Louis, MO). *Gapdh* was used to normalize transcript levels.

Statistics

A students t-test was used for comparison of the different groups using GraphPad Prism. For qRT-PCR experiments fold change in transcript over wild-type was calculated using the $\Delta\Delta\text{Ct}$ method. The average fold-change \pm s.e.m. was then calculated.

Results

Quantitative Real-Time-PCR was used to determine changes in the transcription of *lgals1* and *lgals3*. Galectin-1 transcript was significantly elevated 9.2 fold in the 4-week-old $\text{dy}^{\text{W}}/-$ animals compared to age matched wild-type animals. *lgals1* transcription was reduced in the 8-week-old animals, however it was still significantly elevated 1.7 fold compared to age matched controls (Figure 5.1.A). Four-week-old $\text{dy}^{\text{W}}/-$ animals also showed a significant increase in galectin-3 transcript (70-fold). At 8-weeks of age the increase in transcript was 9.4 fold for galectin-3 which was still significant (Figure 5.1.B).

Western blotting analysis revealed no significant difference in galectin-1 protein levels at 4- or 8-weeks of age between wild-type and $\text{dy}^{\text{W}}/-$ animals (Figure 5.2.A and 5.2.B respectively). There was also no significant difference between the galectin-1 protein when comparing 4- and 8-week old $\text{dy}^{\text{W}}/-$ animals (Figure 5.2.C). Together this data indicates that galectin-1 is probably not a good candidate for an MDC1A biomarker.

At 4-weeks of age the $\text{dy}^{\text{W}}/-$ animals had significantly more galectin-3 protein than the wild-type animals (Figure 5.3.A). The 8-week old $\text{dy}^{\text{W}}/-$ animals also had

significantly greater galectin-3 levels in their muscles when compared with the 4-week-old animals (Figure 5.3.B). Together these results indicate that galectin-3 should be further explored as a potential biomarker for MDC1A.

Discussion

Finding a biomarker to monitor disease progression and therapeutic effect for MDC1A is becoming more important as researchers find therapeutic agents and targets. Currently the tests available for MDC1A include serum creatine kinase and fine needle muscle biopsies. Serum creatine kinase is not an ideal biomarker due to its inherent variability both in a single patient and between patients. Fine needle biopsies are invasive, painful procedures which are impractical to be done on a regular basis and thus, are a poor technique for monitoring disease and response to therapy. Galectins-1 and -3 are readily assayed in serum or urine when monitoring several forms of cancer and heart disease, making them excellent biomarkers^{58;134}.

Galectin-1 plays a role in the modulation of the immune system, cell-growth, differentiation and repair of skeletal muscle, and cell survival^{49;139;140}. The role of galectin-1 in muscle differentiation and survival is due to its ability to dislodge laminin from its binding sites on the $\alpha7\beta1$ integrin which then allows for fusion of the myoblasts or for satellite cells to come into the area to be repaired^{133;141}. Galectin-1 can also induce apoptosis¹⁴². Our results indicate that while galectin-1 transcript is significantly elevated in the $dy^W/-$ animal, however, this does not translate to an elevation in detectable galectin-1 protein. Therefore, galectin-1 does not appear to be a good candidate as a biomarker for MDC1A.

Uniquely, galectin-3 can bind tightly with both glycosylated and nonglycosylated proteins¹³⁴. Galectin-3 is up-regulated in multiple diseases associated with fibrosis such as liver cirrhosis^{143;144}, idiopathic lung fibrosis¹⁴⁵, chronic pancreatitis¹⁴⁶, and similar animal models (Reviewed in de Boer et al¹³⁴). The first suggested use of galectin-3 as a biomarker was made by van Kimmenade for heart failure, a fibrotic condition¹⁴⁷. MDC1A is also a fibrotic condition which supports the further pursuit of galectin-3 as a biomarker for MDC1A.

In this study we show that galectin-3 is significantly elevated at both the transcript and protein levels and, therefore, might serve as an easily obtainable, objective, and minimally invasive biomarker for MDC1A. This may be due to the ability of galectin-3 to regulate the cell cycle and apoptosis (both increasing and decreasing depending upon the situation). Galectin-3 can also bind tightly with CD11b and collagen IV¹³⁴. Again these can be directly associated with MDC1A. Galectin-3 is expressed by macrophages, monocytes, and mast cells^{133;134;136}. It is also associated with fibrosis. Inflammation, particularly of the macrophage and monocyte line, and fibrosis are two of the hallmark features of MDC1A¹²¹. Galectin-3 can also bind tightly with fibronectin, and tenascin-C. Tenascin-C was recently shown to be up-regulated in the $dy^W/-$ mouse model for MDC1A. As disease progresses so do these characteristics and along with them, we would expect to see an increase in galectin-3.

Galectin-3 transcript and protein appear to be highest early in disease progression (Figures 5.1 and 5.3). This pattern is true for gastrocnemius muscle. We need to evaluate serum and other skeletal muscles (such as the Tibialis Anterior muscle which is a fast-twitch muscle as opposed to the slow-twitch gastrocnemius muscle). Transcript

and protein levels of galectin-3, as well as galectin-1, may also go down because of the increased disease in the muscle. One possible reason for the decline in protein and transcript may be that the tissue is fibrotic enough at 8-weeks of age that it is no longer actively producing collagen. This would indicate the presence of fewer fibroblasts and therefore, less galectin-3. We need to test more tissues (including serum) at more time points to more accurately predict what the levels of galectin-3 protein are at different time points in disease.

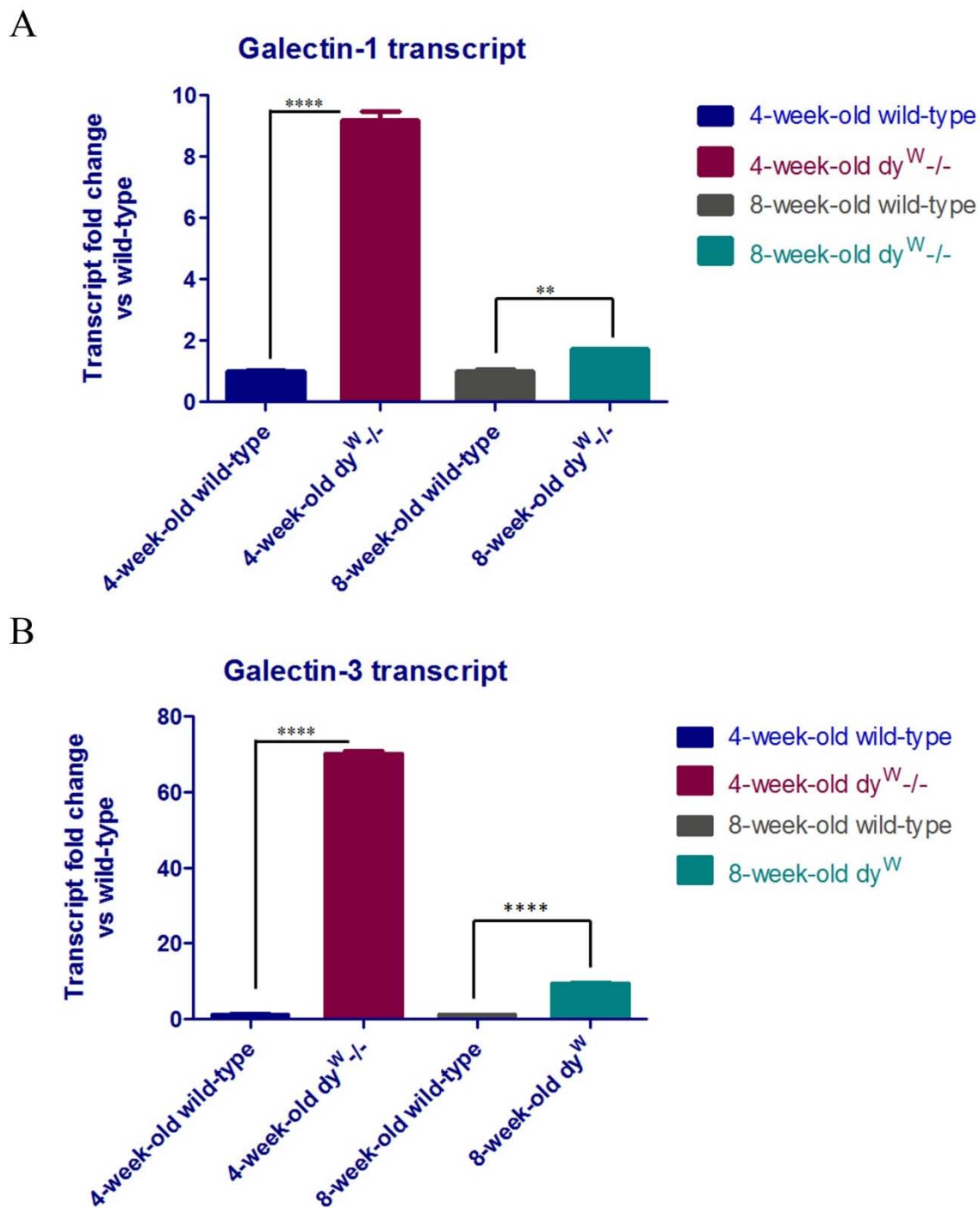


Figure 5.1. Transcription of *lgals1* and *lgals3* are altered in the $dy^{W-/-}$ mouse. (A)

The transcript for *lgals1* (galectin-1) is significantly increased over wild-type in both 4-

and 8-week old animals. (B) Galectin-3 transcript (*lgals3*) is also elevated in both the 4- and 8-week old animals compared to wild-type controls. **P<0.01, ****P<0.00001.

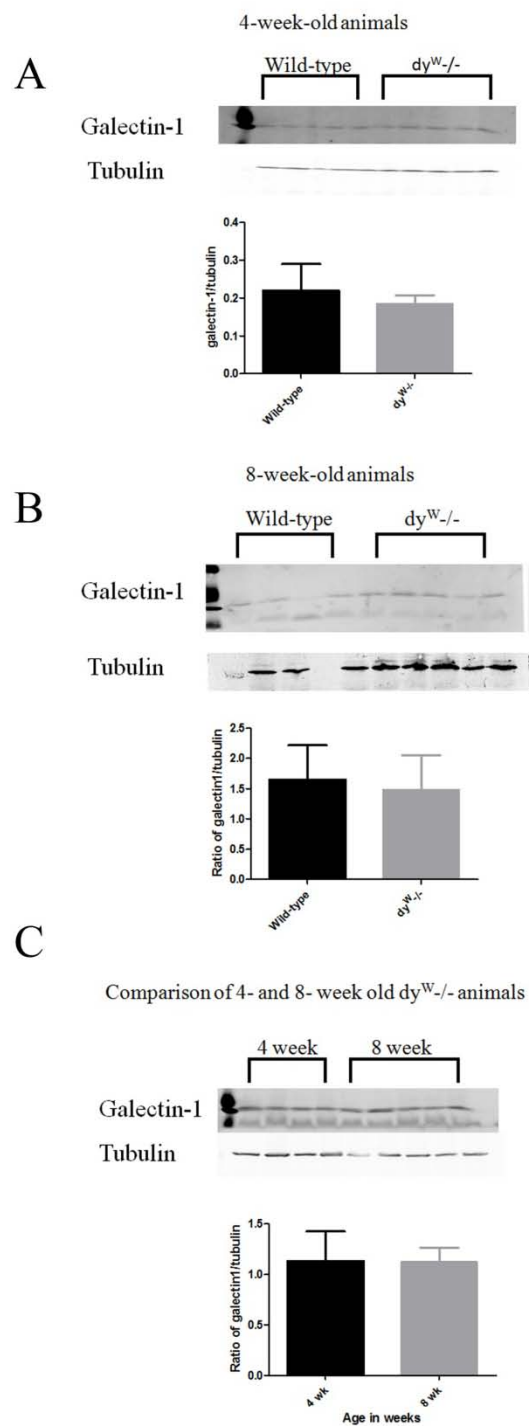


Figure 5.2. Western blotting for galectin-1 in $dy^{W-/-}$ and wild-type mice at 4- and 8-weeks of age. (A) There is no significant difference in galectin-1 protein in the muscles of 4-week-old $dy^{W-/-}$ mice when compared to wild-type animals. (B) The level of

galectin-1 protein in the gastrocnemius muscle of 8-week-old $dy^W/-$ animals compared to wild-type are not significantly different. (C) There is no difference in galectin-1 protein in $dy^W/-$ mice at 4- and 8-weeks of age.

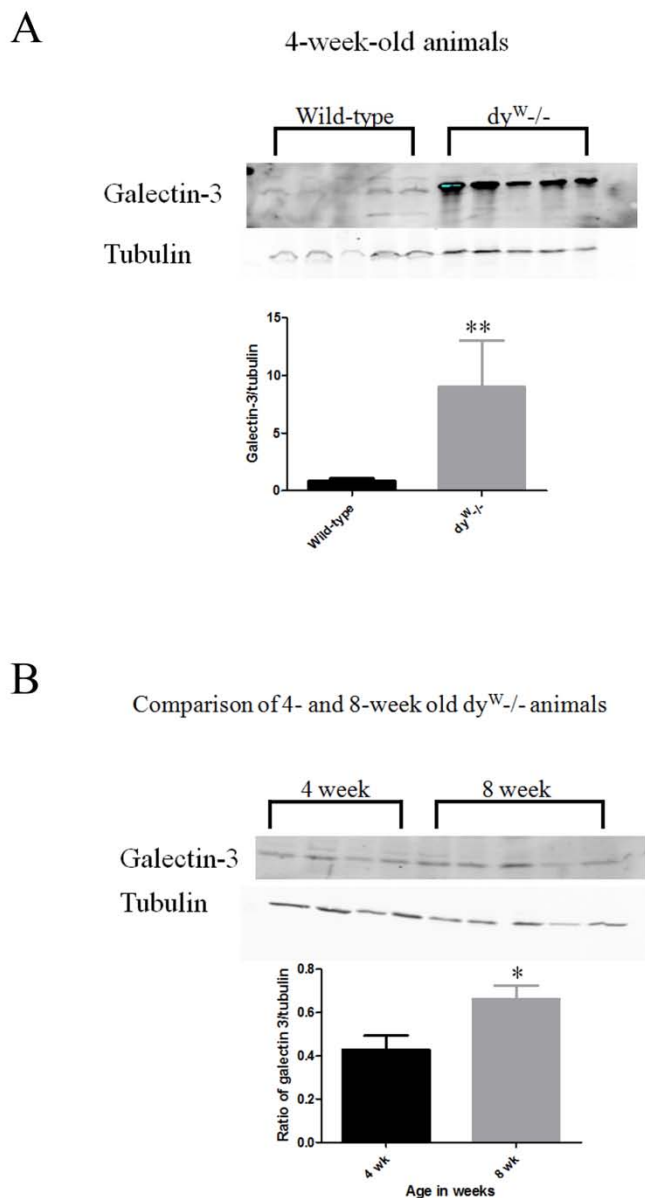


Figure 5.3. Immunoblotting experiments for galectin-3 protein in $dy^{W/-}$ and wild-type animals. (A) There is a significant increase in galectin-3 protein in the $dy^{W/-}$ mice compared to wild-type animals at 4-weeks of age (** $P < 0.01$) (B) There is a significant increase in galectin-3 protein in 8-week old $dy^{W/-}$ mice compared with 4-week-old $dy^{W/-}$ mice.

Chapter 6

Conclusions and future directions

The work presented in this dissertation explores the role of the $\alpha 7$ integrin in the dy^W $-/-$ mouse model of merosin deficient congenital muscular dystrophy 1A (MDC1A). While examining this role we also found a potential biomarker for MDC1A. We have shown that the $\alpha 7$ integrin plays a significant role in MDC1A disease as shown by the improvement seen with enhanced expression of the $\alpha 7$ integrin in the skeletal muscle of a mouse model of MDC1A (the dy^W $-/-$; $itga7$ $+$ animals). The dy^W $-/-$; $itga7$ $+$ animals display reduced muscle pathology at both 4- and 8-weeks of age, have increased longevity, and maintain their strength over time. We have also shown that these changes can be attributed to a stabilization of the extracellular matrix. Even though the matrix is abnormal in the dy^W $-/-$; $itga7$ $+$ mice, allowing it to become stable can lend strength to the myofibers attachment to the matrix and let alternative binding become possible (such as $\alpha 7$ integrin with galectin-1 or -3). Part of the matrix stabilization can be related to increased expression of tissue inhibitor of metalloproteinase 1 (TIMP1) and the decreased expression of matrix metalloproteinase 2 (MMP2). TIMP1 directly inhibits MMP2.

The increased longevity of the dy^W $-/-$; $itga7$ $+$ animals can most likely be explained by reduced diaphragm pathology. The most common cause of death in MDC1A patients is respiratory failure. The diaphragm histopathology data from Chapter 3 and the plethysmography data in Chapter 4 help to support this conclusion. The histology shows that the diaphragm muscle of the dy^W $-/-$; $itga7$ $+$ animals has less variation in fiber size and a reduction in the pathological appearance of the muscle. The plethysmography data show that the respiratory function in the dy^W $-/-$ is impaired, as shown by increases in expiratory and inspiratory time, when compared with wild-type. These parameters of pulmonary disease were not significantly different between the dy^W $-/-$

-;itga7+ animals and wild-type, with the exception of the 4-week-old $dy^W/-;itga7+$ animals. More animals are needed to complete the statistical analysis of the plethysmography data.

While determining the mechanism of $\alpha7$ integrin's rescue of the $dy^W/-$ mouse we found that galectin-1 and galectin-3 were both elevated in the $dy^W/-;itga7+$ animals. These two proteins are already established biomarkers for several different types of cancer and heart disease¹³⁶. Biomarkers are traceable small molecules which are used to either diagnose a disease or monitor the progression of a disease. Galectin-3 can be easily measured in either serum or urine. There are currently no biomarkers being used for MDC1A. Patient monitoring includes serum creatine kinase, a byproduct of muscle breakdown. Unfortunately, serum creatine kinase is highly variable both between patients and within the same patient at different time points. Interestingly, galectin-1 is elevated by valproic acid, a drug that is generating interest as a therapeutic for muscular dystrophy⁴⁹.

This work shows that enhanced expression of the $\alpha7$ integrin in the skeletal muscle of the $dy^W/-$ mouse model of MDC1A increases longevity, reduces muscle pathology, and allows for maintenance of strength. These beneficial effects are attributable to stabilization of the extracellular matrix. This more stable matrix is able to allow for more stable attachments between the muscle fibers and the extracellular matrix. This enhanced attachment occurs in the skeletal muscle (due to the use of the muscle creatine kinase promoter) which includes the diaphragm. Reduced pathology in the diaphragm results in better diaphragm function over time. This is supported by the

plethysmography results. The improved diaphragm function also explains at least a portion of the increased life span noted.

We need to continue with the plethysmography data to continue evaluation of Penh (which is not significantly different at this time but is trending towards being elevated in the 8-week-old mice during methacholine stimulation), inspiratory time, and expiratory time. We also need to evaluate several parameters with the plethysmograph monitors that were not reported here. The effect of the transgene on the NMJs should be further examined as well. Firstly, western blotting should be used as a second method of determining numbers of nACHrs, similarly ligand-binding assays could be used. It is also possible to use a whole mount preparation of the diaphragm muscle since it is only a few cell layers thick, this can then be incubated with α -bungarotoxin to determine number, size, and location of NMJs.

The success of the transgenic approach towards overexpression of the $\alpha 7$ integrin has led us to begin a drug screen looking for compounds which up-regulate $\alpha 7$ integrin. We are scanning several compounds in human cells (both normal control and two different MDC1A lines) for their ability to up-regulate $\alpha 7$ integrin protein production. These compounds were chosen because they have been shown to up-regulate $\alpha 7$ integrin in mouse myoblast lines. This drug screen may lead to a larger scale screen to help identify compounds that enhance $\alpha 7$ integrin expression.

Several therapeutic approaches have been tried in the *mdx* mouse, which have not yet been tested in laminin $\alpha 2$ deficient mice. One of these approaches is the use of the

antifibrotic drug halofuginone¹⁴⁸. Halofuginone has also been associated by increased grip strength and free-running ability with less damage seen after exercise¹⁴⁹.

There are also a number of other transgenic approaches, which have been used to evaluate therapeutic targets for muscular dystrophy. Transgenic upregulation of utrophin has been used in the *mdx* model for DMD; it resulted in decreased CK and CLN as well as causing a restoration of the DGC¹⁵⁰. Similarly, upregulation of heregulin is beneficial for the *mdx*; it acts by regulating the utrophin promoter A¹⁵¹. Increasing nitric oxide synthases is also beneficial in the *mdx* mouse by decreasing inflammation, CLN, fiber size variation and CK¹⁵². Another approach in the *mdx* mouse that appears to work by increasing utrophin is increasing calcineurin levels¹⁵³. Stimulation of calcineurin signaling attenuates the dystrophic pathology in *mdx* mice.

At least one promising therapeutic target in the *mdx* mouse has been shown to have a detrimental effect on *dy*^W animals. Knockout of the protein myostatin improves pathology in the *mdx* mouse by increasing muscle mass, decreasing muscle degeneration and reducing fibrosis^{154;155}. However, myostatin blockade does cause weaker tendons and impaired force generation^{156;157}. This same approach in the *dy*^W mouse leads to earlier mortality. It is believed that this is due to a loss of brown fat in the pups¹⁵⁸.

Ovrexpression of ADAM12 (a disintegrin and metalloproteinase 12) also showed promise in the *mdx* mouse by increasing muscle regeneration and alleviating skeletal muscle pathology; some of its success was attributed to enhanced expression of $\alpha 7$ integrin^{104;159}. ADAM12 was shown to not be beneficial to the *dy*^W mouse.

Transgenic overexpression of Galgt2 has shown promise in both the *mdx* mouse and the *dy*^W mouse. In both models it improves histologic hallmarks of muscular

dystrophy, increases agrin production and increases glycosylation of glycolipids^{104;160}. Its effects on survival were not studied in the dy^W mouse¹⁰⁴. Other transgenic approaches that have been found to alleviate disease in the laminin $\alpha 2$ deficient animals include: expression of laminins $\alpha 2$ and $\alpha 2$, mini-agrin, and linker molecules^{20;29;82;104;115;119}. Linker molecules help to strengthen the association between laminin $\alpha 4$ and the dystroglycans. This helps to form a more stable attachment between the muscle cells and the extracellular matrix; agrin is one example of a linker molecule.

Omigapil is a pharmaceutical agent, which has been tested in the dy^W mouse. It functions by inhibiting an apoptotic pathway (the Gapdh-siah1-cbp/p300-p53 pathway). It reduces apoptosis, reduces weight loss, increases activity, and increases the lifespan of experimental animals¹¹⁴. Doxycycline is another pharmaceutical that has been successfully tested in the dy^W mouse¹¹³. Girgenrath *et al*¹¹³ showed a reduction in inflammation, reduced Bax expression (a pro-apoptotic protein), reduced apoptosis, increased Akt phosphorylation (anti-apoptotic) and increased lifespan. Doxycycline is known to have anti-apoptotic effects that are beneficial in the dy^W mouse¹¹². Another characteristic of the aminoglycoside antibiotics which makes them attractive therapeutic strategies is their ability to induce read through of stop codons. Some of the more common mutations in MDC1A are premature stop codons. However, even though gentamicin was shown to induce read through of a premature stop codon in patient cells, it still did not lead to production of laminin $\alpha 2$ protein¹⁶¹.

Some of the most promising approaches to therapy in the dy^W mouse have included either replacing laminin $\alpha 2$ or re-introducing laminin $\alpha 1$. Transgenic expression of laminin $\alpha 1$ chain using a universal promoter greatly reduces pathology in

the dy^{3K} mice. It also significantly increases lifespan and is able to alleviate the peripheral neuropathy by improving myelination¹⁰⁷. Expression of laminin $\alpha 2$ chain in the skeletal of both the dy^W and dy^{2J} models improves the muscular dystrophy of the animals and the life span (in the dy^W mouse) with no effect on the peripheral neuropathy⁸².

The work presented in this dissertation builds upon previous work. It was previously shown that enhanced expression of the $\alpha 7$ integrin could alleviate the dystrophic phenotype seen in the severely dystrophic $mdx/utr^{-/-}$ mouse (which lacks both dystrophin and utrophin). Along with improving both the skeletal muscle and cardiac muscle phenotype, the overexpression resulted in at least a 4-fold increase in lifespan^{42;45}. In these animals the mechanism of action involves increasing the attachment of the muscle cells to the extracellular matrix by increasing a laminin receptor (the $\alpha 7\beta 1$ integrin). We propose that the effect of overexpressing the $\alpha 7$ integrin in the dy^W mouse involves increased $\alpha 7\beta 1$ integrin associated signaling (including the anti-apoptotic Akt pathway) and stabilizing the extracellular matrix in its altered form (Figure 6.1).

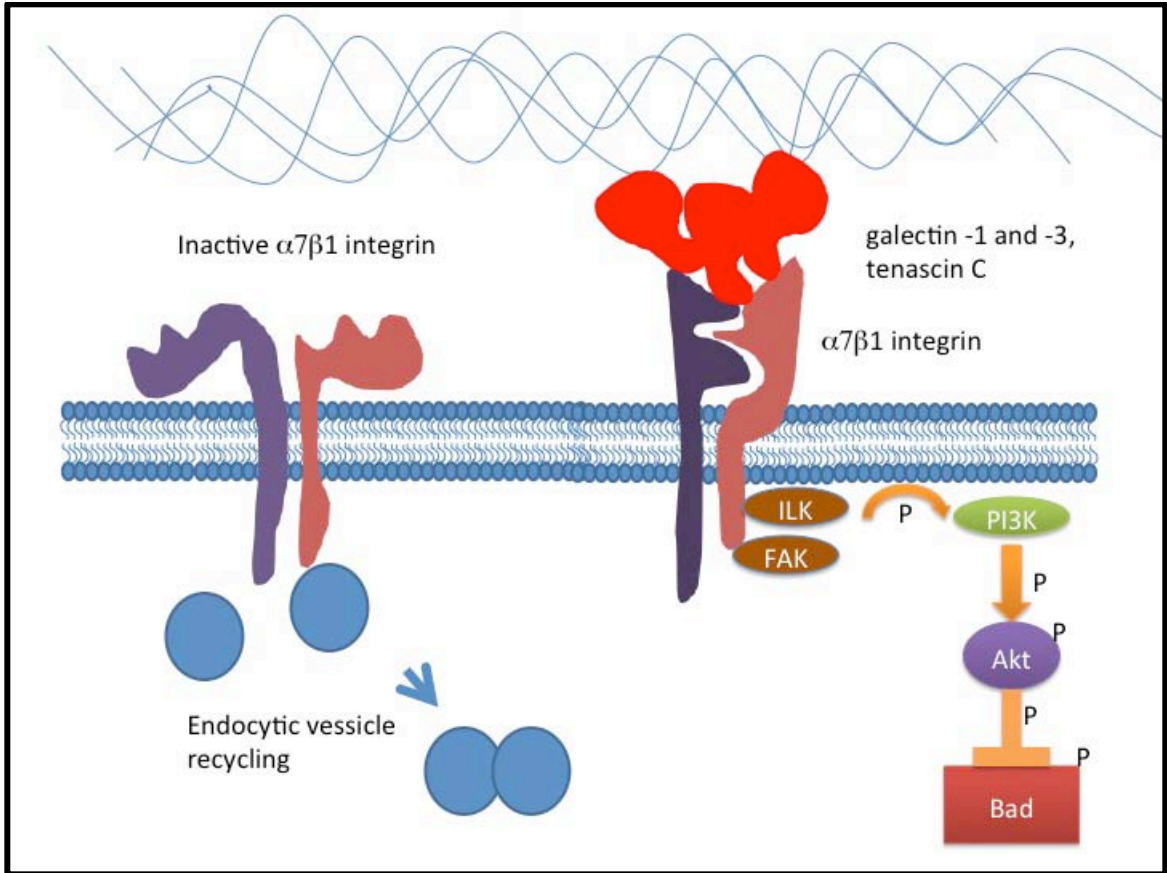


Figure 6.1 Proposed mechanism of action. In the presence of enhanced $\alpha7$ integrin expression, integrin activation occurs and signaling pathways lead to inactivation of Bad and reduced apoptosis.

APPENDIX

APPENDIX A.1

**INFLUENCE OF THE EXTRACELLULAR MATRIX AND INTEGRINS ON
VOLUME-SENSITIVE OSMOLYTE ANION CHANNELS IN C2C12
MYOBLASTS**

Abstract

The purpose of this study was to determine whether extracellular matrix (ECM) composition through integrin receptors modulated the Volume-Sensitive Osmolyte Anion Channels (VSOACs) in skeletal muscle derived C2C12 cells. Cl⁻ currents were recorded in whole-cell voltage clamped cells grown on Laminin (LM), Fibronectin (FN) or in the absence of a defined ECM (NM). Basal membrane currents recorded in isotonic media (300 mosmol/kg) were larger in cells grown on FN (3.8-fold at +100 mV) or LM (8.8-fold at +100 mV) when compared to NM. VSOAC currents activated by cell exposure to hypotonic solution were larger in cells grown on LM (1.72-fold at +100 mV) or FN (1.75-fold at +100 mV) compared to NM. Additionally, the kinetics of VSOAC activation was \approx 27% quicker on FN and LM. These currents were tamoxifen-sensitive, displayed outward rectification, reversed at E_{Cl} and inactivated at potentials > +60 mV. Specific knockdown of β_1 integrin by short hairpin RNA interference (shRNAi) strongly inhibited the VSOAC Cl⁻ currents in cells plated on FN. In conclusion, ECM composition and integrins profoundly influences the biophysical properties and mechanisms of onset of VSOACs.

Keywords

Extracellular matrix, Integrins, Volume Sensitive Osmolyte Anion Channels, Cl⁻ currents, C2C12 mouse myoblasts, shRNAi knockdowns

Introduction

The mechanisms that link cell swelling to activation of volume-sensitive outwardly rectifying Cl⁻ channels (VSOACs) remain unknown even though a number of

intracellular signaling pathways have been implicated^{162;163}. Activation of these channels is believed to be involved in cell volume homeostasis since they may contribute to regulatory volume decreases (RVD) in response to cell swelling¹⁶³⁻¹⁶⁵. The actual stimulus for channel activation may involve mechanical stretch of the membrane or cortical actin cytoskeleton, rather than cell volume changes *per se*, and thus these channels might be mechanosensitive. However, despite numerous attempts, direct evidence supporting the hypothesis that VSOACs may represent a new class of mechanosensitive anion channels has been lacking. Recently, new studies have resurrected the mechanosensitive hypothesis by providing convincing evidence that mechanical stretch of β_1 integrin receptors can activate anion channels. Specifically, an elegant study by Browe & Baumgarten has documented the activation of stretch-activated anion channels (SAC) by mechanical stimulation of the β_1 integrin (see details below) on rabbit ventricular myocytes¹⁶⁶. This integrin-mediated SAC current shared many properties with VSOACs: 1) a reversal potential near E_{Cl} , 2) partial inactivation at potentials $> +10$ mV, 3) a time course of activation that was similar to that of VSOACs evoked by cell swelling, 4) sensitivity to block by tamoxifen (10 μ M), and 5) sensitivity to the PTK inhibitor genistein, and the Src and FAK inhibitor PP2. Subsequent work showed that the β_1 integrin-mediated activation of SAC involves a paracrine/autocrine stimulation of type 1 angiotensin receptor (AT_1R) by angiotensin II (AII) that is locally released by the myocytes during stretch (5). In addition, AT_1R -induced stimulation of SAC involves a redox pathway implicating NADPH oxidase and formation of superoxide anion and H_2O_2 . The nature of the integrin receptor(s) and their ECM ligands along with the molecular identity of the anion channel activated remain undefined.

Mechanical stress of myocytes, mediated by the extracellular matrix and intracellular cytoskeleton, is an important determinant of muscle mechanics. In striated myocytes, integrins are localized to costameres at Z-discs where they contribute to the structural integrity of the muscle and are well positioned to sense mechanical stress generated by muscle contraction. At this site integrin receptors link the ECM to the force-generating actin-myosin cytoskeleton via a number of cytoplasmic proteins. In non-muscle cells integrins have been shown to function as mechanotransducers¹⁶⁷. In myocytes, integrins are proposed to function as bidirectional transducers of both mechanical and molecular signals between the ECM and the cytoplasm. This mechanotransduction regulates the activation of signaling pathways that alter myocyte gene expression and cytoskeletal reorganization. Therefore, integrins are ideal candidates for the role of mechanotransducers in myocytes.

Integrins are heterodimeric α/β glycoprotein receptors. The pairing of specific α and β integrin subunits dictate the extracellular matrix (ECM) proteins the cell can adhere to upon activation¹⁶⁸. Two of the integrin receptors expressed on skeletal myocytes are $\alpha_7\beta_1$ and $\alpha_5\beta_1$ integrin¹⁶⁹. Aside from playing a structural role, integrins can modulate cell behavior and growth through the induction of intracellular signaling pathways. The influence of ECM composition on myoblast phenotype is well documented. Attachment of myoblasts to fibronectin through the $\alpha_5\beta_1$ integrin promotes proliferation while attachment to laminin through the $\alpha_7\beta_1$ integrin promotes differentiation. Accordingly, the laminin receptor, $\alpha_7\beta_1$ integrin, must signal in a manner distinct from the fibronectin

receptor, $\alpha_5\beta_1$ integrin. Therefore, it is important to determine if VSOAC activation is dependent on ECM composition and/or integrin receptor subtype.

Little work has been done to determine if the composition of the ECM to which the integrins bind influence the activation of VSOACs. This study sought to better understand the pathway(s) by which integrins regulate VSOAC activation and/or RVD in myocytes. Specifically we examined if myoblast attachment to different ECM proteins differentially regulated Cl^- channel activation and if channel activation could be blocked in the absence of integrin attachment.

Materials and Methods

Cell culture and reagents

C2C12 mouse myoblasts are cultured in DMEM + 4.5g/L D-glucose, L-glutamine, 110mg/L sodium pyruvate, 10% heat inactivated fetal bovine serum, 100U/ml penicillin and 100mg/ml streptomycin at 37°C in 5% CO_2 . Glass coverslips were coated with 10 $\mu\text{g/ml}$ human fibronectin (gift from J.A. McDonald) or mouse laminin (Invitrogen) for 20 minutes.

Lentiviral transduction

Day 1, 1.6×10^4 C2C12 myoblasts (American Type Culture Collection, Rockville, MD) were seeded on a 100 mm plate and grown at 37°C 5% CO_2 . Day 2, lentiviral particles (TRCN0000066643, TRCN0000066644, TRCN0000066645, TRCN0000066646, Sigma-Aldrich, St. Louis, MO) that contained shRNAi's specific to β_1 integrin) were applied at an MOI of 25 and polybrene (Sigma-Aldrich, St. Louis, MO) at 8 $\mu\text{g/ml}$ was added. Day 3, media was replaced with fresh complete media. Day 4,

puromycin at 1.5 μ g/ml (Sigma) was added. Selection pressure was maintained for 10-12 days until single colonies were formed and cloned.

Protein extraction

Cells were scraped, homogenized in TNET (50 mM Tris HCl, pH 7.4, 150 mM NaCl, 1 mM EDTA and 0.5% Triton X-100) containing 1X protease inhibitor cocktail (Sigma, St. Louis, MO), sonicated (10 s) and centrifuged (13,000 rpm, 10 min, 4°C). Protein concentration in supernatant was determined with BCA Protein Assay Kit (Pierce, Rockford, IL).

Immuno-blot analysis

Immuno-blot analysis was performed as described previously (26). Specifically, 10-40 μ g protein extract/gel lane was electrophoresed on a 4-12% NuPAGE Bis-Tris gradient gel (Invitrogen, Carlsbad, CA) and transferred to Hybond-C Extra nitrocellulose membrane (Amersham, UK). Antibodies used included, AB47 anti α_5 integrin (gift from Dr. John A. McDonald), AB1952 (Millipore) or MC229 (gift from Dr. John A. McDonald) or AB1952 (Chemicon) anti β_1 integrin, B2347 anti α_7 integrin (gift from Dr. Dean Burkin). Un-Scan-It software was used to analyze protein expression on the immune-blots.

Microscopy and immunofluorescent staining

A laser-scanning confocal microscope (Olympus FluoView 1000) was used to collect fluorescent images. Cells were fixed in 3.7% formaldehyde in phosphate buffered saline for 10 minutes. Cells were permeabilized with 0.1% Triton X100, blocked with 1% BSA than stained incubated with FITC-phalloidin, bis-benzamide and 9EG7 (1/20, β_1 integrin specific antibody, gift of D.V. Weber). Primary rat antibody was detected with

biotinylated donkey anti-rat (Jackson ImmunoResearch Laboratories, Inc.) followed by an AlexaTM 594-streptavidin conjugate (Molecular Probes).

Electrophysiological methods

Proliferating C2C12 myoblasts were seeded on coverslips coated with fibronectin (FN), laminin (LM) or in the absence of matrix and allowed to grow in a CO₂ incubator (Thermo Scientific Heraeus, model Hera Cell 150, Waltham, MA) at 37°C for 12-16 hours. Coverslips were set on the stage of an inverted IX-71 Olympus microscope (Center Valley, PA) and superfusion initiated with the isotonic solution described below at a rate of ≈ 1 ml/min. The cells were superfused for at least 5 min prior to any recording. Macroscopic currents were recorded at room temperature in the standard whole-cell configuration mode of the patch clamp technique using a patch clamp amplifier (model PC-505B, Warner Instruments, LLC, Hamden, CT). Patch pipettes (≈ 1 μ m in diameter; tip resistance was 2-4 M Ω when immersed in the external isotonic solution described below) were pulled from borosilicate glass capillaries (Sutter Instrument Company, Novato, CA) with a Sutter P-57 puller (Sutter Instrument Company). Pipette and stray capacitances as well as series resistance were compensated for in all experiments. For most experiments, an Ag/AgCl pellet placed in the bathing chamber was used as the reference electrode. In all ion exchange experiments carried out to determine the relative permeability of the channels to iodide or aspartate relative to chloride, a 3M KCl agar bridge was used instead to minimize changes in junction potential associated with external replacement of Cl⁻ with I⁻ or Asp⁻. Voltage clamp protocols were computer-driven using Digidata 1320 series acquisition system and pCLAMP 9.2 (Molecular Devices, Sunnyvale, CA, USA). Membrane currents were low-

pass filtered at 1 kHz before being acquired at a sampling rate of 1 kHz. After gaining whole-cell access, C2C12 cells were held at the standard holding potential -40 mV, and cell dialysis was allowed to proceed for at least 5 min before any voltage clamp protocol was initiated. In most figures, current was expressed as current density (pA/pF) by dividing the measured current by the cell capacitance, which was estimated by integrating the mean of five consecutive capacitative current transients elicited by 20 ms test pulses from -50 to -60 mV (with Clampfit 9.2, Molecular Devices, Sunnyvale, CA, USA). Cell capacitance was calculated using the following equation: $C = Q/\Delta V$, where C is the whole-cell capacitance (in pF), Q is the amount of charge transferred (in fC), and ΔV is the magnitude of the voltage clamp step.

The K^+ -free pipette and external solutions were designed to minimize the activity of endogenous K^+ channels by including cesium in the internal solution, and tetraethylammonium chloride (TEA) and barium chloride in the superfusate. The external isotonic and hypotonic solutions were made using a common base solution which contained: 90mM NaCl; 0.66mM $MgCl_2$; 1mM $CaCl_2$; 2mM $BaCl_2$; 10mM TEA-Cl; 10mM Hepes; 5.5mM Glucose; pH adjusted to 7.4 with NaOH. The osmolality of this solution was ≈ 220 mosmol/kg H_2O as determined by a high precision osmometer (The Advanced Micro Osmometer, model 3300, Advanced Instruments, Inc., Norwood, MA). Mannitol was added to the base solution to make the isotonic solution with an osmolality of 300 mosmol/kg H_2O . The pipette solution contained (mM): CsCl, 90; TEA-Cl, 18.0; Hepes, 5.0; MgATP, 5.0; EGTA, 5.0; adjusted to pH 7.2 with CsOH. The osmolality of the pipette solution was similarly adjusted to 300 mosmol/kg H_2O by adding mannitol.

All solutions had identical ionic strength. For all anion exchange experiments, NaCl was replaced by an equimolar concentration of NaI or Na-Aspartate (90 mM).

After seal rupture and measurement of cell capacitance, a constant step protocol was subsequently initiated to monitor current magnitude over ~ 5 min while the cell was superfused with the isotonic solution. This allowed for stabilization of membrane current during cell dialysis. For all voltage clamp protocols, the cells were consistently held at a holding potential (HP) of -40 mV. The double-pulse protocol consisted of a 500 ms step to $+80$ mV followed by a return step to -80 mV applied every 10 s. The same protocol was used to monitor the effects on membrane current of switching the external isotonic solution to the hypotonic solution, or to examine the effects of tamoxifen on the VSOAC current elicited by hypotonic medium. Current-voltage (I-V) relationships were obtained by a single pulse protocol consisting of 500 ms steps ranging from -100 to $+120$ mV (10 mV increments at 0.05 Hz). Finally, reversal potential measurements of the VSOAC current in cells exposed to solutions of different anion compositions were carried out using a 2 s ramp protocol ranging from -100 to $+120$ mV (110 mV/s) imposed at a frequency of one ramp every 10 s.

We used the following variant of the Goldman-Hodgkin-Katz equation to determine the relative anion permeability of the VSOAC current under bi-ionic conditions in which external Cl^- was partially replaced by I^- or aspartate $^-$:

$$P_X/P_{\text{Cl}} = \{((\exp(V_{\text{rev}} \times zF/RT)) \times [\text{Cl}^-]_i) - [\text{Cl}^-]_o\}/[X^-]_o$$

Where X represents I^- or Asp $^-$, V_{rev} is the reversal potential measured in the presence of external iodide or aspartate, zF/RT has its standard meaning, $[\text{Cl}^-]_i$ and $[\text{Cl}^-]_o$ are the

internal (107.32 mM) and external (17.8 mM) Cl^- concentrations, respectively, and $[\text{X}]_o$ is the external concentration of Γ or Asp^- (90 mM).

Reagents

TEA and tamoxifen were purchased from Sigma-Aldrich (St. Louis, MO). TEA was directly added to the external solution in powder form whereas tamoxifen (Sigma-Aldrich) was prepared as a 10 mM stock solution in DMSO and kept in small aliquots at 4°C. Each aliquot was diluted in the external solution at a final concentration of 10 μM immediately prior to the experiment. The final concentration of DMSO never exceeded 0.1%, a concentration that had no effect on the basal Cl^- and VSOAC currents.

Statistics

Membrane currents were analyzed with Clampfit 9.2 (Molecular Devices) and Origin 8.0 (OriginLabCorp). All pooled data are expressed as means \pm SEM. Comparisons among multiple means were performed using one-way ANOVA with Bonferroni *post-hoc* test. A *P* value of < 0.05 was considered to be statistically significant.

Results

Influence of matrix proteins on C2C12 phenotype.

ECM composition has a profound influence on myoblast phenotype. C2C12 cells were grown on uncoated coverslips (NM), laminin (LM)-coated or fibronectin (FN)-coated cover slips for 12 hours display an altered distribution of β_1 integrin containing focal adhesions and actin stress fibers. Figure A.1.1 illustrates the diverse phenotypes observed. Cells plated on uncoated coverslips lacked well-defined integrin containing focal adhesions complexes at the cell periphery, had a few thin stress fibers and remained

small and compact in shape (A). In comparison, cells grown on FN contained numerous integrin-containing focal adhesions, an increase in distinct stress fibers and spread extensively (B). In striking contrast, cells plated on LM spread in a manner similar to the FN plated cells but contained numerous thick stress fibers and strong staining of peripheral focal contacts (C). All images were collected with identical camera settings and stained simultaneously. Immuno-blot analysis demonstrated that C2C12 cells grown on uncoated tissue culture plates expressed all three integrin subunits examined in these studies, β_1 , α_5 and α_7 integrin (Figure A.1.1D).

Influence of matrix proteins on the properties of VSOAC currents.

Whole-cell macroscopic volume-sensitive osmolyte anion (VSOAC) currents recorded from C2C12 cells were elicited by reducing the osmolality of the K^+ -free bathing solution from 300 to 220 mosmol/kg H_2O . Figure A.1.2 shows the results of two typical experiments, one from a cultured cell plated on cover slips in the absence of matrix (NM; panel A) and the other plated on fibronectin (FN; panel B). The two graphs in Figure A.1.2Aa and A.1.2Ba illustrate the time course of changes in membrane current density (holding potential = -40 mV) measured at the end of 500 ms steps to +80 mV (filled squares) and at the end of 500 ms return steps to -80 mV (open circles). The equilibrium potential for Cl^- was purposely set to 0 mV to help visualize current rectification when stepping to +80 and -80 mV. Figures A.1.2Ab and A.1.2Bb each depicts sample traces recorded in isotonic (top) and hypotonic (middle) solutions in response to the voltage clamp protocol shown below. Measurements from these traces are indicated by the filled circle and filled triangles and reported in the corresponding graph. Basal membrane current in isotonic solution was very small after 5 min of cell

dialysis for cells plated in the absence of matrix (Figure A.1.2A). In contrast, a small outwardly rectifying membrane current was clearly detectable in the cell plated on fibronectin (Figure A.1.2B). For both cells, switching the solution to hypotonic media at time = 0 led to delayed activation of a current bearing properties consistent with VSOAC displaying outward rectification (panels Aa and Ba) and voltage-dependent inactivation at +80 mV (panels Ab and Bb), especially the cell plated on FN. There were two notable differences between the two conditions: 1) the time required for activation of the current was significantly longer for the cell plated without matrix than the one grown on FN; 2) the magnitude of the hypotonic-induced current in the cell grown on FN was larger than NM. Figure A.1.2C reports mean \pm SEM times for half-maximal activation of membrane current evoked by a switch to hypotonic solution for C2C12 plated on NM, FN and LM. The data indicate that activation of the hypotonic-mediated current was faster for cells grown on FN or LM when compared to NM.

We next sought to determine the voltage-dependence of membrane currents recorded from C2C12 cells plated on NM, FN or LM, in isotonic and hypotonic solutions. Figure A.1.3 shows representative families of current traces for each condition elicited by the voltage clamp protocol displayed at the bottom center. All current traces are expressed as current density in pA/pF. For each surface-coating condition, the currents recorded in isotonic and hypotonic media were recorded from the same cell. Currents registered in isotonic medium were very small in the absence of matrix (Figure A.1.3Aa). However, plating the cells on FN led the appearance of a basal conductance having signature features for VSOAC currents including outward rectification and voltage-dependent inactivation (Figure A.1.3Ba). Such a basal conductance was also

apparent and even accentuated in cells plated on LM (Figure A.1.3Ca; notice the different size of the calibration bar). Typical VSOAC-like currents were evoked by the hypotonic solution. In addition to outward rectification and voltage-dependent inactivation at positive potentials, voltage-dependent reactivation was also observed following return to the holding potential (-40 mV) in the cells plated on matrix proteins (Figure A.1.3Bb and A.1.3Cb). Similar to the currents recorded with the isotonic solution, the magnitude of the elicited currents was much larger in cells plated on matrix versus no matrix (FN \approx LM > NM; Fig. 3Ab, Bb and Cb). Figure A.1.4 shows pooled data for similar experiments to those described in Figure A.1.3. The graphs display the mean current-voltage (I-V) relationships (HP = -40 mV) for the early instantaneous current (Early; panels A and C) or late (Late; panels B and D) current measured at the beginning or the end of 500 ms steps, respectively, which ranged from -100 to +120 mV in 10 mV-increments. For a proper comparison, the I-V relationships recorded from cells plated on NM, FN or LM were generated only in cells exposed to both isotonic (panels A and B) and hypotonic (panels C and D) solutions. Currents recorded from all conditions reversed near the predicted equilibrium potential for Cl⁻ suggesting that this anion is the main charge carrier of both isotonic- and hypotonic-induced currents. Whilst the early instantaneous current displayed slight outwardly rectifying (LM and FN) or linear (NM) properties in isotonic conditions, late current for cells plated on FN and LM showed clear signs of inward rectification at potentials \geq +70 mV, an observation consistent with time- and voltage-dependent inactivation. Both the instantaneous (Figure A.1.4A) and late (Figure A.1.4B) currents were larger in cells plated on matrix; for example at +100 mV, late outward current was 3.8-fold and 8.8-fold larger in cells grown on FN and LM,

respectively, relative to those proliferating on NM (Figure A.1.4B). Matrix proteins also had a profound influence on hypotonic-induced membrane currents. Both the early instantaneous (Figure A.1.4C) and late (Figure A.1.4D) currents were similarly enhanced in cells plated on either matrix protein vs. no matrix. For example, the late current in hypotonic solution was 75% greater on FN and 72% greater on LM compared to NM. Taken together, these results demonstrate that matrix proteins differentially stimulate a basal ionic conductance in isotonic conditions as well as a membrane currents triggered by hypotonic medium.

In order to establish that the hypotonic-induced membrane current is indeed generated by VSOACs in C2C12 cells, we performed anion replacement experiments to confirm that Cl^- is the main charge carrier and assessed whether matrix proteins alter the anion permeability sequence of the induced conductance. Figure A.1.5 shows three typical experiments during which extracellular Cl^- was sequentially replaced with Γ^- and aspartate (Asp^-). All traces were recorded in the steady state after at least 15 min of exposure to hypotonic medium. A 5 s voltage ramp ranging from -100 to +120 mV was used to elicit each trace as explained in the Methods. For all three groups of cells, total replacement of external Cl^- with Γ^- led to a small leftward shift of the reversal potential and increase in slope conductance at positive potentials, observations consistent with the higher relative permeability of Γ^- to Cl^- of VSOACs. In contrast and also consistent with this hypothesis, cell exposure to the less permeant organic anion aspartate consistently caused a positive shift in reversal potential and a reduced slope conductance in the entire voltage range analyzed. The relative permeability of external ions (X) with respect to Cl^- (P_X/P_{Cl}) was estimated by measuring the shifts in reversal potential of the current under

bionic conditions and calculated using the Goldman-Hodgkin-Katz equation as outlined in the Methods. Mean data pooled from several experiments with cells grown under the three conditions revealed a relative permeability of Γ and Asp^- over Cl^- that was statistically indistinguishable among the three groups (Figure A.1.6A); P_X/P_{Cl} were $\Gamma:\text{Cl}^-:\text{Asp}^- \cong 1.3:1.0:0.75$. The $\Gamma > \text{Cl}^- > \text{Aspartate}$ sequence is identical to the Eisenman “weak field strength” lyotropic series and supports the idea that hypotonic-induced current is an anion current. We also analyzed the impact of ion replacement on the conductance of the hypotonic-induced current in the three conditions (Figure A.1.6B). Linear regression was used to calculate the slope conductance in the negative (-100 to -50 mV) and positive range (+20 to +80 mV) of membrane potentials. As for P_X/P_{Cl} , the relative slope conductances of the current in the two voltage ranges measured in the presence of Γ or Asp^- relative to Cl^- (G_X/G_{Cl}) were also similar between the three conditions. Whilst G_{Γ}/G_{Cl} was not significantly different from unity, $G_{\text{Asp}^-}/G_{\text{Cl}}$ in both voltage ranges was significantly smaller than one supporting the concept that ion permeation was partially inhibited in the presence of aspartate.

VSOACs are very sensitive to block by the estrogen receptor modulator Tamoxifen (TMX)¹⁶². We thus tested the effects of TMX on currents from C2C12 plated on different matrices and exposed to isotonic and hypotonic media. Figure A.1.7 depicts experiments in which the effects of TMX were tested on hypotonic-induced currents recorded in C2C12 cells plated on FN. Panel A shows sample recordings and measurements from these traces are reported on the corresponding graph below, which illustrates the time course of changes in magnitude of late current before and during the application of TMX. The inhibitor potently blocked the hypotonic-induced current.

Figure A.1.7B shows a graph illustrating mean \pm SEM percent block by TMX of late current recorded in hypotonic solution in cells plated on NM, FN or LM. TMX produced over 96% block of late current in hypotonic solution in cells grown on any of the matrices. Taken together, these data support the notion that matrix proteins exert a profound influence on the properties of a membrane current resembling the volume-regulated chloride channel described in many cell types.

Role of β_1 integrin in the regulation of VSOACs.

One hypothesis to explain the influence of matrix proteins on VSOACs is that C2C12 cells plated on FN or LM trigger integrin signaling, which somehow regulates the activity and/or expression of VSOACs. Heterodimeric associations of β_1 integrin with multiple α integrins provide the molecular basis of the predominant receptors for the extracellular matrix proteins laminin, collagen and RGD-containing proteins such as fibronectin. $\alpha_5\beta_1$ and $\alpha_7\beta_1$ are the major integrin receptors for fibronectin and laminin, respectively, in muscle and both are highly expressed in C2C12 cells (see Figure A.1.1D above) ¹⁷⁰. We used an shRNAi strategy to induce a selective knockdown (KD) of β_1 integrin in C2C12 cells and to assess whether this intervention altered VSOACs in cells plated on FN. Lentiviral particles containing four independent target sequences specific to β_1 integrin were used to transiently infect C2C12 cells. After screening for β_1 integrin knockdown by immuno-blot analysis (data not shown), two of the lentiviral constructs were used to generate and clone two stable independent KD cell lines. Antibody specific to β_1 integrin identified a band at 130kDa consistent with β_1 integrin. Figure A.1.8A is a representative immune-blot that illustrates the expression level of β_1 integrin in C2C12

cells (lane 1, 100%), cell line C-9 (lane 2, < 1%) and cell line B-7 (lane 3 \approx 5%). Figure A.1.8B and C respectively show I-V relationships of membrane currents recorded in isotonic and hypotonic conditions in wild-type (WT) cells, or in the two KD cell lines. For both the B-7 and C-9 cell lines, the basal Cl^- current in isotonic solution was not significantly different from WT cells (Figure A.1.8B) although a clear tendency for the C-9 cell line (99% KD of β_1 integrin) to exhibit a smaller current is notable. The VSOAC current activated by hypotonic solution was attenuated by a little more than 60% at all voltages in the B-7 cell line, and by > 87% in the C-9 cell line ($P < 0.001$). These experiments demonstrate that integrins play an integral role in the activation of VSOACs in C2C12 cells.

Discussion

Various classes of integrins have been shown to regulate a number of ion channels including hERG K^+ channels, large conductance Ca^{2+} -dependent K^+ channels, L-type Ca^{2+} channels, stretch-activated non-selective cation, and Cl^- channels^{166;171-179}. There is also evidence for activation of β_1 integrin caused by the opening of the voltage-gated K^+ channel Kv1.3 in response to membrane depolarization in human T lymphocytes¹⁸⁰. Most of the above studies examined the effects of various acute interventions designed to alter key signaling components involved in integrin activation. Similar to the study by Hofmann et al. on hERG in FLG 29.1 cells, a human leukemic preosteoclastic cell line, we first investigated whether VSOACs in C2C12 murine myoblast cells would be influenced by having the cells adhere on fibronectin or laminin, the major ligands for $\alpha_5\beta_1$ and $\alpha_7\beta_1$ integrins, respectively¹⁷¹. Our data showed that compared to cells plated on glass cover slips with no matrix (NM), cells cultured on FN

or LM displayed a basal anion conductance in iso-osmotic condition that shared many properties to those of VSOACs evoked by cell exposure to hypotonic solution. Cell adhesion to FN and LM triggered structural reorganizations consistent with activation of integrins manifested by the appearance of peripheral focal adhesions (FN and LM) and the formation of thick stress fibers (LM). The hypotonic-induced VSOAC current recorded from cells plated on FN or LM displayed an earlier onset and was larger after reaching a steady state than that registered from cells growing on NM. Specific genetic knockdown of β_1 integrin in cells plated on FN suppressed both the basal Cl^- conductance recorded in isotonic solution as well as the VSOAC elicited by hypo-osmotic solution. These results support the concept that integrins are an essential component of the signaling pathway triggering the activation of the volume-regulated chloride conductance in C2C12 myoblast cells.

Extracellular Matrix Proteins Stimulate Cl^- Conductances in C2C12 Cells.

When C2C12 myoblasts are cultured on ECM, the nature of the ECM (FN or LM) is known to influence cell phenotype. This response is clearly demonstrated in our studies by the pattern of β_1 integrin clustering and stress fiber formation in the presence/absence of ECM coating. It is at these β_1 integrin containing focal adhesion points, that stress fibers are anchored and that signals are generated to regulate gene expression, cell motility, cell differentiation and growth¹⁸¹⁻¹⁸³. At focal adhesions, integrins are thought to serve as mechanotransducers. It is logical to assume that an integrin attached to the ECM and anchored to stress fibers in the cytoplasm will sense a larger mechanical force (such as the force generated by cell swelling) than an integrin that is not attached to the ECM (no opposing force). Therefore, we postulate a more efficient conversion of the

mechanical force into a chemical signal. This model correlates nicely with our observations as follows. One interesting difference between C2C12 cells plated on NM versus FN or LM was the increased induction of stress fibers in cells plated on NM < FN < LM. These “progressive” structural changes correlated well with the very small or sometimes inexistent basal Cl⁻ conductance in cells grown on NM, and the intermediate and large basal Cl⁻ conductance seen in cells plated on FN and LM, respectively. Furthermore, reorganization of the cytoskeleton by the two ECM proteins accelerated the time course of activation of the VSOAC current and increased the size of the maximally activated hypotonic-induced current to a similar degree suggesting that the ECM-induced changes “primed” the volume sensing machinery leading to opening of the Cl⁻ channel. Whether stimulation of $\alpha_5\beta_1$ and $\alpha_7\beta_1$ integrins by fibronectin and laminin converge to a common pathway or are able to somehow cooperate synergistically in promoting the activation of the VSOAC will require additional experiments.

Nature of the Cl⁻ conductances influenced by ECM proteins in C2C12 myoblasts.

Are the anion conductances detected in isotonic and hypotonic media generated by the same channel? This cannot be answered unequivocally because the molecular identity encoding for the volume-sensitive Cl⁻ conductance is still unresolved^{162;163}. However, the basal conductance and current elicited by hypotonic solution have several biophysical properties in common that allow us to at least propose that they may be the product of the same ion channel. With a symmetrical Cl⁻ gradient, both currents reversed near the predicted Nernst potential of 0 mV, an observation consistent with Cl⁻ being the main charge carrier. Ion replacement experiments showed an identical anion permeability sequence of I⁻ > Cl⁻ > Aspartate⁻ for currents recorded in isotonic or

hypotonic conditions in cells plated on NM, FN or LM, in accord with a low electric field ion selectivity profile or Eisenman's sequence I; the magnitude of the permeability (P_I/P_{Cl} and P_{Asp}/P_{Cl}) conductance (G_I/G_{Cl} and G_{Asp}/G_{Cl}) ratios of the Cl^- currents recorded in all groups were not significantly different from each other. The fully activated instantaneous current measured in the different conditions displayed modest outward rectification. At potentials positive to $\approx +50$ mV, currents inactivated in a time- and voltage-dependent manner, which led to appearance of a flattening of the current-voltage relationship (inward rectification) for the current measured at the end of the pulse. Finally, the VSOAC current induced by hypotonic solution in cells plated on NM, FN or LM was similarly and potently blocked by the estrogen receptor tamoxifen, a commonly used organic inhibitor of volume-regulated Cl^- channels^{162;163;184;185}. Although not systemically studied in detail, the basal conductance in cells plated on all three matrices was also sensitive to block by tamoxifen. Moreover, the over 97% block of the hypotonic-induced VSOAC current in all groups is consistent with the idea that the basal Cl^- conductance apparent in isotonic condition is generated by the same channel since the amount block achieved by tamoxifen surpassed the blocking of hypotonic-induced current alone. Taken together, these results suggest that specific adherence of C2C12 myoblasts to matrix proteins may have shifted the set point for activation of VSOACs to a lower threshold or elevated the maximal response resulting in basal activation rather than by eliciting the expression of another basal anion conductance superimposed with a distinct VSOAC. This hypothesis is of course not in conflict with the possibility that matrix protein interactions with the cell membrane may have enhanced the expression,

turnover rate, trafficking and/or function of the pore-forming subunit or one of its regulators.

β_1 integrin is essential for activation of the basal Cl^- and VSOAC conductances.

Immunofluorescence and confocal imaging experiments showed that specific interactions of FN and LM with C2C12 promoted clustering and in the case of LM, a potent stimulation of stress fiber biosynthesis. These changes were paralleled by induction of a basally activated Cl^- conductance in isotonic medium and increased VSOAC activation profile. Using a lentivirus, a shRNAi gene knockdown strategy was used to down-regulate β_1 integrin protein. The β_{1A} integrin isoform is the predominant isoform expressed in undifferentiated myoblasts, and our immuno-blot analysis revealed KD of a band at the appropriate molecular weight¹⁸⁶⁻¹⁸⁸. Analysis of two independent “stable” cell lines containing different shRNAi constructs yielded a titrated inhibitory effect on the magnitude of the basal Cl^- and VSOAC currents; in one cell line (B7), KD had no effect on the basal Cl^- current and partially inhibited the VSOAC current, while in the other (C9) both currents were strongly inhibited. Some of this variation could be due to loss of suppression of β_1 integrin by the shRNAi constructs over time. In fact, recent immuno-blot analysis conducted after all the patch-clamp analysis revealed a progressive increase in β_1 integrin expression ($\approx 20\%$ of wild type, data not shown) in both B7 and C9 cell lines after repeated freeze thaw cycles. Additionally, the large SEM seen on the I-V plot (Figure 8B) for cell line B7 may indicate a mixed population of KD in this “stable” cell line. Regardless of the mechanisms involved in these differences, the fact that two distinct shRNAi sequences both inhibited the basal and VSOAC conductances strongly

suggests that β_1 integrin is not just a mere regulator of channel function but is key for activation of VSOACs in C2C12 myoblasts.

Browe and Baumgarten provided evidence for involvement of this integrin in the activation by stretch of an outwardly rectifying tamoxifen-sensitive Cl^- current in rabbit ventricular myocytes¹⁶⁶. Paramagnetic beads coated with a β_1 integrin antibody were deposited on the cell surface and the beads were pulled upward by applying a constant magnetic field to stretch the membrane. Similar to VSOACs, inhibitors of focal adhesion kinase (FAK) and c-Src blocked the stretch-activated Cl^- current. A subsequent study from the same group showed that activation of this current occurred through an autocrine mechanism whereby stretch would elicit the endogenous release of angiotensin II (AII) would bind to the AT_1 receptor subclass and trigger a cascade of biochemical events leading to stimulation of sarcolemmal NADPH oxidase, production of reactive oxygen species (ROS) and ultimately activation of the stretch-activated Cl^- current¹⁷⁸. More recently, these investigators reported that the AII-ROS signaling pathway was also involved in activation of VSOACs in rabbit cardiac myocytes, providing support to the proposal that VSOACs and the β_{1D} integrin-stretch-activated Cl^- current are probably generated by the same channel¹⁸⁹. Whether the β_1 integrin is absolutely required for activation of the Cl^- channels in the heart is unknown. In preliminary experiments (unpublished observations) and in contrast to the above studies, H_2O_2 in the range of 100 to 500 μM failed to elicit a VSOAC current in C2C12 bathed in isotonic solution, which suggests that the downstream signaling events are different.

The mechanism of activation of the volume-stimulated osmolyte and anion channel is still unknown and this is to a large extent due to the lack of knowledge of the

molecular identity of the pore-forming subunit of this channel^{162;163}. However, studies performed by Walsh and Zhang have shown that the magnitude and kinetics of VSOAC ($I_{Cl, \text{swell}}$) activation in rat neonatal ventricular myocytes is regulated by FAK and Src¹⁹⁰. FAK phosphorylation and activity is directly linked to integrin activation and extracellular matrix composition. Our data showed that skeletal muscle myoblast cells grown on specific matrix proteins triggers substantial remodeling of the cytoskeleton altering the properties of a chloride channel that plays an important role in regulation of cell volume, apoptosis, cell differentiation and growth. Furthermore, β_1 integrin appears to be central to this process. Future studies should be carried out to determine if the actions of $\alpha_5\beta_1$ (FN receptor) and $\alpha_7\beta_1$ (LM receptor) integrins, all of which are expressed in C2C12 cells, are coordinated or whether these two integrins work independently in the regulation of VSOACs and the specific downstream signaling pathways they trigger.

Acknowledgements

This research was supported by the National Institutes of Health COBRE 5P20RR015581-09 to MV and NL and the NIH R01 HL 075477 to NL.

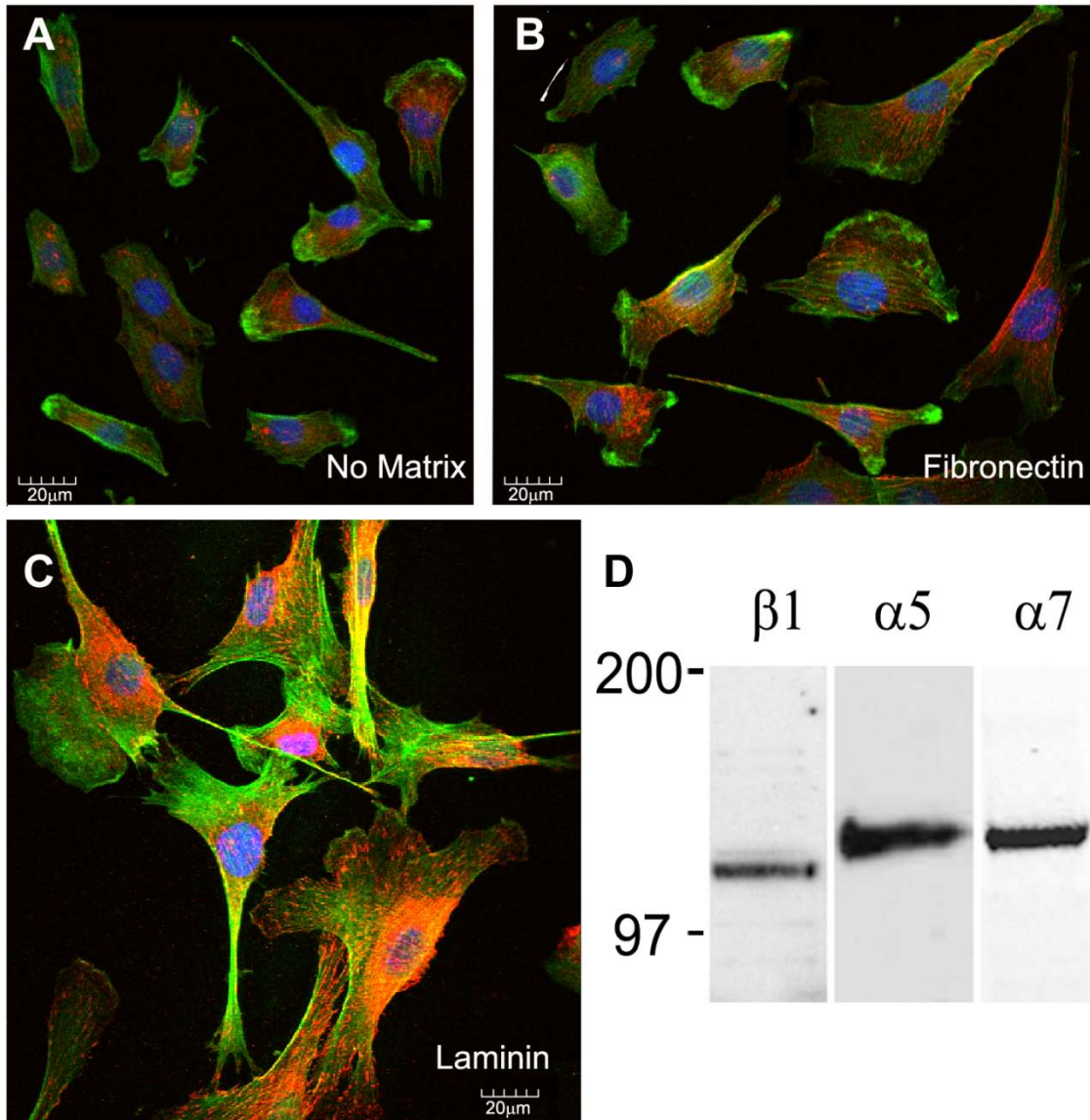


Figure A.1.1. Immunofluorescent staining of C2C12 reveals that ECM composition has a profound influence on myoblast phenotype. C2C12 cells plated on uncoated coverslips (A), fibronectin (B) or laminin (C) were stained with antibody 9EG7, to identify β_1 integrin containing focal adhesions (red), FITC phalloidin to detect actin containing stress fibers (green) and bis-benzamide to detect nuclei (blue). Note the profound differences in focal contact distribution and stress fiber formation. All images

were stained simultaneously and collected with identical settings. The immune-blot shown in panel D, illustrates the expression of β_1 , α_5 and α_7 integrins in C2C12 cells grown on standard tissue culture plates.

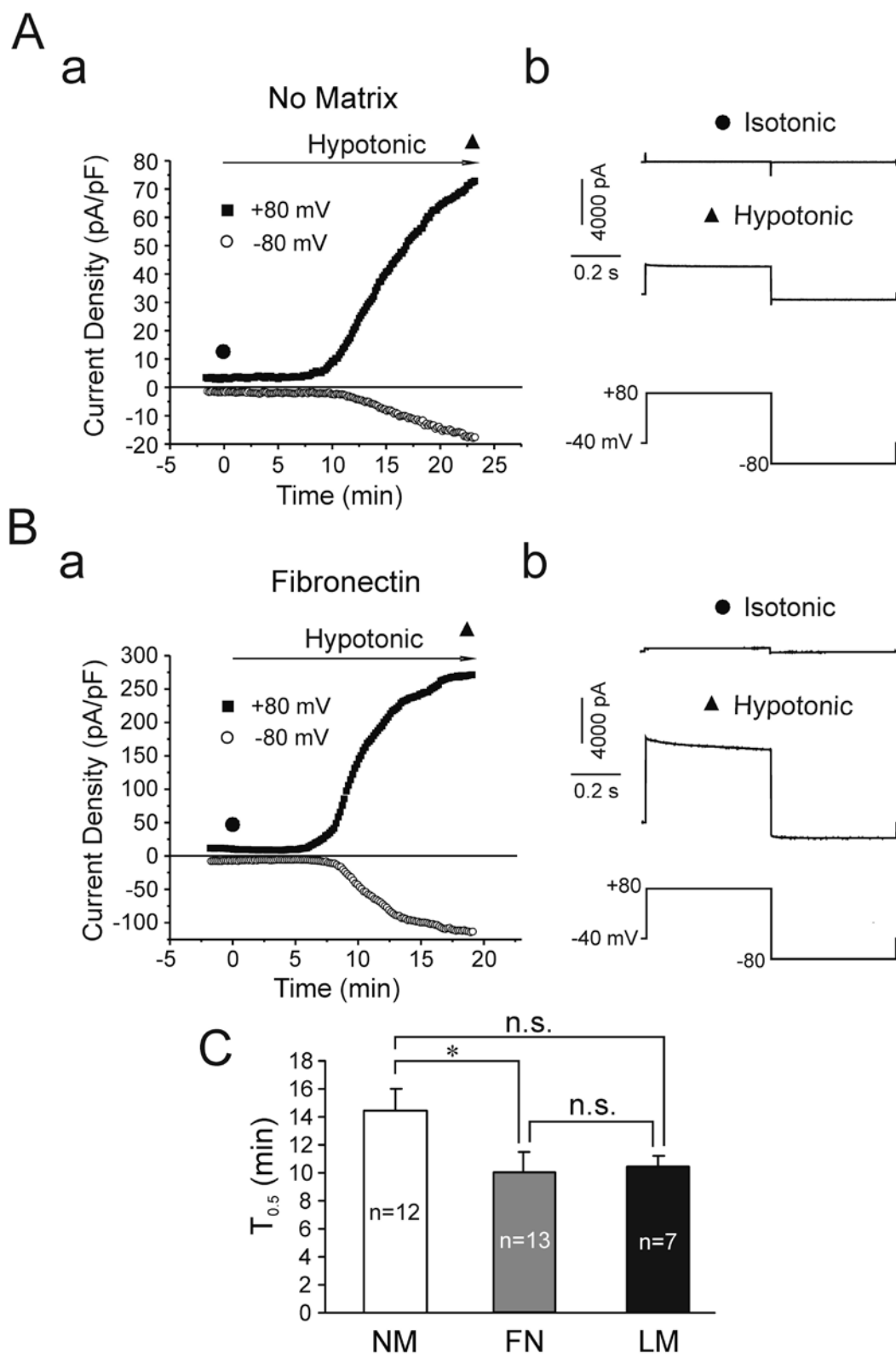


Figure A.1.2. Alteration in the time course of changes in membrane currents elicited by switching from isotonic to hypotonic solutions in C2C12 cells plated on fibronectin. Panels A and B respectively show results representative of experiments carried out in a C2C12 cell cultured in the absence of matrix and another one plated on fibronectin. For both panels A and B, panel a shows a plot of the time course of changes in membrane currents evoked by the voltage clamp protocol displayed at the bottom of panel b. As indicated, the holding potential was set to -40 mV. A repetitive double-pulse protocol consisting of an initial 500 ms step to +80 mV followed by a 500 ms repolarizing step to -80 mV was applied at a frequency of 0.1 Hz. The graph in panel a plots current density measured at the end of each step to +80 (filled squares) and -80 mV (empty circles) as a function of time before and after exposure to hypotonic solution as indicated by the arrow above the plots. The filled circle and triangle indicate when the representative traces registered in isotonic and hypotonic solutions in panel b were recorded. Isotonic and hypotonic solutions were respectively set to 300 and 220 mosmol/kg H₂O. C. Bar graph summarizing the mean \pm SEM half maximal time for activation of the VSOAC current ($T_{0.5}$) after switching from isotonic to hypotonic solutions for cells grown in the absence of substrate (NM), on fibronectin (FN) or laminin (LM). n: number of cells; * $P < 0.05$; n.s.: not significant.

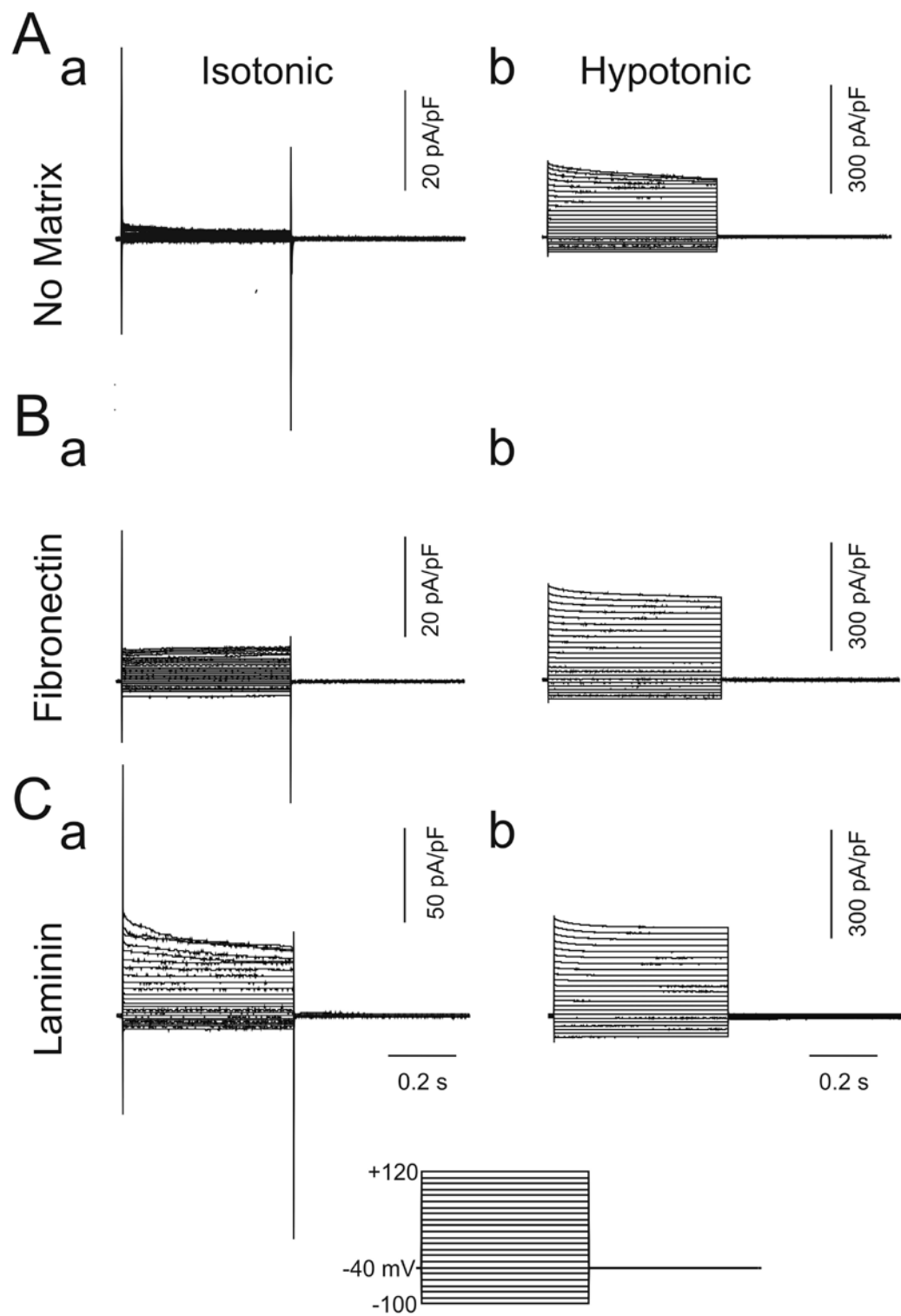


Figure A.1.3. Typical families of membrane current recorded in isotonic and hypotonic conditions from C2C12 myoblasts grown in the absence or presence of matrix proteins. All families of membrane current were evoked by the protocol shown at the bottom, which consisted of 500 ms steps ranging from -100 to +120 mV applied in 10 mV increments from a holding potential of -40 mV. Panels A, B and C show membrane currents recorded expressed as current density in pA/pF from cells plated on no matrix, fibronectin or laminin, respectively. For each of the three panels, panels a and b were respectively obtained in the same cell exposed initially to isotonic solution and after a new steady state was detected in hypotonic solution. All traces shown are representative of mean data presented in Figure 3 ($\approx \pm 1$ S.D.).

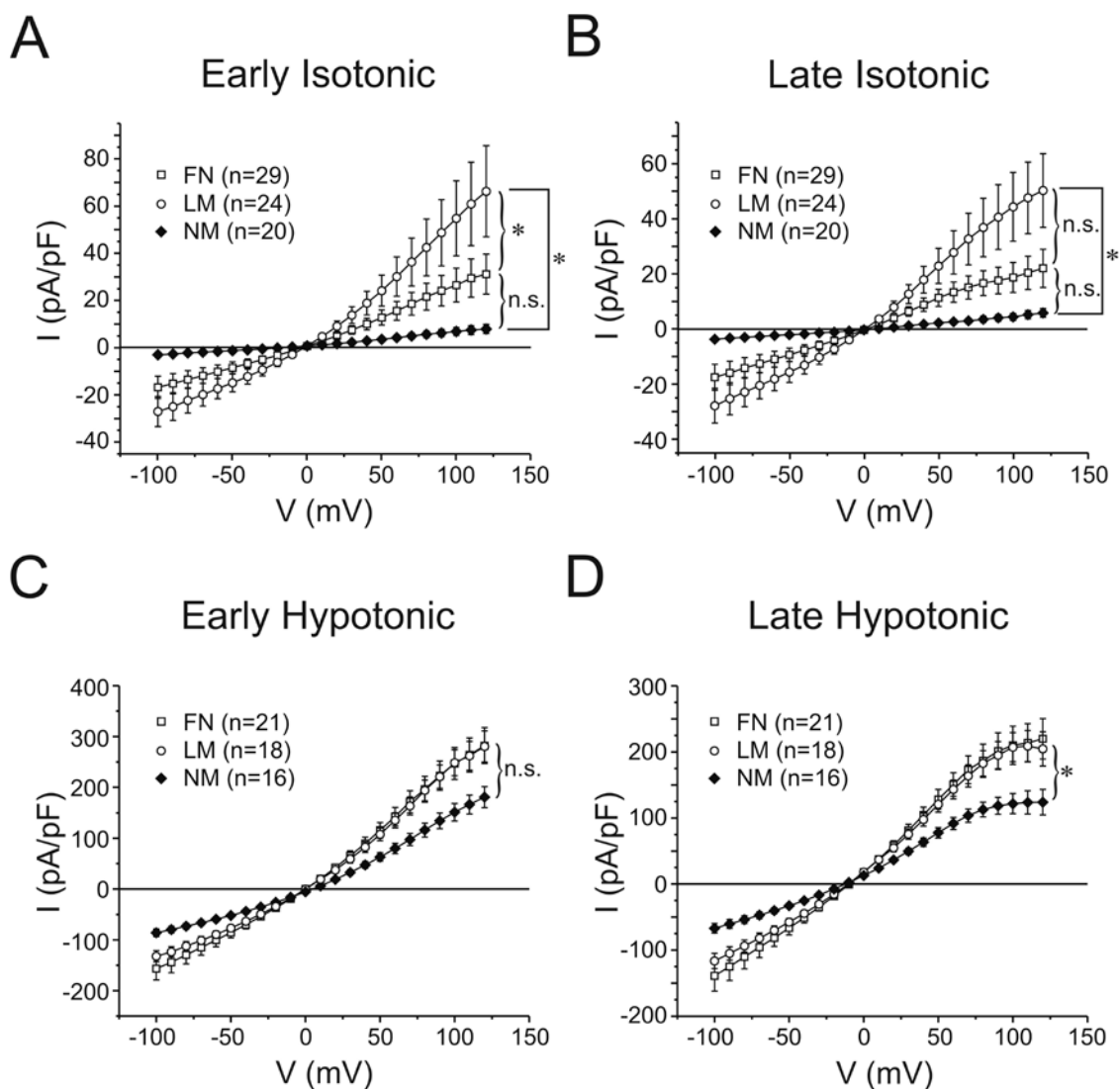


Figure A.1.4. Voltage-dependence of membrane current recorded in isotonic and hypotonic conditions in C2C12 cells grown in the absence or presence of matrix proteins. (A) Mean I-V relationships for the current measured at the beginning of steps ranging from -100 to +120 mV from holding potential of -40 mV (see description of Fig. 2) in cells exposed to isotonic medium (Early Isotonic) and plated on no matrix (NM), fibronectin (FN) or laminin (LM). One-way ANOVA test revealed significant differences between the means with $P < 0.005$ (*). (B) The same as panel A except that the current

was measured at the end of the 500 ms steps (Late Isotonic; see Fig. 2). One-way ANOVA test revealed significant differences between the means with $P < 0.005$ (*). (C) The same as panel A except that the cells were exposed to hypotonic solution (Early Hypotonic). One-way ANOVA test revealed no significant differences between the means although the P value was just at the limit of significance ($P = 0.0518$). (D) The same as panel B except that the cells were exposed to hypotonic solution (Late Hypotonic). One-way ANOVA test revealed significant differences between the means with $P < 0.05$ (*). For all panels, the number in parentheses refers to the number of cells and n.s.: not significant. Note the enhancement of membrane current in isotonic and hypotonic solutions for cells grown on FN or LM vs. NM. Also, irrespective of the presence or absence of matrix proteins, all currents recorded in isotonic and hypotonic media reversed near the predicted equilibrium potential for Cl^- (≈ 0 mV).

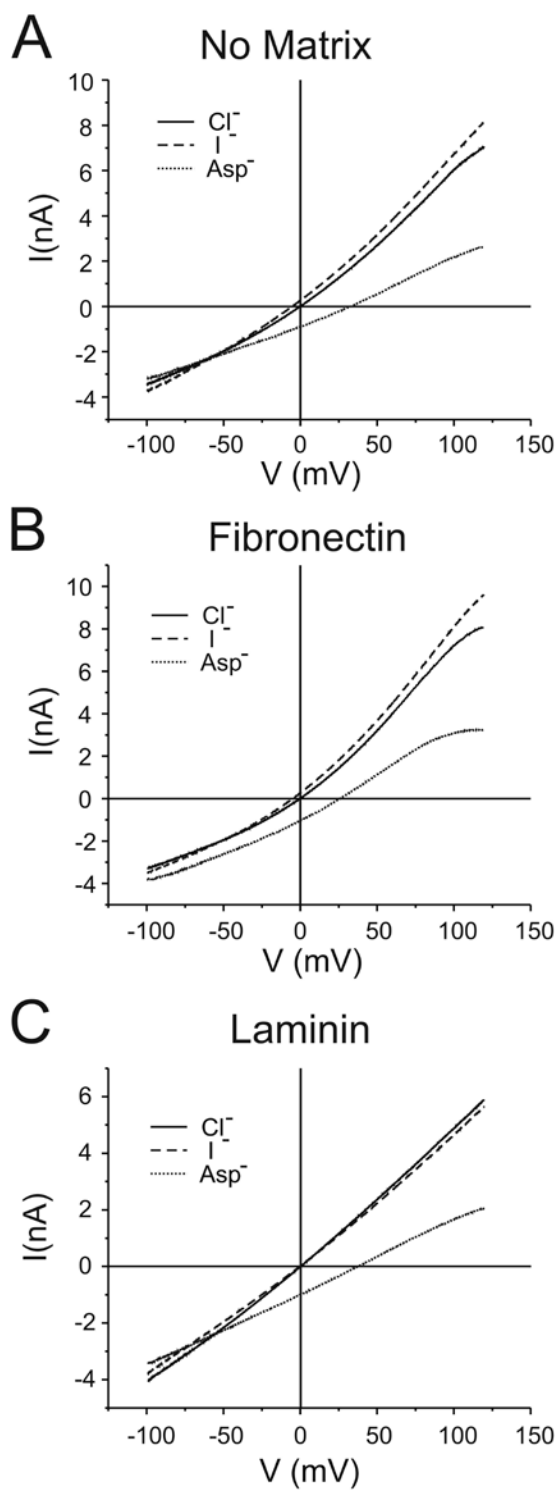


Figure A.1.5. Anion selectivity of hypotonic-induced membrane current recorded from C2C12 grown in the absence or presence of matrix proteins. Panels A, B and C

show sample experiments from C2C12 cells plated respectively in the absence of matrix, or on fibronectin or laminin. For all traces, membrane current was elicited by 5 s voltage ramp protocols ranging from -100 to +120 mV (44 mV/s) and imposed at a rate of 1 ramp every 10 s. In each panel, the three traces were obtained in the same cell after a sequential equimolar replacement of NaCl (solid line labeled Cl⁻) with NaI (dotted line labeled I⁻) and then with Na-Aspartate (dashed line labeled Asp⁻). Not eh small but significant negative shift in reversal potential when external chloride is replaced with iodide, and the large positive shift in reversal potential when the solution is switching to the one containing Na-Aspartate.

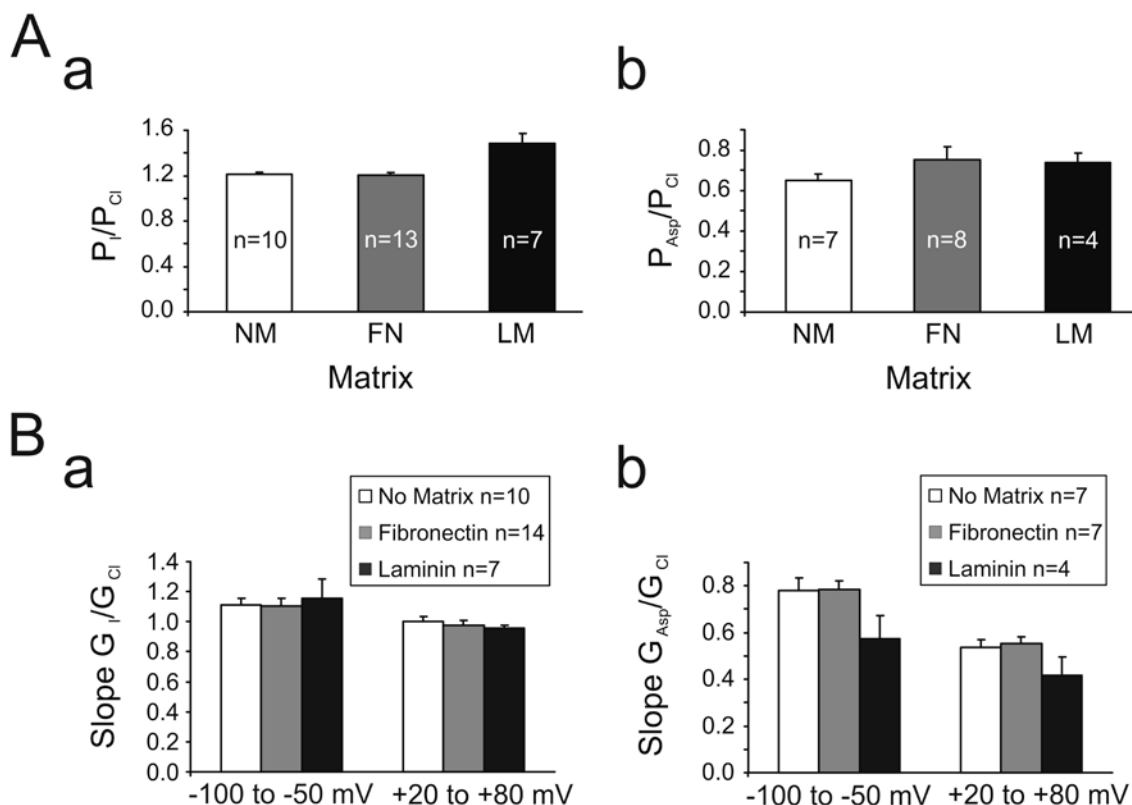


Figure A.1.6. Selectivity and permeability profiles of hypotonic-induced VSOAC currents in C2C12 myoblasts grown in the absence or presence of matrix proteins.

(A) Bar graphs reporting the mean calculated relative permeability of iodide to chloride (P_I/P_{Cl} ; panel a) and aspartate to chloride (P_{Asp}/P_{Cl} ; panel b) for VSOAC currents recorded in C2C12 cells plated on no matrix (NM), fibronectin (FN) or laminin (LM).

The shifts in reversal potential measured from anion replacement experiments identical to those shown in Figure 5 were computed to determine P_I/P_{Cl} and P_{Asp}/P_{Cl} using the proper form of the Goldman-Hodgkin-Katz equation under bi-ionic conditions as described in the Methods. There were no significant differences for P_I/P_{Cl} and P_{Asp}/P_{Cl} of the VSOAC current between the cells plated on the three different substrates. B. The relative slope conductance over two ranges of membrane potential for iodide over chloride (G_I/G_{Cl}) and

aspartate over chloride ($G_{\text{Asp}}/G_{\text{Cl}}$) of VSOAC currents were measured in cells plated with NM, FN or LM, and plotted in the bar graphs shown in panels a and b, respectively.

There were no significant differences for $G_{\text{I}}/G_{\text{Cl}}$ and $G_{\text{Asp}}/G_{\text{Cl}}$ of the VSOAC current between the cells plated on the three different substrates. For panels A and B, there were no significant differences noted between the means within each group of data.

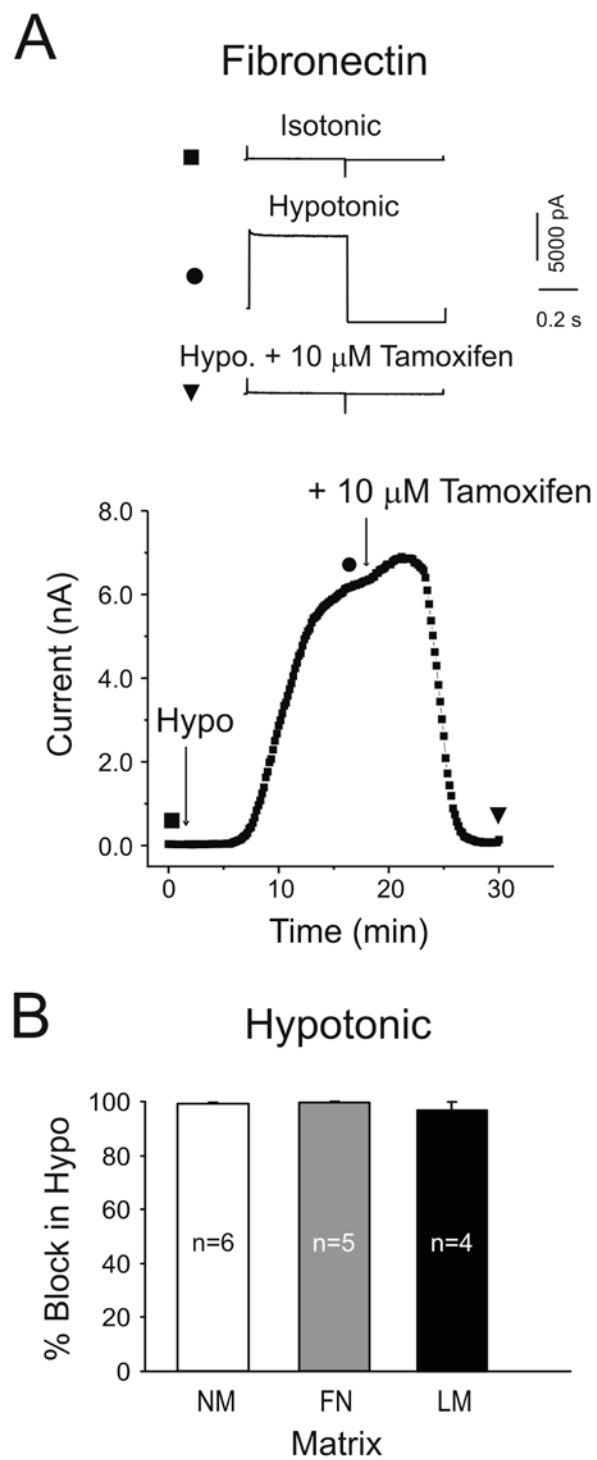


Figure A.1.7. Tamoxifen sensitivity of the hypotonic-induced VSOAC current recorded in cells grown in the absence or presence of matrix protein. (A) Typical

experiment showing the sensitivity to block by the anion channel blocker tamoxifen of the VSOAC current recorded from a C2C12 cell plated on fibronectin. The traces above the graph were obtained in isotonic solution, after a switch to hypotonic solution elicited maximal stimulation, and after a steady state inhibition by adding 10 μ M tamoxifen to the hypotonic solution was observed. Each trace was evoked by an identical voltage clamp protocol to that described in Figure 2. Measurements from each trace are correspondingly labeled in the graph below with the symbol shown beside each trace. The graph shows the time course of development of the VSOAC current after the switch to hypotonic solution, and its suppression by tamoxifen. Measurements were made at the end of 500 ms steps to +80 mV (one step every 10 s) from a holding potential of -40 mV.

(B) Bar graph reporting the mean % block by 10 μ M tamoxifen of the VSOAC current at +80 mV in cells plated on no matrix (NM), fibronectin (FN) or laminin (LM). No significant differences were found between the means of the three groups.

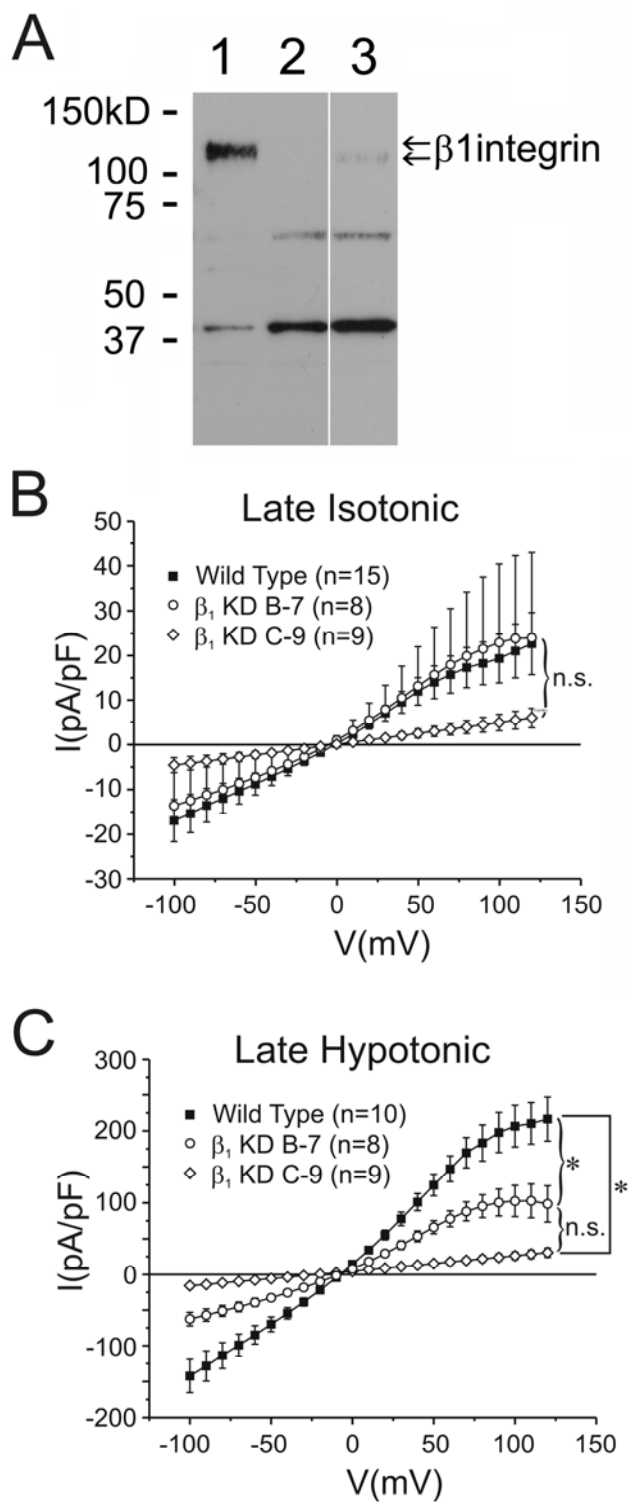


Figure A.1.8. Specific genetic β_1 integrin knockdown inhibits the basal and hypotonic-induced VSOAC current in cells plated on fibronectin. (A) Immuno blot analysis of β_1 integrin expression in C2C12 cells (lane 1), KD C9 (lane 2) and KD B7 (lane 3). Note, lane 3 is added from a non adjacent lane of the same gel as lanes 1 and 2. (B) Mean *I-V* relationships for the current measured at the end of steps ranging from -100 to +120 mV from holding potential of -40 mV (see description of Fig. 4) in Wild-type C2C12 cells exposed to isotonic medium (Late Isotonic) and plated on fibronectin, and two cell lines (β_1 KD B-7 and β_1 KD C-9) in which a variable degree of β_1 integrin knock down was achieved by shRNAi. (C) Identical nomenclature to panel C except that the results were analyzed from the same pool of cells after exposure to hypotonic solution. One-way ANOVA test revealed significant differences between the means with $P < 0.001$ (*). For panels C and D, the number in parentheses refers to the number of cells and n.s.: not significant. Note the significant inhibition of both the basal anion and VSOAC currents in the β_1 integrin knockdown C-9 cell line in which 99% of the protein was successfully down-regulated.

Reprinted with the permission of the American Physiological Society. Published as:
Influence of the extracellular matrix and integrins on volume-sensitive osmolyte anion
channels in C2C12 myoblasts. Neveux I, Doe J, Leblanc N, Valencik ML. American
Journal of Physiology Cell Physiology, 2010 May;298(5):C1006-17

Bibliography

- (1) Allamand V, Guicheney P. Merosin-deficient congenital muscular dystrophy autosomal recessive (MDC1A, MIM#156225, LAMA2 gene coding for α 2 chain of laminin). *European Journal of Human Genetics* 2002;10:91.
- (2) Peat RA, Smith JM, Compton AG et al. Diagnosis and etiology of congenital muscular dystrophy. *Neurology* 2008;71:312-321.
- (3) Tubridy N, Fontaine B, Eymard B. Congenital myopathies and congenital muscular dystrophies. *Current Opinion in Neurology* 2001;14:575-582.
- (4) Muntoni F, Voit T. The congenital muscular dystrophies in 2004: a century of exciting progress. *Neuromuscular Disorders* 2004;14:635-649.
- (5) Mendell JR, Boue DR, Martin PT. The congenital muscular dystrophies: Recent advances and molecular insights. *Pediatric and Developmental Pathology* 2006;9:427-443.
- (6) Helbling-Leclerc A, Zhang X, Topaloglu H et al. Mutations in the laminin α 2-chain gene (LAMA2) cause merosin-deficient congenital muscular dystrophy. *Nat Genet* 1995;11:216-218.
- (7) Naom IS, DAlessandro M, Topaloglu H et al. Refinement of the laminin α 2 chain locus to human chromosome 6q2 in severe and mild merosin deficient congenital muscular dystrophy. *Journal of Medical Genetics* 1997;34:99-104.
- (8) Chae JH, Lee JS, Hwang H et al. Merosin-deficient congenital muscular dystrophy in Korea. *Brain and Development* 2009;31:341-346.
- (9) Di Blasi C, He Y, Morandi L, Cornelio F, Guicheney P, Mora M. Mild muscular dystrophy due to a nonsense mutation in the LAMA2 gene resulting in exon skipping. *Brain* 2001;124:698-704.

- (10) Mora M, Moroni I, Uziel G et al. Mild clinical phenotype in a 12-year-old boy with partial merosin deficiency and central and peripheral nervous system abnormalities. *Neuromuscular Disorders* 1996;6:377-381.
- (11) Taratuto AL, Lubieniecki F, Diaz D et al. Merosin-deficient congenital muscular dystrophy associated with abnormal cerebral cortical gyration: an autopsy study. *Neuromuscul Disord* 1999;9:86-94.
- (12) Jones KJ, Morgan G, Johnston H et al. The expanding phenotype of laminin alpha 2 chain (merosin) abnormalities: case series and review. *Journal of Medical Genetics* 2001;38:649-657.
- (13) Timpl R, Rohde H, Robey PG, Rennard SI, Foidart JM, Martin GR. Laminin--a glycoprotein from basement membranes. *J Biol Chem* 1979;254:9933-9937.
- (14) Tzu J, Marinkovich MP. Bridging structure with function: structural, regulatory, and developmental role of laminins. *Int J Biochem Cell Biol* 2008;40:199-214.
- (15) Aumailley M, Bruckner-Tuderman L, Carter WG et al. A simplified laminin nomenclature. *Matrix Biology* 2005;24:326-332.
- (16) Colognato H, Yurchenco PD. Form and function: The laminin family of heterotrimers. *Developmental Dynamics* 2000;218:213-234.
- (17) Aumailley M, Smyth N. The role of laminins in basement membrane function. *J Anat* 1998;193 (Pt 1):1-21.
- (18) Gullberg D, Tiger CF, Velling T. Laminins during muscle development and in muscular dystrophies. *Cell Mol Life Sci* 1999;56:442-460.
- (19) Sasaki T, Giltay R, Talts U, Timpl R, Talts JF. Expression and Distribution of Laminin [alpha]1 and [alpha]2 Chains in Embryonic and Adult Mouse Tissues: An Immunochemical Approach. *Experimental Cell Research* 2002;275:185-199.

- (20) Gawlik KI, Durbeej M. Skeletal muscle laminin and MDC1A: pathogenesis and treatment strategies. *Skelet Muscle* 2011;1:9.
- (21) Sewry CA, Chevallay M, Tome FM. Expression of laminin subunits in human fetal skeletal muscle. *Histochem J* 1995;27:497-504.
- (22) Pedrosa-Domellof F, Tiger CF, Virtanen I, Thornell LE, Gullberg D. Laminin chains in developing and adult human myotendinous junctions. *J Histochem Cytochem* 2000;48:201-210.
- (23) Patton BL, Connolly AM, Martin PT et al. Distribution of ten laminin chains in dystrophic and regenerating muscles. *Neuromuscular Disorders* 1999;9:423-433.
- (24) Vachon PH, Loechel F, Xu H, Wewer UM, Engvall E. Merosin and laminin in myogenesis; specific requirement for merosin in myotube stability and survival. *J Cell Biol* 1996;134:1483-1497.
- (25) Kuang W, Xu H, Vachon PH, Engvall E. Disruption of the lama2 Gene in Embryonic Stem Cells: Laminin [alpha]2 Is Necessary for Sustenance of Mature Muscle Cells. *Experimental Cell Research* 1998;241:117-125.
- (26) Kuang W, Xu H, Vilquin JT, Engvall E. Activation of the lama2 gene in muscle regeneration: Abortive regeneration in laminin alpha 2-deficiency. *Laboratory Investigation* 1999;79:1601-1613.
- (27) Miyagoe-Suzuki Y, Nakagawa M, Takeda S. Merosin and congenital muscular dystrophy. *Microscopy Research and Technique* 2000;48:181-191.
- (28) Cohn RD, Campbell KP. Molecular basis of muscular dystrophies. *Muscle & Nerve* 2000;23:1456-1471.

- (29) Gawlik K, Miyagoe-Suzuki Y, Ekblom P, Takeda S, Durbeej M. Laminin {alpha}1 chain reduces muscular dystrophy in laminin {alpha}2 chain deficient mice. *Hum Mol Genet* 2004;13:1775-1784.
- (30) Colognato H, Winkelmann DA, Yurchenco PD. Laminin polymerization induces a receptor-cytoskeleton network. *J Cell Biol* 1999;145:619-631.
- (31) Gu M, Wang W, Song WK, Cooper DN, Kaufman SJ. Selective modulation of the interaction of alpha 7 beta 1 integrin with fibronectin and laminin by L-14 lectin during skeletal muscle differentiation. *J Cell Sci* 1994;107:175-181.
- (32) Vachon PH, Xu H, Liu L et al. Integrins (alpha 7 beta 1) in muscle function and survival - Disrupted expression in merosin-deficient congenital muscular dystrophy. *Journal of Clinical Investigation* 1997;100:1870-1881.
- (33) Hodges BL, Hayashi YK, Nonaka I, Wang W, Arahata K, Kaufman SJ. Altered expression of the alpha7beta1 integrin in human and murine muscular dystrophies. *J Cell Sci* 1997;110:2873-2881.
- (34) Hynes RO. Integrins: versatility, modulation, and signaling in cell adhesion. *Cell* 1992;69:11-25.
- (35) Hynes RO. Integrins: Bidirectional, Allosteric Signaling Machines. *Cell* 2002;110:673-687.
- (36) Hayashi YK, Chou FL, Engvall E et al. Mutations in the integrin alpha7 gene cause congenital myopathy. *Nat Genet* 1998;19:94-97.
- (37) Song WK, Wang W, Foster RF, Bielser DA, Kaufman SJ. H36-alpha 7 is a novel integrin alpha chain that is developmentally regulated during skeletal myogenesis. *J Cell Biol* 1992;117:643-657.

- (38) Guo C, Willem M, Werner A et al. Absence of α 7 integrin in dystrophin-deficient mice causes a myopathy similar to Duchenne muscular dystrophy. *Hum Mol Genet* 2006;15:989-998.
- (39) Rooney JE, Welser JV, Dechert MA, Flintoff-Dye NL, Kaufman SJ, Burkin DJ. Severe muscular dystrophy in mice that lack dystrophin and α 7 integrin. *J Cell Sci* 2006;119:2185-2195.
- (40) Martin PT, Sanes JR. Integrins mediate adhesion to agrin and modulate agrin signaling. *Development* 1997;124:3909-3917.
- (41) Velling T, Collo G, Sorokin L, Durbeej M, Zhang H, Gullberg D. Distinct α 7A β 1 and α 7B β 1 integrin expression patterns during mouse development: α 7A is restricted to skeletal muscle but α 7B is expressed in striated muscle, vasculature, and nervous system. *Dev Dyn* 1996;207:355-371.
- (42) Burkin DJ, Wallace GQ, Nicol KJ, Kaufman DJ, Kaufman SJ. Enhanced Expression of the α 7 β 1 Integrin Reduces Muscular Dystrophy and Restores Viability in Dystrophic Mice. *J Cell Biol* 2001;152:1207-1218.
- (43) Burkin DJ, Kaufman SJ. The α 7 β 1 integrin in muscle development and disease. *Cell and Tissue Research* 1999;296:183-190.
- (44) Boppart MD, Burkin DJ, Kaufman SJ. α 7 β 1-Integrin regulates mechanotransduction and prevents skeletal muscle injury. *Am J Physiol Cell Physiol* 2006;290:C1660-C1665.
- (45) Burkin DJ, Wallace GQ, Milner DJ, Chaney EJ, Mulligan JA, Kaufman SJ. Transgenic Expression of α 7 β 1 Integrin Maintains Muscle Integrity, Increases Regenerative Capacity, Promotes Hypertrophy, and Reduces Cardiomyopathy in Dystrophic Mice. *Am J Pathol* 2005;166:253-263.

- (46) Gawlik KI, Li JY, Petersen A, Durbeej M. Laminin {alpha}1 chain improves laminin {alpha}2 chain deficient peripheral neuropathy. *Hum Mol Genet* 2006;15:2690-2700.
- (47) Zanotti S, Saredi S, Ruggieri A et al. Altered extracellular matrix transcript expression and protein modulation in primary Duchenne muscular dystrophy myotubes. *Matrix Biol* 2007;26:615-624.
- (48) van Lunteren E, Moyer M, Leahy P. Gene expression profiling of diaphragm muscle in {alpha}2-laminin (merosin)-deficient dy/dy dystrophic mice. *Physiol Genomics* 2006;25:85-95.
- (49) Camby I, Le MM, Lefranc F, Kiss R. Galectin-1: a small protein with major functions. *Glycobiology* 2006;16:137R-157R.
- (50) Cooper DN, Massa SM, Barondes SH. Endogenous muscle lectin inhibits myoblast adhesion to laminin. *J Cell Biol* 1991;115:1437-1448.
- (51) Belot N, Rorive S, Doyen I et al. Molecular characterization of cell substratum attachments in human glial tumors relates to prognostic features. *Glia* 2001;36:375-390.
- (52) Wanninger J, Weigert J, Wiest R et al. Systemic and hepatic vein galectin-3 are increased in patients with alcoholic liver cirrhosis and negatively correlate with liver function. *Cytokine* 2011.
- (53) Almkvist J, Karlsson A. Galectins as inflammatory mediators. *Glycoconj J* 2004;19:575-581.
- (54) Hsu DK, Yang RY, Pan Z et al. Targeted disruption of the galectin-3 gene results in attenuated peritoneal inflammatory responses. *Am J Pathol* 2000;156:1073-1083.

- (55) Massa SM, Cooper DN, Leffler H, Barondes SH. L-29, an endogenous lectin, binds to glycoconjugate ligands with positive cooperativity. *Biochemistry* 1993;32:260-267.
- (56) Woo HJ, Shaw LM, Messier JM, Mercurio AM. The major non-integrin laminin binding protein of macrophages is identical to carbohydrate binding protein 35 (Mac-2). *J Biol Chem* 1990;265:7097-7099.
- (57) Lok CN, Chan KF, Loh TT. Effects of protein kinase modulators on transferrin receptor expression in human leukaemic HL-60 cells. *FEBS Lett* 1995;365:137-140.
- (58) Canesin G, Gonzalez-Peramato P, Palou J, Urrutia M, Cordon-Cardo C, Sanchez-Carbayo M. Galectin-3 expression is associated with bladder cancer progression and clinical outcome. *Tumour Biol* 2010;31:277-285.
- (59) Weigert J, Neumeier M, Wanninger J et al. Serum galectin-3 is elevated in obesity and negatively correlates with glycosylated hemoglobin in type 2 diabetes. *J Clin Endocrinol Metab* 2010;95:1404-1411.
- (60) Reist NE, Werle MJ, McMahan UJ. Agrin released by motor neurons induces the aggregation of acetylcholine receptors at neuromuscular junctions. *Neuron* 1992;8:865-868.
- (61) Eusebio A, Oliveri F, Barzaghi P, Ruegg MA. Expression of mouse agrin in normal, denervated and dystrophic muscle. *Neuromuscul Disord* 2003;13:408-415.
- (62) Nitkin RM, Smith MA, Magill C et al. Identification of agrin, a synaptic organizing protein from Torpedo electric organ. *J Cell Biol* 1987;105:2471-2478.

- (63) Gesemann M, Cavalli V, Denzer AJ, Brancaccio A, Schumacher B, Ruegg MA. Alternative splicing of agrin alters its binding to heparin, dystroglycan, and the putative agrin receptor. *Neuron* 1996;16:755-767.
- (64) Glass DJ, Bowen DC, Stitt TN et al. Agrin acts via a MuSK receptor complex. *Cell* 1996;85:513-523.
- (65) Williams S, Ryan C, Jacobson C. Agrin and neuregulin, expanding roles and implications for therapeutics. *Biotechnol Adv* 2008;26:187-201.
- (66) Denzer AJ, Brandenberger R, Gesemann M, Chiquet M, Ruegg MA. Agrin binds to the nerve-muscle basal lamina via laminin. *J Cell Biol* 1997;137:671-683.
- (67) Denzer AJ, Schulthess T, Fauser C et al. Electron microscopic structure of agrin and mapping of its binding site in laminin-1. *EMBO J* 1998;17:335-343.
- (68) Kammerer RA, Schulthess T, Landwehr R et al. Interaction of agrin with laminin requires a coiled-coil conformation of the agrin-binding site within the laminin gamma1 chain. *EMBO J* 1999;18:6762-6770.
- (69) Wang YG, Ji X, Pabbidi M, Samarel AM, Lipsius SL. Laminin acts via focal adhesion kinase/phosphatidylinositol-3' kinase/protein kinase B to down-regulate beta1-adrenergic receptor signalling in cat atrial myocytes. *J Physiol* 2009;587:541-550.
- (70) Samarel AM. Costameres, focal adhesions, and cardiomyocyte mechanotransduction. *Am J Physiol Heart Circ Physiol* 2005;289:H2291-H2301.
- (71) Chen HC, Guan JL. Association of focal adhesion kinase with its potential substrate phosphatidylinositol 3-kinase. *Proc Natl Acad Sci U S A* 1994;91:10148-10152.

- (72) Gao Y, Ordas R, Klein JD, Price SR. Regulation of caspase-3 activity by insulin in skeletal muscle cells involves both PI3-kinase and MEK-1/2. *J Appl Physiol* 2008;105:1772-1778.
- (73) Ginsberg MH, Partridge A, Shattil SJ. Integrin regulation. *Curr Opin Cell Biol* 2005;17:509-516.
- (74) Matheny RW, Jr., Adamo ML. Current perspectives on Akt activation and Actions. *Exp Biol Med (Maywood)* 2009;234:1264-1270.
- (75) Song WK, Wang W, Sato H, Bielser DA, Kaufman SJ. Expression of alpha 7 integrin cytoplasmic domains during skeletal muscle development: alternate forms, conformational change, and homologies with serine/threonine kinases and tyrosine phosphatases. *J Cell Sci* 1993;106 (Pt 4):1139-1152.
- (76) Schwartz MA, Ginsberg MH. Networks and crosstalk: integrin signalling spreads. *Nat Cell Biol* 2002;4:E65-E68.
- (77) Welser JV, Lange N, Singer CA et al. Loss of the alpha 7 integrin promoted extracellular signal-regulated kinase activation and altered vascular remodeling. *Circulation Research* 2007;101:672-681.
- (78) Xu H, Wu XR, Wewer UM, Engvall E. Murine muscular dystrophy caused by a mutation in the laminin [alpha]2 (Lama2) gene. *Nat Genet* 1994;8:297-302.
- (79) Sunada Y, Bernier SM, Kozak CA, Yamada Y, Campbell KP. Deficiency of merosin in dystrophic mice and genetic linkage of laminin M chain gene to dy locus. *J Biol Chem* 1994;269:13729-13732.
- (80) Chun SJ, Rasband MN, Sidman RL, Habib AA, Vartanian T. Integrin-linked kinase is required for laminin-2-induced oligodendrocyte cell spreading and CNS myelination. *J Cell Biol* 2003;163:397-408.

- (81) Bateson DS, Parry DJ. Motor units in a fast-twitch muscle of normal and dystrophic mice. *J Physiol* 1983;345:515-523.
- (82) Kuang W, Xu H, Vachon PH et al. Merosin-deficient congenital muscular dystrophy - Partial genetic correction in two mouse models. *Journal of Clinical Investigation* 1998;102:844-852.
- (83) Miyagoe Y, Hanaoka K, Nonaka I et al. Laminin [alpha]2 chain-null mutant mice by targeted disruption of the Lama2 gene: a new model of merosin (laminin 2)-deficient congenital muscular dystrophy. *FEBS Letters* 1997;415:33-39.
- (84) Guo LT, Zhang XU, Kuang W et al. Laminin [alpha]2 deficiency and muscular dystrophy; genotype-phenotype correlation in mutant mice. *Neuromuscular Disorders* 2003;13:207-215.
- (85) Nakagawa M, Miyagoe-Suzuki Y, Ikezoe K et al. Schwann cell myelination occurred without basal lamina formation in laminin alpha2 chain-null mutant (dy3K/dy3K) mice. *Glia* 2001;35:101-110.
- (86) Hager M, Gawlik K, Nystrom A, Sasaki T, Durbeej M. Laminin {alpha}1 chain corrects male infertility caused by absence of laminin {alpha}2 chain. *Am J Pathol* 2005;167:823-833.
- (87) Philpot J, Cowan F, Pennock J et al. Merosin-deficient congenital muscular dystrophy: the spectrum of brain involvement on magnetic resonance imaging. *Neuromuscul Disord* 1999;9:81-85.
- (88) Philpot J, Bagnall A, King C, Dubowitz V, Muntoni F. Feeding problems in merosin deficient congenital muscular dystrophy. *Arch Dis Child* 1999;80:542-547.
- (89) Martin PT, Ettinger AJ, Sanes JR. A synaptic localization domain in the synaptic cleft protein laminin beta 2 (s-laminin). *Science* 1995;269:413-416.

- (90) Rooney JE, Gurpur PB, Yablonka-Reuveni Z, Burkin DJ. Laminin-111 restores regenerative capacity in a mouse model for alpha7 integrin congenital myopathy. *Am J Pathol* 2009;174:256-264.
- (91) Occhi S, Zambroni D, Del Carro U et al. Both Laminin and Schwann Cell Dystroglycan Are Necessary for Proper Clustering of Sodium Channels at Nodes of Ranvier. *J Neurosci* 2005;25:9418-9427.
- (92) Burkin DJ, Gu M, Hodges BL, Campanelli JT, Kaufman SJ. A Functional Role for Specific Spliced Variants of the alpha 7beta 1 Integrin in Acetylcholine Receptor Clustering. *J Cell Biol* 1998;143:1067-1075.
- (93) Burkin DJ, Kim JE, Gu M, Kaufman SJ. Laminin and alpha7beta1 integrin regulate agrin-induced clustering of acetylcholine receptors. *J Cell Sci* 2000;113:2877-2886.
- (94) Collo G, Starr L, Quaranta V. A new isoform of the laminin receptor integrin alpha 7 beta 1 is developmentally regulated in skeletal muscle. *J Biol Chem* 1993;268:19019-19024.
- (95) Ziober BL, Vu MP, Waleh N, Crawford J, Lin CS, Kramer RH. Alternative extracellular and cytoplasmic domains of the integrin alpha 7 subunit are differentially expressed during development. *J Biol Chem* 1993;268:26773-26783.
- (96) von der MH, Williams I, Wendler O, Sorokin L, von der MK, Poschl E. Alternative splice variants of alpha 7 beta 1 integrin selectively recognize different laminin isoforms. *J Biol Chem* 2002;277:6012-6016.
- (97) Patarroyo M, Tryggvason K, Virtanen I. Laminin isoforms in tumor invasion, angiogenesis and metastasis. *Semin Cancer Biol* 2002;12:197-207.

- (98) Flintoff-Dye NL, Welsch J, Rooney J et al. Role for the alpha 7 beta 1 integrin in vascular development and integrity. *Developmental Dynamics* 2005;234:11-21.
- (99) Nawrotzki R, Willem M, Miosge N, Brinkmeier H, Mayer U. Defective integrin switch and matrix composition at alpha 7-deficient myotendinous junctions precede the onset of muscular dystrophy in mice. *Hum Mol Genet* 2003;12:483-495.
- (100) Mayer U, Saher G, Fassler R et al. Absence of integrin alpha 7 causes a novel form of muscular dystrophy. *Nat Genet* 1997;17:318-323.
- (101) Martin PT, Kaufman SJ, Kramer RH, Sanes JR. Synaptic integrins in developing, adult, and mutant muscle: selective association of alpha1, alpha7A, and alpha7B integrins with the neuromuscular junction. *Dev Biol* 1996;174:125-139.
- (102) Boppart MD, Volker SE, Alexander N, Burkin DJ, Kaufman SJ. Exercise promotes alpha7 integrin gene transcription and protection of skeletal muscle. *Am J Physiol Regul Integr Comp Physiol* 2008;295:R1623-R1630.
- (103) Rooney JE, Gurpur PB, Burkin DJ. Laminin-111 protein therapy prevents muscle disease in the mdx mouse model for Duchenne muscular dystrophy. *Proc Natl Acad Sci U S A* 2009;106:7991-7996.
- (104) Xu R, Chandrasekharan K, Yoon JH, Camboni M, Martin PT. Overexpression of the cytotoxic T cell (CT) carbohydrate inhibits muscular dystrophy in the dy(w) mouse model of congenital muscular dystrophy 1A. *Am J Pathol* 2007;171:181-199.
- (105) Ringelmann B, Roder C, Hallmann R et al. Expression of laminin alpha1, alpha2, alpha4, and alpha5 chains, fibronectin, and tenascin-C in skeletal muscle of dystrophic 129ReJ dy/dy mice. *Exp Cell Res* 1999;246:165-182.

- (106) Pegoraro E, Mancias P, Swerdlow SH et al. Congenital muscular dystrophy with primary laminin alpha2 (merosin) deficiency presenting as inflammatory myopathy. *Ann Neurol* 1996;40:782-791.
- (107) Gawlik KI, Mayer U, Blomberg K, Sonnenberg A, Ekblom P, Durbeej M. Laminin [alpha]1 chain mediated reduction of laminin [alpha]2 chain deficient muscular dystrophy involves integrin [alpha]7[beta]1 and dystroglycan. *FEBS Letters* 2006;580:1759-1765.
- (108) Patton BL, Miner JH, Chiu AY, Sanes JR. Distribution and function of laminins in the neuromuscular system of developing, adult, and mutant mice. *J Cell Biol* 1997;139:1507-1521.
- (109) Chen X, Li Y. Role of matrix metalloproteinases in skeletal muscle: migration, differentiation, regeneration and fibrosis. *Cell Adh Migr* 2009;3:337-341.
- (110) Dumic J, Dabelic S, Flogel M. Galectin-3: an open-ended story. *Biochim Biophys Acta* 2006;1760:616-635.
- (111) Furtak V, Hatcher F, Ochieng J. Galectin-3 mediates the endocytosis of beta-1 integrins by breast carcinoma cells. *Biochem Biophys Res Commun* 2001;289:845-850.
- (112) Girgenrath M, Dominov JA, Kostek CA, Miller JB. Inhibition of apoptosis improves outcome in a model of congenital muscular dystrophy. *Journal of Clinical Investigation* 2004;114:1635-1639.
- (113) Girgenrath M, Beermann ML, Vishnudas VK, Homma S, Miller JB. Pathology is alleviated by doxycycline in a laminin-alpha2-null model of congenital muscular dystrophy. *Ann Neurol* 2009;65:47-56.

- (114) Erb M, Meinen S, Barzaghi P et al. Omigapil ameliorates the pathology of muscle dystrophy caused by laminin- α 2 deficiency. *J Pharmacol Exp Ther* 2009;331:787-795.
- (115) Bentzinger CF, Barzaghi P, Lin S, Ruegg MA. Overexpression of mini-agrin in skeletal muscle increases muscle integrity and regenerative capacity in laminin- α 2-deficient mice. *FASEB J* 2005;19:934-942.
- (116) Kalamida D, Poulas K, Avramopoulou V et al. Muscle and neuronal nicotinic acetylcholine receptors. Structure, function and pathogenicity. *FEBS J* 2007;274:3799-3845.
- (117) Pato C, Stetzkowski-Marden F, Gaus K, Recouvreur M, Cartaud A, Cartaud J. Role of lipid rafts in agrin-elicited acetylcholine receptor clustering. *Chem Biol Interact* 2008;175:64-67.
- (118) Werle MJ. Cell-to-cell signaling at the neuromuscular junction: the dynamic role of the extracellular matrix. *Ann N Y Acad Sci* 2008;1132:13-18.
- (119) Moll J, Barzaghi P, Lin S et al. An agrin minigene rescues dystrophic symptoms in a mouse model for congenital muscular dystrophy. *Nature* 2001;413:302-307.
- (120) Tourovskaia A, Li N, Folch A. Localized acetylcholine receptor clustering dynamics in response to microfluidic focal stimulation with agrin. *Biophys J* 2008;95:3009-3016.
- (121) Doe JA, Wuebbles RD, Allred ET, Rooney JE, Elorza M, Burkin DJ. Transgenic overexpression of the α 7 integrin reduces muscle pathology and improves viability in the dyW mouse model of merosin-deficient congenital muscular dystrophy type 1A. *J Cell Sci* 2011;124:2287-2297.

- (122) Cockcroft DW. Direct challenge tests: Airway hyperresponsiveness in asthma: its measurement and clinical significance. *Chest* 2010;138:18S-24S.
- (123) Behr J, Furst DE. Pulmonary function tests. *Rheumatology (Oxford)* 2008;47 Suppl 5:v65-v67.
- (124) Bozanich EM, Janosi TZ, Collins RA et al. Methacholine responsiveness in mice from 2 to 8 wk of age. *J Appl Physiol* 2007;103:542-546.
- (125) Philpot J, Bagnall A, King C, Dubowitz V, Muntoni F. Feeding problems in merosin deficient congenital muscular dystrophy. *Arch Dis Child* 1999;80:542-547.
- (126) Glaab T, Taube C, Braun A, Mitzner W. Invasive and noninvasive methods for studying pulmonary function in mice. *Respir Res* 2007;8:63.
- (127) Lundblad LK, Irvin CG, Adler A, Bates JH. A reevaluation of the validity of unrestrained plethysmography in mice. *J Appl Physiol* 2002;93:1198-1207.
- (128) Lomask M. Further exploration of the Penh parameter. *Exp Toxicol Pathol* 2006;57 Suppl 2:13-20.
- (129) Hamelmann E, Schwarze J, Takeda K et al. Noninvasive measurement of airway responsiveness in allergic mice using barometric plethysmography. *Am J Respir Crit Care Med* 1997;156:766-775.
- (130) Adler A, Cieslewicz G, Irvin CG. Unrestrained plethysmography is an unreliable measure of airway responsiveness in BALB/c and C57BL/6 mice. *J Appl Physiol* 2004;97:286-292.
- (131) Zatz M, Rapaport D, Vainzof M et al. Serum creatine-kinase (CK) and pyruvate-kinase (PK) activities in Duchenne (DMD) as compared with Becker (BMD) muscular dystrophy. *J Neurol Sci* 1991;102:190-196.

- (132) Perillo NL, Marcus ME, Baum LG. Galectins: versatile modulators of cell adhesion, cell proliferation, and cell death. *J Mol Med (Berl)* 1998;76:402-412.
- (133) Hughes RC. Secretion of the galectin family of mammalian carbohydrate-binding proteins. *Biochim Biophys Acta* 1999;1473:172-185.
- (134) de Boer RA, Yu L, van Veldhuisen DJ. Galectin-3 in cardiac remodeling and heart failure. *Curr Heart Fail Rep* 2010;7:1-8.
- (135) Cleves AE, Cooper DN, Barondes SH, Kelly RB. A new pathway for protein export in *Saccharomyces cerevisiae*. *J Cell Biol* 1996;133:1017-1026.
- (136) Henderson NC, Sethi T. The regulation of inflammation by galectin-3. *Immunol Rev* 2009;230:160-171.
- (137) Rivera M, Seetharaman R, Girdhar D et al. The reduction potential of cytochrome b5 is modulated by its exposed heme edge. *Biochemistry* 1998;37:1485-1494.
- (138) Liu FT, Patterson RJ, Wang JL. Intracellular functions of galectins. *Biochim Biophys Acta* 2002;1572:263-273.
- (139) Rabinovich GA, Riera CM, Landa CA, Sotomayor CE. Galectins: a key intersection between glycobiology and immunology. *Braz J Med Biol Res* 1999;32:383-393.
- (140) Cerri DG, Rodrigues LC, Stowell SR et al. Degeneration of dystrophic or injured skeletal muscles induces high expression of Galectin-1. *Glycobiology* 2008;18:842-850.
- (141) Cooper DN, Barondes SH. Evidence for export of a muscle lectin from cytosol to extracellular matrix and for a novel secretory mechanism. *J Cell Biol* 1990;110:1681-1691.

- (142) Liu FT, Patterson RJ, Wang JL. Intracellular functions of galectins. *Biochim Biophys Acta* 2002;1572:263-273.
- (143) Hsu DK, Dowling CA, Jeng KC, Chen JT, Yang RY, Liu FT. Galectin-3 expression is induced in cirrhotic liver and hepatocellular carcinoma. *Int J Cancer* 1999;81:519-526.
- (144) Henderson NC, Mackinnon AC, Farnworth SL et al. Galectin-3 regulates myofibroblast activation and hepatic fibrosis. *Proc Natl Acad Sci U S A* 2006;103:5060-5065.
- (145) Nishi Y, Sano H, Kawashima T et al. Role of galectin-3 in human pulmonary fibrosis. *Allergol Int* 2007;56:57-65.
- (146) Wang L, Friess H, Zhu Z et al. Galectin-1 and galectin-3 in chronic pancreatitis. *Lab Invest* 2000;80:1233-1241.
- (147) van Kimmenade RR, Januzzi JL, Jr., Ellinor PT et al. Utility of amino-terminal pro-brain natriuretic peptide, galectin-3, and apelin for the evaluation of patients with acute heart failure. *J Am Coll Cardiol* 2006;48:1217-1224.
- (148) McLoon LK. Focusing on fibrosis: halofuginone-induced functional improvement in the mdx mouse model of Duchenne muscular dystrophy. *Am J Physiol Heart Circ Physiol* 2008;294:H1505-H1507.
- (149) Huebner KD, Jassal DS, Halevy O, Pines M, Anderson JE. Functional resolution of fibrosis in mdx mouse dystrophic heart and skeletal muscle by halofuginone. *Am J Physiol Heart Circ Physiol* 2008;294:H1550-H1561.
- (150) Tinsley JM, Potter AC, Phelps SR, Fisher R, Trickett JI, Davies KE. Amelioration of the dystrophic phenotype of mdx mice using a truncated utrophin transgene. *Nature* 1996;384:349-353.

- (151) Krag TO, Bogdanovich S, Jensen CJ et al. Heregulin ameliorates the dystrophic phenotype in mdx mice. *Proc Natl Acad Sci U S A* 2004;101:13856-13860.
- (152) Wehling M, Spencer MJ, Tidball JG. A nitric oxide synthase transgene ameliorates muscular dystrophy in mdx mice. *J Cell Biol* 2001;155:123-132.
- (153) Stupka N, Gregorevic P, Plant DR, Lynch GS. The calcineurin signal transduction pathway is essential for successful muscle regeneration in mdx dystrophic mice. *Acta Neuropathol* 2004;107:299-310.
- (154) McPherron AC, Lawler AM, Lee SJ. Regulation of skeletal muscle mass in mice by a new TGF-beta superfamily member. *Nature* 1997;387:83-90.
- (155) Bogdanovich S, Krag TO, Barton ER et al. Functional improvement of dystrophic muscle by myostatin blockade. *Nature* 2002;420:418-421.
- (156) Mendias CL, Bakhurin KI, Faulkner JA. Tendons of myostatin-deficient mice are small, brittle, and hypocellular. *Proc Natl Acad Sci U S A* 2008;105:388-393.
- (157) Amthor H, Macharia R, Navarrete R et al. Lack of myostatin results in excessive muscle growth but impaired force generation. *Proceedings of the National Academy of Sciences of the United States of America* 2007;104:1835-1840.
- (158) Li Zf, Shelton GD, Engvall E. Elimination of Myostatin Does Not Combat Muscular Dystrophy in dy Mice but Increases Postnatal Lethality. *Am J Pathol* 2005;166:491-497.
- (159) Kronqvist P, Kawaguchi N, Albrechtsen R et al. ADAM12 Alleviates the Skeletal Muscle Pathology in mdx Dystrophic Mice. *Am J Pathol* 2002;161:1535-1540.

- (160) Nguyen HH, Jayasinha V, Xia B, Hoyte K, Martin PT. Overexpression of the cytotoxic T cell GalNAc transferase in skeletal muscle inhibits muscular dystrophy in mdx mice. *Proc Natl Acad Sci U S A* 2002;99:5616-5621.
- (161) Allamand V, Bidou L, Arakawa M et al. Drug-induced readthrough of premature stop codons leads to the stabilization of laminin alpha2 chain mRNA in CMD myotubes. *J Gene Med* 2008;10:217-224.
- (162) Jentsch TJ, Stein V, Weinreich F, Zdebik AA. Molecular structure and physiological function of chloride channels. *Physiol Rev* 2002;82:503-568.
- (163) Hoffmann EK, Lambert IH, Pedersen SF. Physiology of cell volume regulation in vertebrates. *Physiol Rev* 2009;89:193-277.
- (164) Inoue H, Okada Y. Roles of volume-sensitive chloride channel in excitotoxic neuronal injury. *J Neurosci* 2007;27:1445-1455.
- (165) Okada Y, Maeno E, Shimizu T, Dezaki K, Wang J, Morishima S. Receptor-mediated control of regulatory volume decrease (RVD) and apoptotic volume decrease (AVD). *J Physiol* 2001;532:3-16.
- (166) Browe DM, Baumgarten CM. Stretch of beta 1 integrin activates an outwardly rectifying chloride current via FAK and Src in rabbit ventricular myocytes. *J Gen Physiol* 2003;122:689-702.
- (167) Puklin-Faucher E, Sheetz MP. The mechanical integrin cycle. *J Cell Sci* 2009;122:179-186.
- (168) Sonnenberg A. Integrins and their ligands. *Curr Top Microbiol Immunol* 1993;184:7-35.
- (169) de Melker AA, Sonnenberg A. Integrins: alternative splicing as a mechanism to regulate ligand binding and integrin signaling events. *Bioessays* 1999;21:499-509.

- (170) Ross RS. Molecular and mechanical synergy: cross-talk between integrins and growth factor receptors. *Cardiovasc Res* 2004;63:381-390.
- (171) Hofmann G, Bernabei PA, Crociani O et al. HERG K⁺ channels activation during beta(1) integrin-mediated adhesion to fibronectin induces an up-regulation of alpha(v)beta(3) integrin in the preosteoclastic leukemia cell line FLG 29.1. *J Biol Chem* 2001;276:4923-4931.
- (172) Kawasaki J, Davis GE, Davis MJ. Regulation of Ca²⁺-dependent K⁺ current by alphavbeta3 integrin engagement in vascular endothelium. *J Biol Chem* 2004;279:12959-12966.
- (173) Wu X, Yang Y, Gui P et al. Potentiation of large conductance, Ca²⁺-activated K⁺ (BK) channels by alpha5beta1 integrin activation in arteriolar smooth muscle. *J Physiol* 2008;586:1699-1713.
- (174) Waitkus-Edwards KR, Martinez-Lemus LA, Wu X et al. alpha(4)beta(1) Integrin activation of L-type calcium channels in vascular smooth muscle causes arteriole vasoconstriction. *Circ Res* 2002;90:473-480.
- (175) Wu X, Mogford JE, Platts SH, Davis GE, Meininger GA, Davis MJ. Modulation of calcium current in arteriolar smooth muscle by alphav beta3 and alpha5 beta1 integrin ligands. *J Cell Biol* 1998;143:241-252.
- (176) Formigli L, Meacci E, Sassoli C et al. Sphingosine 1-phosphate induces cytoskeletal reorganization in C2C12 myoblasts: physiological relevance for stress fibres in the modulation of ion current through stretch-activated channels. *J Cell Sci* 2005;118:1161-1171.
- (177) Sbrana F, Sassoli C, Meacci E et al. Role for stress fiber contraction in surface tension development and stretch-activated channel regulation in C2C12 myoblasts. *Am J Physiol Cell Physiol* 2008;295:C160-C172.

- (178) Browe DM, Baumgarten CM. Angiotensin II (AT1) receptors and NADPH oxidase regulate Cl⁻ current elicited by beta1 integrin stretch in rabbit ventricular myocytes. *J Gen Physiol* 2004;124:273-287.
- (179) Browe DM, Baumgarten CM. EGFR kinase regulates volume-sensitive chloride current elicited by integrin stretch via PI-3K and NADPH oxidase in ventricular myocytes. *J Gen Physiol* 2006;127:237-251.
- (180) Levite M, Cahalon L, Peretz A et al. Extracellular K⁽⁺⁾ and opening of voltage-gated potassium channels activate T cell integrin function: physical and functional association between Kv1.3 channels and beta1 integrins. *J Exp Med* 2000;191:1167-1176.
- (181) Askari JA, Buckley PA, Mould AP, Humphries MJ. Linking integrin conformation to function. *J Cell Sci* 2009;122:165-170.
- (182) Formigli L, Meacci E, Sassoli C et al. Cytoskeleton/stretch-activated ion channel interaction regulates myogenic differentiation of skeletal myoblasts. *J Cell Physiol* 2007;211:296-306.
- (183) Legate KR, Wickstrom SA, Fassler R. Genetic and cell biological analysis of integrin outside-in signaling. *Genes Dev* 2009;23:397-418.
- (184) Fatherazi S, Izutsu KT, Wellner RB, Belton CM. Hypotonically activated chloride current in HSG cells. *J Membr Biol* 1994;142:181-193.
- (185) Nilius B, Eggermont J, Voets T, Buyse G, Manolopoulos V, Droogmans G. Properties of volume-regulated anion channels in mammalian cells. *Prog Biophys Mol Biol* 1997;68:69-119.
- (186) Belkin AM, Retta SF, Pletjushkina OY et al. Muscle beta1D integrin reinforces the cytoskeleton-matrix link: modulation of integrin adhesive function by alternative splicing. *J Cell Biol* 1997;139:1583-1595.

- (187) Belkin AM, Zhidkova NI, Balzac F et al. Beta 1D integrin displaces the beta 1A isoform in striated muscles: localization at junctional structures and signaling potential in nonmuscle cells. *J Cell Biol* 1996;132:211-226.
- (188) van der Flier A, Gaspar AC, Thorsteinsdottir S et al. Spatial and temporal expression of the beta1D integrin during mouse development. *Dev Dyn* 1997;210:472-486.
- (189) Ren Z, Raucci FJ, Jr., Browe DM, Baumgarten CM. Regulation of swelling-activated Cl(-) current by angiotensin II signalling and NADPH oxidase in rabbit ventricle. *Cardiovasc Res* 2008;77:73-80.
- (190) Walsh KB, Zhang J. Regulation of cardiac volume-sensitive chloride channel by focal adhesion kinase and Src kinase. *Am J Physiol Heart Circ Physiol* 2005;289:H2566-H2574.